INFORMATION TO USERS

The most advanced technology has been used to photograph and reproduce this manuscript from the microfilm master. UMI films the text directly from the original or copy submitted. Thus, some thesis and dissertation copies are in typewriter face, while others may be from any type of computer printer.

The quality of this reproduction is dependent upon the quality of the copy submitted. Broken or indistinct print, colored or poor quality illustrations and photographs, print bleedthrough, substandard margins, and improper alignment can adversely affect reproduction.

In the unlikely event that the author did not send UMI a complete manuscript and there are missing pages, these will be noted. Also, if unauthorized copyright material had to be removed, a note will indicate the deletion.

Oversize materials (e.g., maps, drawings, charts) are reproduced by sectioning the original, beginning at the upper left-hand corner and continuing from left to right in equal sections with small overlaps. Each original is also photographed in one exposure and is included in reduced form at the back of the book.

Photographs included in the original manuscript have been reproduced xerographically in this copy. Higher quality 6" x 9" black and white photographic prints are available for any photographs or illustrations appearing in this copy for an additional charge. Contact UMI directly to order.

U·M·I

University Microfilms International
A Bell & Howell Information Company
300 North Zeeb Road, Ann Arbor, MI 48106-1346 USA
313/761-4700 800/521-0600

Order Number 9119695

The molecular properties of NAD-coenzymes bound to various dehydrogenases: A classical raman difference study

Zheng, Jie, Ph.D.

City University of New York, 1991

U·M·I
300 N. Zeeb Rd.
Ann Arbor, MI 48106

A

THE MOLECULAR PROPERTIES OF NAD-COENZYMES BOUND TO VARIOUS DEHYDROGENASES: A CLASSICAL RAMAN DIFFERENCE STUDY

By Jie Zheng

A dissertation submitted to the Graduate Faculty in Physics in partial fulfillment of the requirements for the degree of Doctor of Philosophy, The City University of New York

1991

The manuscript has been read and accepted for the Graduate Faculty in Physics in satisfaction of the dissertation requirement for the degree of Doctor of Philosophy.

Jan. 10, 1991
Date

Robert Callender
Chair of Examining Committee

Jan 22, 1991
Date

Joseph B. Krieger
Executive Officer

Supervisory Committee

The City University of New York

Abstract

THE MOLECULAR PROPERTIES OF NAD-COENZYMES BOUND TO VARIOUS DEHYDROGENASES: A CLASSICAL RAMAN DIFFERENCE STUDY

by

Jie Zheng

Adviser: Professor Robert H. Callender

The Raman spectrum of a small molecule or molecular moiety when bound to proteins can be measured by using difference techniques developed in our laboratory. In the thesis, we have applied this method in obtaining the Raman spectra of NAD(P)-coenzymes and their analogies when bound to lactate dehydrogenase (LDH) and dihydrofolate reductase (DHFR). The binding of the coenzymes to the proteins causes significant changes in the Raman spectra of these molecules relative to spectra obtained in the absence of enzymes. When the coenzymes bind to LDH, the molecular motions of the adenine moiety of both NAD^+ and NADH as well as adenine containing analogues of these coenzyme produce Raman bands that are essentially identical to each other but very different from solution spectra, suggesting that the binding of adenine to the enzyme is the same regardless of the nicotinamide head-group nature. Protonation of the bound adenine ring at the 3-position is offered as a possible explanation for the changes observed in the Raman spectra of adenine when it binds to these two

enzymes relative to its solution spectrum. Significant shifts are observed in both the stretching frequency of the carboxamide carbonyl of the NAD^+ and analogues and the rocking motion of the carboxamide NH_2 group of NADH. We ascribe these shifts to the formation of strong hydrogen bonding between the cofactor's carbxamide group and the apoenzyme. We suggest that this hydrogen bonding is responsible for the very high degree of stereochemistry fidelity observed with this enzyme. When the coenzymes bound to DHFR, the binding properties of nicotinamide-head are found to be quite similar to those bound for LDH. However, the adenine moiety shows different Raman spectra. We suggest that when the cofactor binds to the DHFR, the adenine moiety fits into a hydrophobic pocket and does not change its protanation state. Finally, we use the C-H (C-D) stretching mode at the C4 position of nicotinamide to probe the possibility of the pucker state of the nicotinamide ring when it binds to dehydrogenases. We find considerable ring puckers for NADH upon binding to LDH and DHFR and little ring puckering for NADH in solution. We discuss this in relationship to the enzymatic properties of LDH and DHFR.

To my Parents and my Teachers

Acknowledgements

I would like to express my sincere gratitude to my thesis advisor Professor Robert H. Callender, for patiently guiding me through this work, as well as for his great contributions to my professional and personal growth.

I wish to dedicate this thesis to the memory of Professor Donald L. Sloan, and express my deepest appreciation to him for his help and many valuable discussions.

I am greatly indebted to Dr. John Burgner at Purdure University for his guidance and help in my thesis research.

I am grateful to Professor Timothy Boyer, who is the graduate student advisor in the Physics Department, for his help and cares.

I thank the members of my thesis committee for their time and guidance.

I thank Dr. Hua Deng for his collaboration and assistance.

I thank Dr. Danny Manor, Dr. Jim Ball, Miss Gezhi Weng, Mr. Yong Q. Chen, and Mr Liewen Huang for their valuable discussions and generous help. And also, I would like to thank Dr. Manor for his proof reading the manuscript and many valuable suggestions.

I thank Mrs. Naomi Hellman for her help during the years when I study in Professor Callender's Laboratory.

Table of Contents

page

List of Figures

List of Symbols Acronyms

NAD^+	oxidized β-nicotinamide adenine dinucleotide
NADH	reduced β-nicotinamide adenine dinucleotide
$NADP^+$	oxidized β-nicotinamide adenine dinucleotide phosphate
NADPH	reduced β-nicotinamide adenine dinucleotide phosphate
9-EtAd	9-ethyladenine
NMNH	reduced β-nicotinamide mononucleotide
NMN^+	oxidized β-nicotinamide mononucleotide
ADPR	adenosine 5'-diphosphate ribose
ATPR	adenosine 5'-diphosphate ribose phosphate
$APAD^+$	acetylpyridine adenine dinucleotide
$APADP^+$	acetylpyridine adenine dinucleotide phosphate
LDH	lactate dehydrogenase
LADH	liver alcohol dehydrogenase
DHFR	dihydrofolate reductase
OMA	optical multichannel analyzer

Chapter 1

INTRODUCTION

Enzymes, the catalysts of biological systems, are remarkable molecular device that determine the pattern of chemical transformations. They also mediate the transformations of different forms of energy. The most striking characteristics of enzymes are their catalytic power and specificity. Furthermore, the actions of many enzymes are regulated. Nearly all know enzymes are proteins.
From ***Biochemistry***, 3rd ed, by L. Stryer.

After enzymes were discovered in 1830, they have become a subject of great interest. Many scientists have spend their whole lifetime in their study. In 1913, L. Michaelis and M. L. Menten derived an equation, the Michaelis-Menten equation, which made it possible to understand and describe the kinetic behaver of enzymes. In the following six to seven decades, a lot of work having to do with enzymatic kinetics has been done, and now we can say that the kinetic behavior of many enzymes is clear.

But, how do the enzymes work? Some aspects of this question can be answered by kinetic studies, but structural probes, like X-ray crystallographic studies, have yielded deep insights into this molecular question. We can directly see the three-dimensional structure of enzyme. But, in the X-ray diffraction studies, it is very difficult to locate the positions of hydrogen atoms in proteins because the electron density of the H atoms is so weak. Also, X-ray diffraction studies cannot gave the directly information characterizing the interaction between two molecular fragments.

Raman spectroscopy is known for its ability to provide the detail information concerning such molecular properties of molecules and the interactions between molecules such as those that occur when a substrate binds at the active site of an enzyme. Indeed, using resonance Raman spectroscopy, the binding property of colored chromospheres to protein have been well studied. But, most protein ligands are not colored, so resonance Raman studies have been of limited use. Recently, our lab has developed ultrasensitive Raman difference techniques to study the binding properties of coenzymes and substrates to proteins. This technique (see below) permits the study of virtually any bound ligand.

In the period of my thesis research study, we used the difference Raman technique to study the binding probities of the NAD^+ and NADH coenzymes to lactate dehydrogenase (EC1.1.1.27, LDH) and dihydrofolate reductase (EC1.5.1.3, DHFR). Both LDH and DHFR belong to the large family (over 250 members) of NAD(P)-linked dehydrogenases. Those enzymes are among the earliest to be subjected to detailed kinetic studies. Also, good X-ray structure of both LDH and DHFR are available. The reaction catalyzed are of the type shown in Scheme 1.1. LDH is a NAD-linked enzyme while the DHFR is a NADP-linked one.

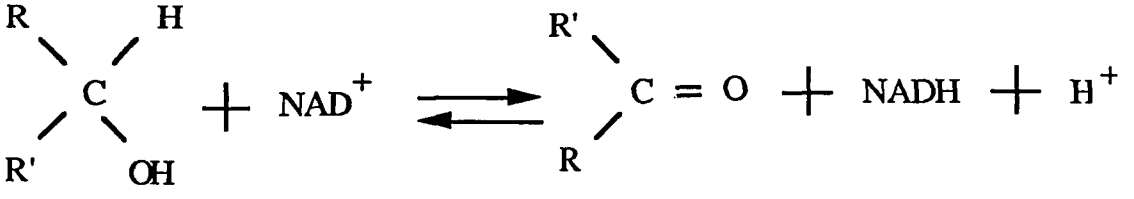

Scheme 1.1

Chapter 2
RAMAN EFFECT AND ITS DETECTION

2.1. Raman Effect

When a beam of monochromatic light is incident on a sample (e.g. a liquid), the majority of scattered light is due to elastic scattering and has a identical energy (or wavelength) to the incident beam. That is called Reyleigh scattering. A small portion of the scattered light (about 10^{-5}) however, is slightly shifted in energy from the incident light as a result of an inelastic scattering. This is known as the Raman effect after the Indian scientist C.V. Raman who with his colleague K.S. Krishnan first reported the effect in 1928 (Raman & Krishnan, 1928). The physical origin of Ramam scattering lies in inelastic collisions between the molecules composing the liquid and the photons of the incident light. The electric field of the light perturbs the electronic distribution of the molecule and induces periodic vibrations, thereby producing oscillating electric moments. Such oscillating electrons become new sources for emitting radiation, that is, the scattered light. If the scatter photons have a lower frequency than the incident light, it is called Stokes Raman scattering. Oppositely, if the scatter photon has higher frequency than the incident light, it is called anti-Stokes Raman scattering.

2.1.a. A model for Raman scattering based on classical physics

A light wave is a travelling wave composed of electric and magnetic fields, of which only the electric component gives rise to Raman scattering. When a light wave meets a molecule consisting of

electrons and nuclei, the electric field will exert the same force on all electrons in the molecule and will tend to displace them from their their average positions around the positively charged nuclei. Crucially, for the Raman process this displacement results in an *induced dipole moment* π in the molecule which is, to a good approximation, proportional to the electric field strength $\boldsymbol{E}$. Thus $\pi = \alpha \boldsymbol{E}$, where the proportionality factor α is called the electric polarizability of the molecule. In general the α is not a simple scalar, therefore the vector π will have a different direction from that of the vector $\boldsymbol{E}$. In fact, α is a tensor but in a simplified treatment we can limit the problem to with the relationship between just one component of the tensor, α_{zz} and the components of π and $\boldsymbol{E}$ in the z direction.

The electric field of the light wave varies with time. If a fixed molecule is irradiated with monochromatic radiation of ν_0, expressed in Hertz, which is plane polarized in the z direction, E_z as a function of time is given by

$$E(t) = E_{max} \cos(2\pi\nu_0 t)$$

where E_{max} is the value of E_z at its maximum and t is the time in seconds from an arbitrary starting time. Thus, for the E_z component of π

$$\pi_z = \alpha_{zz} E_{max} \cos(2\pi\nu_0 t)$$

Polarizability α here is caused by the vibration of the molecule and determined by the structure of the molecule. In the simple case of a diatomic molecule, α depends linearly on the nuclear coordinate q(t) and can be expanded around the equilibrium configuration of the molecule as

$$\alpha_{zz}(t) = \alpha_{zz}(0) + a'_{zz}\,\Delta q(t)$$

where $a_{zz}(0)$ is the equilibrium value of polarizability and a'_{zz} is the first order derivative of a_{zz} with respect to the nuclear coordinates q. The time dependence of q(t) due to molecular vibration is given by the relation

$$\Delta q(t) = q_o \cos(2\pi\nu_v t)$$

where ν_v is the molecular vibrational frequency, q_o is the amplitude of q(t).

Now the time dependence of the dipole moment can be explicitly written as

$$\pi_z(t) = a_{zz}(0)\, E_z \cos(2\pi\nu t) + (1/2)a'_{zz}\,\Delta q_o\, E_z \cos 2\pi(\nu + \nu_v)t + (1/2)a'_{zz}\,\Delta q_o\, E_z \cos 2\pi(\nu - \nu_v)t$$

In classical physics, an oscillating dipole radiates energy and the total power radiated (**P**) is given by (Jackson, 1975)

$$\mathbf{P}(t) = (8/3)(\pi^4/c^3)(\nu)^4 |\,\pi(t)\,|^2$$

When we put the two equations together, we obtain the total power radiated from an oscillating dipole in terms of the incident light frequency and the vibrational frequency of the molecule. From the above equation, it can be seen that the intensity of the scattered light varies as the fourth power of the incident light frequency.

As a result of the first term in the first equation, light of incident frequency ν will be emitted and observed in all directions. This is the phenomenon of Raleigh scattering. The scattered light arising from the second term is known as anti-Stokes Raman scattering. The third term will give light quanta of frequency $\nu-\nu_v$, and is known as Stokes Raman scattering. The coefficient of the cosine factor in each of these terms give the intensity of the Raleigh

or Raman scattering.

When the molecule is excited with a light of frequency close to its absorption maximum, a large increase in the intensity of the Raman lines is observed. This resonance phenomenon, known as the resonance Raman effect, cannot be explained through the classical approach outlined above. A semi-classical approach to the problem, discussed below, explains the observed resonance effect.

2.1.b. Semi-classical approach and resonance Raman effect

The basic theory of Raman scattering was developed by Placzek (Placzek, 1934). This theory was first applied in detail to molecular systems by Albrecht (Albrecht, 1961) and since then a considerable amount of theoretical work has been done in the field of Raman and resonance Raman scattering (Tang and Albrecht, 1968, 1970; Johnson and Peticolas, 1976). In the semi-classical Placzek's theory of Raman scattering, the radiation field is described classically and the molecule is treated quantum mechanically. The Raman intensity $I_{g0->g1}$ for the transition from the lowest vibrational state i=0 to the vibrational state i=1 (Stokes process), both in the ground electronic state g, is proportional to the square of the corresponding term in the polarizability tensor and is given by (just as in the case of classical description given above)

$$I_{g0\rightarrow g1} = \frac{2^7\pi^5}{9c^4} I_0 (\nu_s)^4 \sum_{\rho\sigma} \left| \alpha^{\rho\sigma}_{g0,g1}(\nu_L) \right|^2$$

where I_0 is the incident flux, ν_L is the incident light (laser) frequency, $\nu_s = \nu_L - \nu_0$ is the scattered light frequency, where ν_0 is the energy separation between the vibrational levels g0 and g1.

The $\alpha^{\rho\sigma}_{g0,g1}(\nu_L)$ component of the polarizability tensor is given

by

$$\alpha^{\rho\sigma}_{g0\,g1}(\nu_L) = \sum_{e,j} \frac{\langle g0|M^{\rho}_{eg}(Q)|ej\rangle\langle ej|M^{\sigma}_{eg}(Q)|g1\rangle}{\Delta E_{eg} - h\nu_L + \varepsilon_j + i\Gamma_{ej}} + \frac{\langle g0|M^{\sigma}_{eg}(Q)|ej\rangle\langle ej|M^{\rho}_{eg}(Q)|g1\rangle}{\Delta E_{eg} + h\nu_s + \varepsilon_j + i\Gamma_{ej}}$$

where |ej> denotes the jth vibrational level in the eth excited state, ej is the vibrational energy of that level, and ΔE_{eg} is the energy difference between the ground and excited electronic state. $M_{eg}(Q)$ is the electronic transition dipole moment expressed as a function of the nuclear coordinates Q, ρ and σ are the polarization vectors of the incident and scattered light. The factor $i\Gamma_{ej}$ in the denominators of equation is the phenomenological line width factor which takes in to account the finite lifetime of each of the molecular state.

It can be seen that when $\Delta E_{eg} \approx h\nu_L$, the denominator in the first term in above equation becomes small giving rise to a large enhancement of Raman intensity (resonance Raman effect). In this case the sum over electronic state may reduce to a single term in which case the vibrational sum over j pertains to the vibronic states of the excited electronic state in resonance with the incident photon. The second term in the equation makes, in general, negligible contribution to the Raman intensity and can be neglected in the resonance condition. In the first approximation, the electronic transition dipoles are assumed independent of nuclear coordinates, i.e. $M_{eg}(Q) = M_{eg}(0)$, and we obtain

$$\alpha^{\rho\sigma}_{g0\,g1}(\nu_L) = M^{\rho}_{eg}(0)\; M^{\sigma}_{eg}(0) \sum_j \frac{\langle g0|ej\rangle\langle ej|g1\rangle}{\Delta E_{eg} - h\nu_L + \varepsilon_j + i\Gamma_{ej}}$$

This is the so called Albrecht A term discussed first by Albrecht

(1961). In this term, <g0|ej> and <ej|g1> are overlap integrals between vibrational wave functions of the ground and excited states. The factors <g0|ej> are the Franck-Condon integrals which determine the appearance of vibrational progressions in absorption or fluorescence spectroscopy. Raman intensity goes to zero when these terms are small. This means that the A term will have significant contribution to the Raman intensity only for the vibrations that appear as progressions in electronic spectra.

In the off-resonance situation, particularly when $\Delta E_{eg} >> h\nu_L$, the polarizability is independent of the incident light frequency but involves contributions from all excited vibronic and electronic states. The A term, in this case, goes to zero and an expansion of $M_{eg}(Q)$ about $Q = Q_{eq}$, Herzberg-Teller approximation, leads to a so called B term. The B term is the major contributor to the Raman intensity when the laser photon is far from resonance with the excited state. And by simplified the B term, we can get a similar result for Raman intensity as we get in classical model.

2.2. Optical Multichannel Analyzer System

In our lab, Raman spectra are be measured using one of two spectrometer systems as depicted in following figure 2.1.

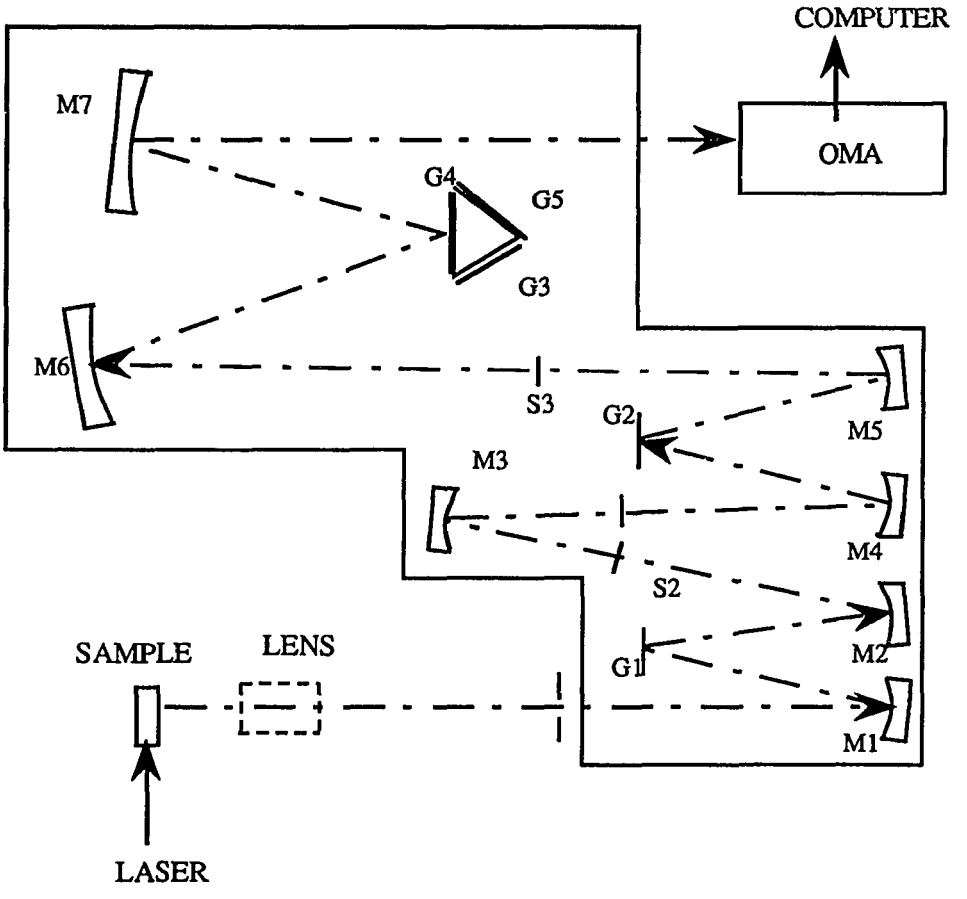

Figure 2.1 Experimental set up for Raman spectroscopy with a multichannel array detection system.

Both spectrometers consists of a 1877 Triplemate spectrometer (Spex Industries) equipped with either a Model 1420 reticon solid state detector system photodiode array and a model 1218 Controller

(EG&G, Princeton Applied Research) or a model DIDA-1000 reticon detector connected to a ST-100 detector controller (Princeton Instruments). The two detectors are interfaced to an LSI-11/2 microcomputer (Digital Equipment Corp.) or MAC II microcomputer (Apple Computer) which are used for data collection, manipulation and analysis, and equipment control. Both spectrometer systems, including the exciting lasers, are mounted on vibration free tables. Typically, 200 mW of the 488 nm line or 514.5 nm line from an argon-ion laser (Spetral-Physics, Model 165 or Model 164 or Coherent Innova 200) is used to excite Raman scattering.

2.2.a. Triplemate Spectrometer

Spex's 1877 triplemate spectrometer is a spectrograph specially tailored to provide the low-stray light and flat, undistrorted focal plane ideal for sensitive work with optical multichannel analyzer detector.

The Triplemate has two main sections (shown in Fig2.1). The first is a 0.22 m double monochrometer with gratings locked in a subtractive-dispersion mode. It acts as a variable-wavelength, selectable-bandpass filter that feeds a non-dispersed segment of radiation from a sample into the entrance slit of the second, or spectrograph stage. The 0.6-m, single-monochromator spectrograph stage, in turn, disperses the radiation over the detector. The optical path of the Triplemate is shown in the figure 2.1. Light passes into the entrance slit (S1) to be collimated by the first mirror (M1) onto the first grating (G1) (600 grooves/mm, 50x50 mm; 500 nm blaze,) where it is dispersed onto the second mirror (M2). After pass through the second slit (S2), which determines the bandpass of the

filter stage, the light strikes the spatial-filter mirror (M3) and passes through a fixed slit which eliminates much of the stray light. Again the light is collimated by next mirror (M4), and dispersed in an opposing direction by the second grating (G2), to conceal the effects of the initial dispersion, the focused by mirror 5 (M5) onto the exit slit of the first stage (S3). In this stage, by changing the intermediate slit (S2), we can choose the nominal bandpass, and we can select the center of the bandpass by changing direction of the grating. In the final stage, the light is again collimated the mirror (M6) and dispersed on whichever of threw turreted grating (G4) is selected. There are three grating available there; G3 with 600 grooves/mm; G4 with 1200 grooves/mm; and G5 with 2400 grooves/mm. Usually, we use a 64x64 mm plane grating with 1200 grooves per millimeter. Finally, the camera mirror, (M7) projects a flat image onto the focal plane.

The resolution of the spectrometer is determined by the third slit and the last grating, G4 (or G3; G5). Normally, we use the so-call 'resolving power' R to compare different optics instruments. The definition of the R is the following; with two lines of equal intensity of wavelengths λ_1 and $\lambda_2=\lambda_1 + \delta\lambda$, if we can just resolved them by a practical instrument, then we say the 'resolving power' $R=\lambda_1/\delta\lambda$. For an ideal grating with N grooves, R=KN, where the K is the diffraction order number.

Inside a grating monochrometor, the width of the entrance slit W, the focal length f and diameter d of the collimator lens, the diffracting angle θ, all effect the resolving power. Considering all these factors, the R should be as the following equation (S. A.

Chuster, "An introduction to the theory of optics"):

$$R = K \cdot N \cdot \frac{\lambda}{W} \cdot \frac{f}{d} \cdot \frac{1}{\cos\theta}$$

In our Spex' 1877 triplemate spectrometer, the size of G4 grating is 64 mm × 64 mm with 1200 grooves/mm, so N = 76800. We also take f/d =10, λ = 5000 Å, W= 0.1 mm, and $\cos\theta \approx 1$. Then we have R = 3840, and $\delta\lambda$ = 1.25 Å, or $\Delta\lambda$ =5 cm^{-1}. So at λ = 5000 Å, the resolution of this triplemate is about 5 cm^{-1}.

2.2.b. The optical multichannel detector

The theory of operation for both optical multichannel detectors, (from EG&G, Princeton Applied Research and from Princeton Instruments) intensified photodiode arrays (IPDAs), are almost same, as depicted in the figure 2.2.

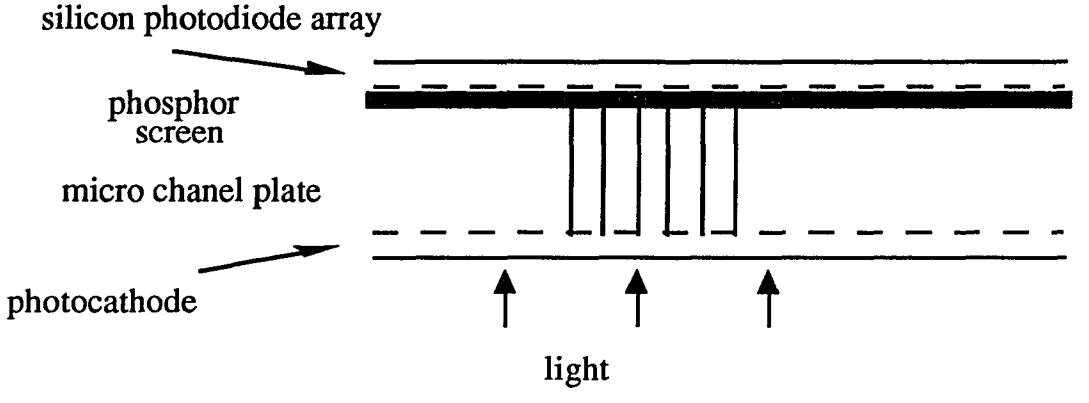

Figure 2.2 A schematic of reticon.

It consists of a microchannel plate (MCP) image intensifier optically coupled to a self-scanned linear Reticon silicon photodiode array

(SPD) as the multichannel readout/storage device.

Operation theory: The MCP image intensifier consists of an input photocathode followed by an MCP wafer which is in turn followed by a phosphor output. Focusing of the photo-electron image produced by the photocathode transducer is achieved by applying a strong electrical-field across the photocathode-to-MCP gap (200μm), i.e., the proximity-focusing method. The MCP is a a disk-shaped continuous-dynode electron multiplier imager. It consists of millions of hollow microchannels formed in a glass substrate, where each channel, which is 12-25μm in diameter, is semi-conducting. Each channel acts as an individual electron multiplier with an absolute geometric registration between the input and output plates of the device. An electrical gain of about 1000 is typical of MCPs.

A self-scanned linear photodiode array is a large integrated circuit fabricated on a single monolithic silicon crystal. It contains a row of photodiode sensors, typically on 25-μm centers, along with a scanning circuitry for sequential readout (figure 2.3.a.). The photodiode geometry is defined by diffused p-type bars in a n-type silicon substrate (figure 2.3b.). The center-to-center distance between the diode defines the resolution in the scan direction. The height of the diode sensing area is determined by an aperture in a metal mask, which runs perpendicular to the p-type bars, typically about 2.5mm. Light incident on the sensing area generates a charge, which is collected and stored on the p-type bars during the integration period. The accumulated charge are then sequentially switched into the video output for readout. The n-type as well as the p-type silicon surface is photosensitive.

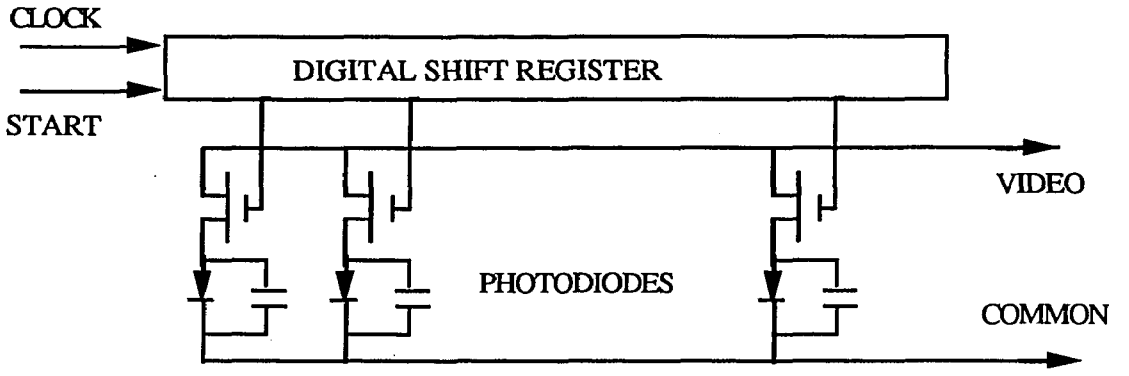

Figure 2.3.a Simplified schematic diagram of typical self-scanned photodiode array.

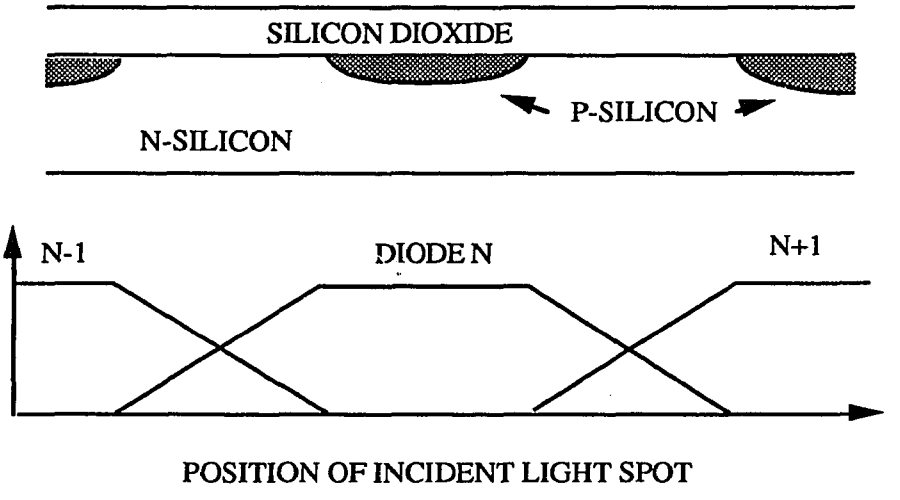

Figure 2.3.b Sensor (diode) geometry and idealized aperture function.

Light incident on one of the p-regions will generate charge, which is stored on that diode. Charge generated by light incident on the n-type surface between two p-regions will divide between the adjacent diodes to produce the idealized response function shown at

the bottom of Fig 2.3b. Included on the silicon chip for readout of the diodes are two arrays of MOSFET multiplex switches, two 256-bit shift registers to drive the switches, and four video output lines.

Typically the 'neighborhood coupling' is only one pixel, so the resolution of the diode array should be equal 3 × 0.025 mm (diode width) × reciprocal linear dispersion (cm^{-1}/mm). For our 0.6m triplemate spectrometer with the 1200 grooves/mm grating at 5000 Å, the dispersion is about 55 cm^{-1}/mm. Thus the resolution we get here is about 4 cm^{-1}. This essential matches the resolution of the triplemate spectrometer, 5 wavenumbers.

2.2.c. Noise of the detector and S/N enhancement

Normally, there are two major kinds of the noise, the random noise and the fixed pattern noise.

Random noise: For a signal which contains n pluses, suppose the probability for our detector to test one single pulse is p, then, the probability of the detector to obtain m pulses for that signal is P(m),

$$P(m) = \binom{n}{m} p^m (1 - p)^n$$

This probability distribution is known as the *binomial distribution.* When the pn and n are large, the above formula can be simplified as:

$$P(m) = \frac{1}{\sqrt{2\pi\sigma}} \exp\left(-\frac{1}{2}\frac{(pn - m)^2}{\sigma^2}\right)$$

where $\sigma = 2\sqrt{np(1-p)}$ is a measure of the width of the distribution. It is so-called *Gaussian distribution* and is shown in figure 2.4. The maximum value of P(m) is at m=np. That means our detector can detect np pulses with the error is $\sqrt{np(1-p)}$. So the signal to noise ratio is $np/\sqrt{np(1-p)}$ or $\sqrt{m/(1-p)}$, so the signal to noise ratio is

proportional to the square root of number of the pulses which the detector can be test. That kind of "square root" noise is the very common case in the electronic equipments.

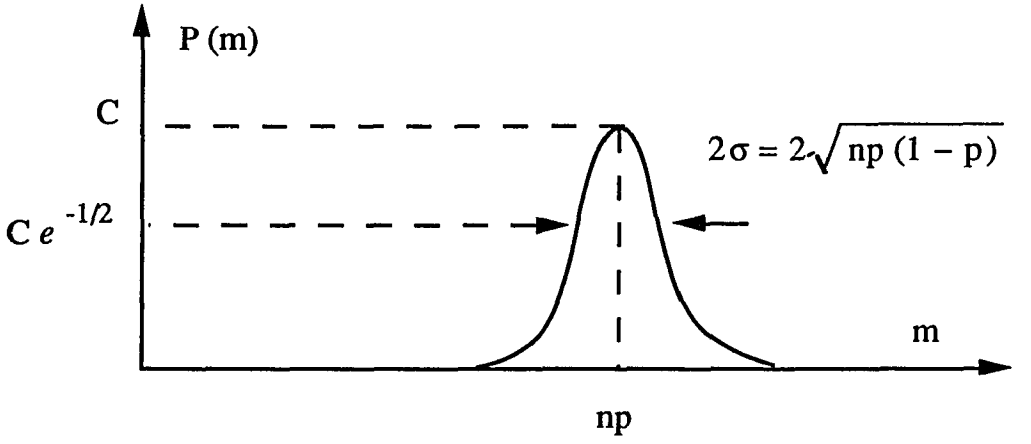

Figure 2.4 A Gaussian distribution. The maximum value of P(m) is at m=np.

Each readout of the diode array generates some 'count' of noise. This result is from a number of sources: dark shot noise, photon shot noise and intensifier noise, resetting noise of the diode array, and the noise due to the preamplifier.

All silicon image detectors are subject to thermally generated dark current and its associated statistical fluctuations (shot noise), square root of the number of electrons in the dark signal charge. The dark current can be reduce significantly by cooling down the diode arrays. In our systems, the thermodiode coupled with tap water are used to cool down the chips to about -20 °C.

The photocathode response is normally in the 10-25% range

over the UV-VIS region. Therefore for lower light input, the shot noise of the input light will be increase a quite bit by the intensifier stage. Combined the preamplifier noise and resting noise of the diode, Simposon (Simposon, 1978) concluded the on-chip integration improves the signal to noise ratio proportionately to the exposure time, while the averaging multiple collections ("on-computer integration") only improves the signal to noise ratio proportionately to the square root of the exposure time. This is very true in our experiment. Since the on-chip integration time is limited by the A/D saturation 16K "count", in our experiment we always try to set the integration time to the maxima, near 16K counts, to get better signal to noise ratio.

Fixed Pattern : Each diode array have a characteristic fixed pattern ("spectrum"). That is caused by stray capacitive coupling of the transients arising from the clock driving signals to video lines by external stray capacitances and by diode-to-diode dark charge variations. The level of this fixed pattern is typically 1%-2% of the full scale range. This kind of the noise can be limited either by subtracting or dividing a good gain collection. In principle, the subtracting and dividing do the same job, actually, because we always have some dark count, so the subtracting should be little bit better. But the subtraction requires the gain collection more critically, and it is not very easy to get a requested good gain collection, so in the experiments, we like use dividing a gain collection to minimized the noise. An example is shown in figure 2.5, where the Raman spectrum of acetonitrile in fluercein (a) and of fluercein alone (b) were measured. While the typical CN stretching

vibration mode of acetonitrile is barely visible in the raw data(a), division(c) and subtraction (d) by the fluorescein spectrum can increases the signal to noise by about 10 fold. Thus, these modes now dominated the spectrum.

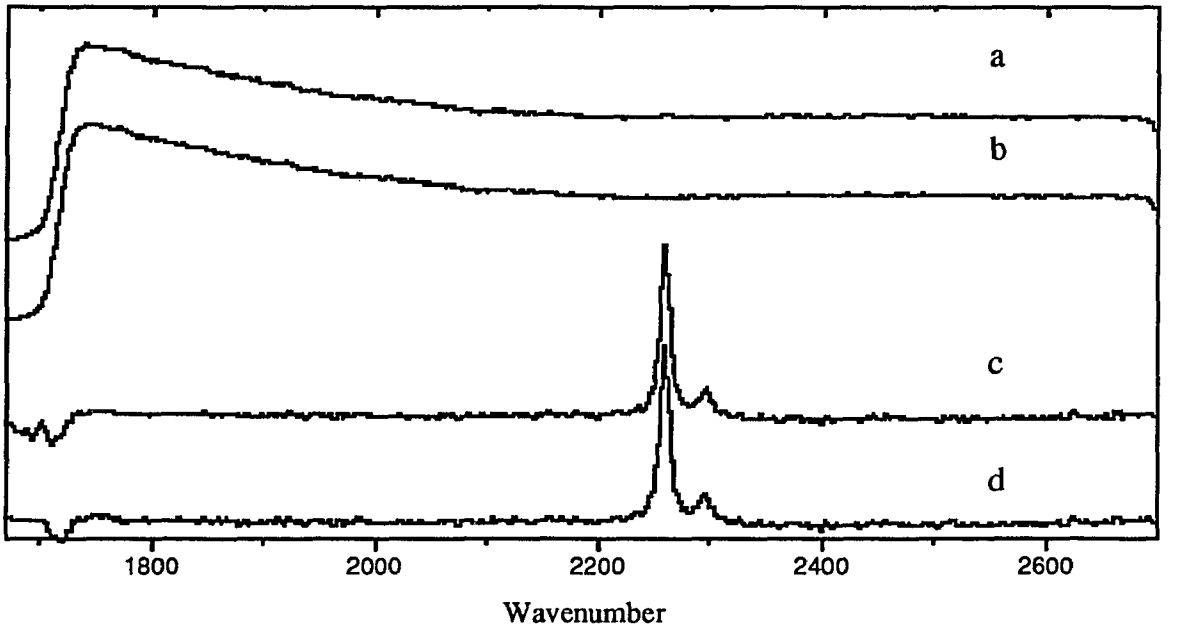

Figure 2.5 By using the substation and division we can improve the signal to noise ratio significantly. (a) the spectrum of 0.5% v/v of acetonitrile in the solution of 0.01 μm of Fluorescein in neutral pH, and (b) is the spectrum of the Fluorescein solution, which is used as gain collection. 200 mW, 514.5 nm laser line was used to probe the sample, and about 20 mins accumulating time for each spectrum. (c) is (a) divided by (b), and (d) is (a) subtracted from (b).

2.3. Difference Raman spectroscopy

Double-beam spectrometers are extensively used in IR, visible, and UV absorption in order to cancel the background absorption by water or solvent. In Raman spectroscopy, we also have the similar problem, in that one may want to remove the solvent's spectra from the samples Raman spectra. In addition, a major part of our work involves obtaining the Raman spectrum of small ligands when bound to various proteins, and comparing it with the spectrum of the ligand "free" in solution. Can we do the some difference procedure as is done in UV-vision abortion?

After using a good gain collection to normalization the spectrum, we are able to obtain a classical Raman spectrum of a protein solution, with a concentration of about 10% by weight, yielding a noise-to-signal ratio of 0.1% within an integration time of about 2 hours using our OMA systems. Hence the determining factor limiting accurate subtractions of two spectra arises from systematic factors.

The most critical factor leading to an inaccurate subtraction of two spectra, say A and B, is that the signal from run A hits the OMA detector with a small displacement with respect to that obtained in run B. The effect is that the two spectra are apparently shifted in frequency, and two identical signals present in two runs do not subtract to zero but yield a 'derivative'-looking difference spectrum. The apparent frequency difference can be very small but still yield a substantial difference intensity as has been noted before. The systematic error can be reduced to an effective shift in frequency between the two samples.

To assess the factor, we shall assume that both runs A and B are applied to an identical sample. Let the signal from A be I(ν) and that from B be I(ν + δ) where δ is the small apparent frequency shift due to effective spectrometer misalignment. For small enough d, we have an apparent difference intensity of

$$\Delta I(\upsilon) = I(\upsilon + \delta) - I(\upsilon) \approx \frac{\partial I(\upsilon)}{\partial \upsilon}\delta$$

We can calculate the magnitude of the maximum in ΔI(δ), which we shall call ΔI_{max} , if we know the lineshape of ΔI(δ). Assuming that the spectrum is Gaussian with intensity at center I(n) and the full width at half-maximum Γ, we find that

$$\frac{\Delta I_{max}}{I(0)} = 1.4\,\frac{\delta}{\Gamma}$$

A Lorentzian line will change the numerical value to 1.9. It is apparent from this equation that the apparent difference signal become very small if the Γ is very large. That is why the method of the difference spectroscopy is widely accepted in UV-Vision absorption spectra studied, since absorption bands are usually very broad. But most the Raman peaks are very sharp, so a small frequency difference will give a significant difference signal.

In order to get a good difference Raman spectrum, we need a very high degree of wavelength accuracy. In scanning spectrometers, like in the double monochromator, the wavelength accuracy is mechanically limited, and it is very hard to get a good difference Raman spectrum. To overcome that problem, Rousseau (Rousseau, 1981) developed a divided rotating cell. In their studies, they put two samples into a divided, rotating cell, and each sample is rotated into the laser interaction area in turn. Gated electronics collect the

two signals, under computer control, which are subsequently subtracted. The spectrometer is maintained at a particular wavelength for a given integration time and the sample cell rotates fairly quickly so that each sample passes through the laser beam many times during the desired integration time. The spectrometer is then stepped to a new wavelength, and the procedure repeated. This scheme minimized systematic factors, spectrometer irreproducibility and wavelength drift, for example, and results in accurate subtractions to the few percent level or better. Very small spectral shifts between the two samples can be detected.

Unlike the scanning spectrometer, the OMA system has excellent wavelength accuracy, making the performance of the difference Raman spectroscopy easier and more reliable. The systematic errors mainly come from vibration and thermal expansion of the optic components, and the stability of the light source. The wavelength accuracy of the OMA system is directly related to geometric (spatial) accuracy of the grating, a spectral-to-spatial transformer.

In our experimental set up, we took several precautions to minimize systematic errors. The entire spectrometer system, including the exciting laser, is mounted on a vibration-free table. Ambient room temperature is controlled to within ± 1.5 °C and relative humidity to within $\pm 3\%$. Sample positioning is another cricial factor. The instruments' response in both signal intensity and wavelength repeatability is sensitive to the optical path of the Raman signal, i.e. the exact geometry of the focused exciting laser beam within the sample and reference cuvettes, and the relative position

of the cuvettes to the spectrometer. It is therefore necessary to alignment the optics path very carefully.

We used the following two procedures which generally minimize the systematic errors arising from sample alignment. One is the use of accurate positioning equipment. The cuvette holder is attached to a translator stage-stepping motor combination (model Unidex XI with ATS302 stages, Aerotech Inc., Pittsburg, PA) so that the sample and reference cell cuvettes can be moved in and out of the Raman exciting laser beam to within ± 0.1 μm. The second procedure is the use of specially fabricated cuvettes. We found that the use of separate sample and reference cuvettes introduced unpredictable and sometime large false differences signals. We believe that this is due to small differences in the width of the cell wall and/or small departures from the square in the nominally rectangular cuvettes from one cell to another. These differences from one cell to another can change the optical path of the exciting Raman signal and modify, slightly, the positioning of the signal incident on the OMA detector. To overcome this, we employ specially fabricated cells whereby a cell divider is inserted into a normal cuvette, which divides the cell into two parts. The two separate samples are placed into the two sides. These cells yield better consistency and some of the best difference spectra in this thesis. Figure 2.6, shows one test experiment, where toluene was loaded into both the A and B side and the difference spectrum was obtained by subtraction of the two spectra, shown in (b). It should be noted that the size of the false signal in the difference spectrum is less than 0.25% of the peak of toluene signal shown in (a).

Finally, we take one more procedure to minimize the systematic error due to the vibration and thermal expansion of the optics components, mostly coming from the last grating in the triplemate. We take A and B's spectra in the interleaved ABABAB..AB fashion. The spectrometer drift will tend to affect the sum of the A measurements in the same way as the sum of the B measurements, and subtract out of the difference provided the drift time is larger than the time used in individual A and B measurements (Chen et al.,1987).

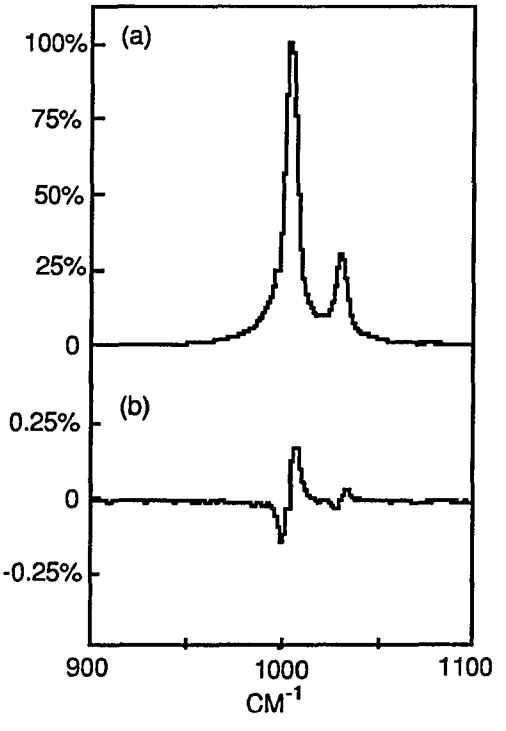

Figure 2.6 (a) the Raman spectrum of toluene in the 900-1000cm^{-1} range and (b) the difference spectrum.

Overall, we are able to obtain a difference Raman spectrum of two protein solutions, with a concentration of about 10% by weight, yielding a noise-to-signal ratio of 0.1% within an integration time of about 2 hours using our OMA systems.

Chapter 3
THE BINDING PROPERTIES OF COENZYMES TO LACTATE DEHYDROGENASE

3.1 Introduction

Recently, in our lab, by using the ultasensitive difference techniques described in chapter, very good classical spectra of substrates bound at the active site of liver alcohol dehydrogenase enzyme were reported (Yue, et al., 1984; Chen et al., 1987). In this chapter we report the Raman spectra of NADH and NAD^+ and fragments of these molecules bound to lactate dehydrogenase, LDH. As shown in the scheme 3.1, this enzyme catalyzes the stereospecific oxidation of *l*-lactate by NAD^+ to pyruvate forming the reduced coenzyme NADH. (Warburg and Christian, 1936; Euler et al., 1936).

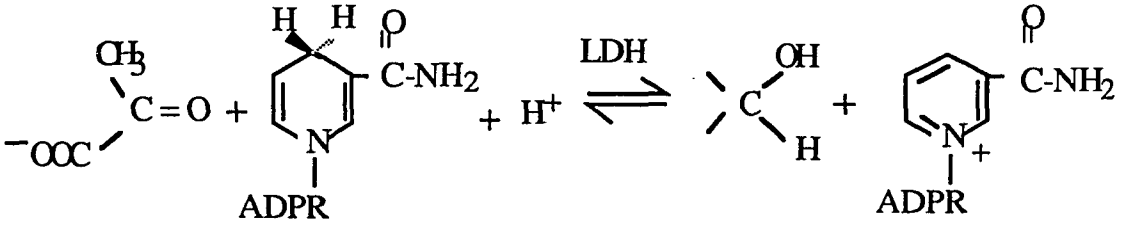

pyruvate NADH lactate NAD^+

Scheme 3.1 The chemical reaction which is catalyzed by LDH

Unlike in LADH, there is no metal ion involved in the catalytic pathway of LDH, and NADH is not as tightly bound to LDH as LADH. A smaller blue shift (< 5 nm) of the NADH absorption band at 340 nm is observed upon binding to LDH compared to that observed for LADH (15 nm) (Fisher et al., 1969). Moderately high resolution crystallographic studies of coenzyme complexes with LDH have been performed (White et al., 1976; Grau et al., 1981) which show similarities to and differences with the coenzyme binding pocket found in LADH (Eklund et al., 1981; 1984; Eklund & Brändèn 1986).

In analyzing the difference spectra, we first compared data obtained from NADH, NAD^+ and a molecular fragment of these coenzymes, ADPR. From these comparisons, we assigned the observed bands to molecular motions located on one or another of the nicotinamide, adenine and phosphate moieties of NADH and NAD^+. We found that pronounced changes in some of these molecular motions accompany the binding of the adenine and reduced nicotinamide moieties when NADH binds, as judged from the dramatic changes that occur in the Raman spectra between that of solution NADH and bound NADH. For instance, strong hydrogen bonding between the C=O and $-NH_2$ moieties of the nicotinamide carboxamide group and the enzyme is observed, and the interaction energies can be estimated from the data. The aromatic nature of the oxidized nicotinamide moiety of NAD^+ is not significantly affected by binding. In addition, the data strongly suggest that the adenine moiety protonates when the coenzymes bind. The spectra of bound NADH and NAD^+ are compared to the analogous spectra obtained in our recent study on LADH. We find that the spectral features of both

the adenine and nicotinamide moieties when NADH binds to either LDH or LADH are very similar, but with interesting differences.

3.2 Materials and Methods

NADH (100%) and NAD^+ (100%) were purchased from Boehringer Mannheim Co. (Indianapolis, IN); ADPR was purchased from Sigma Chemical Co. (St. Louis, MO); and they were used without further purification. Pig H4 LDH was prepared according to the procedure described in Burgner & Ray (Burgner & Ray,1984). Fresh or frozen pig hearts were extracted and the extracts passed through an oxamate-Sepharose affinity column (1×10 cm) according to the procedure of O'Carra & Barry (O'Carra & Barry,1972). The column was washed first with 50 mL of 0.05 M sodium phosphate, pH 7.2, containing 0.5 M NaCl and 0.2 mM NADH and then with 100mL of the same phosphate buffer containing 0.2 mM NADH and 10 mM potassium oxamate. The eluded enzyme was treated with an amount of pyruvate equivalent to twice the NADH present, rapidly diluted 3-fold, and immediately placed on a (Whatman) DE-52 column, 5×10 cm, which had been equilibrated with 0.05 sodium phosphate, pH7.2. After the column was washed with 100 mL more of the equilibrium buffer, the enzyme was eluded with a gradient of 0-0.3 M NaCl in 0.5 M sodium phosphate, pH 7.2. The enzyme was precipitated with $(NH_4)_2SO_2$ (2.6 M) for storage (at 4 °C).

Before Raman experiments, the LDH suspension was centrifuged at 4 °C at 6000×g for 20 minutes to collect the crystals. The pellet was redissolved in the 0.1 M potassium phosphate buffer pH7.2, then it was dialyzed against 0.1 M phosphate buffer at pH 7.2 and 4 °C for several hours. After removing insoluable protein by centrifugation, the enzyme solution was concentrated to about 1 mM, corresponding to a binding site concentration of 4 mM, using a

centricon centrifuge concentrator (Amicon, Lexington, MA). The enzyme activity was measured before and after each Raman experiment; no significant activity loss was detected. Concentrations of enzyme and coenzymes were determined by UV-Vis absorption spectroscopy, using ε_{280}=200000 $M^{-1}cm^{-1}$ for LDH, ε_{340}=6220 $M^{-1}cm^{-1}$ for NADH, ε_{259}=18000 $M^{-1}cm^{-1}$ for NAD^+, and ε_{259}=15200 $M^{-1}cm^{-1}$ for ADPR. Since LDH contains four independent active sites, binary complexes of LDH were prepared by mixing a 1:<4 molar ratio of LDH to NADH, NAD^+ or ADPR. Since the concentration of the enzyme is significantly larger than the dissociation constants for each of the coenzymes and analogs used here (Stinson and Holbrook, 1973), typically better than 90% of the coenzymes (or analogs) were bound.

Raman spectra were measured using an optical multichannel analyzer (OMA) system, which we described in the chapter 2. Typically, 200 mW of 488 nm line from an argon laser was used to excite Raman scattering. Under these conditions, about 800 cm^{-1} can be detected simultaneously. The instrument was calibrated against known assignments of the toluene spectrum. Band positions are accurate to 2 cm^{-1}, and the slits were set to achieve a resolution of 8 cm^{-1}. None of the spectra presented here have been smoothed.

3.3 Results

Spectra: Figure 3.1 shows the Raman spectrum of LDH and its binary complex with NADH. Most of the Raman scattering of the binary complex is due to the enzyme, although a shoulder is clearly observed near 1680 cm^{-1} in the binary complex spectrum which is not seen in the LDH data. While the Raman spectrum of LDH is not analyzed in detail here, it is worth noting some of its most prominent features (see, eg., Carey, 1982, for a discussion of protein bands). The strong broad protein band near 1660 cm^{-1} is the amide I band which arises from polypeptide backbone amide C=0 stretching motions. The frequency of an amide I mode is dependent on hydrogen bonding environment, and hence protein secondary structure. For example, a frequency near 1650 cm^{-1} is suggestive of the relatively strong hydrogen bonding environment found in α-helical structure, while frequencies near 1670 and 1665 cm^{-1} are typically found in antiparallel β-pleated sheet and disordered structures. The amide III region, also sensitive to secondary structure, lies from 1230-1300 cm^{-1} and is due to polypeptide backbone N-H in-plane bending and C-N stretching motions. The bands at 1340 cm^{-1} and 1450 cm^{-1} are the γ-CH_2 and δ-CH_2 bands respectively. These vibrations are relatively insensitive to the secondary structure of the protein.

Using previously described procedures (see chapter 2), we calculated the difference spectrum, shown in figure 3.2.a, between the LDH/NADH binary complex and LDH (figures 3.1.a and 3.1.b respectively). As we noted above, the band intensities of the Raman spectrum of NADH are about 3-10% that of LDH. All the labelled

peaks in figure 3.2a have been consistently observed in at least ten different experiments. For comparison, the difference spectrum between the binary complex of liver alcohol dehydrogenase (LADH) with NADH and LADH (from Chen et al., 1987) is shown in figure 3.2.b, and the spectrum of NADH in solution (from Yue et al., 1986) is shown in figure 3.2.c.

Bands observed in the difference spectra may arise from any of a number of differences between the protein binary complex and the protein itself. The most significance differences are caused by the presence of the bound coenzyme. We found previously (Yue et al., 1986) that the classical Raman bands of NADH (or NAD^+) arise from molecular motions generally located on smaller moieties of the larger molecule. Peaks may be labelled as either adenine (A), nicotinamide (N), ribose (R), phosphate (P), or pyrophosphate (PP). We have so labelled all the peaks in the NADH data of figure 3.2.c in this way. In some cases, a band is found to be largely located on a particular moiety but its position and/or strength is somewhat dependent on a connecting group. Some of the peaks of adenine are influenced by ribose binding to form adenosine, for example. We use the nomenclature A/δR to identify such peaks. Other peaks are strongly associated with two moieties, and these are labelled like A/R. In some cases an observed band contains contributions from two normal modes. The peak at 1422 cm^{-1} in figure 3.2.c is an example of the sum of two bands, one located on the nicotinamide head group (responsible for about 90% of the total intensity) and the other on adenine (the remaining 10%). We have labelled this peak by (N,A) to denote this degeneracy and similarly for the other degenerate bands.

Bands in the difference spectra can also arise from changes in the secondary structure of the protein that occur when the coenzyme binds. As we have pointed out above, the positions of some protein bands are sensitive to secondary structure; and LDH undergoes a conformational change when NADH binds (Holbrook et al., 1975). Another possibility that may result in the observation of a peak in the difference spectrum is when an interaction between NADH and surrounding protein moiety significantly affects a mode of the protein moiety. In these latter cases, a trough of intensity in the difference spectrum, corresponding to the unperturbed position of the Raman active band, would be observed along with a concomitant increase in intensity at the perturbed position.

In our previous work on NADH and complexes of NADH with LADH (Yue et al., 1986; Chen et al., 1987), we found that the peaks observed in the difference spectrum between LADH/NADH and LADH in figure 3.2.b arose from bound NADH, and could be assigned to NADH moieties as is the case for the solution spectrum of NADH in figure 3.2.c. We have labelled the peaks in figure 3.2.b based on these results. We observed no major bands which might arise from the protein conformational change which occurs when NADH binds to LADH or from perturbed protein modes. The assignments were based on the observations that most prominent features observed in figure 3.2.b were positive peaks and could be associated often with features found in the NADH spectrum in solution (figure 3.2.c). Moreover, the corresponding peaks to those in figure 3.2.b due to the adenine moiety were conserved in the bound ADPR spectrum (see figure 3.4.b). ADPR binding, unlike NADH binding, does not induce a

conformational change when it binds to LADH (Eklund et al., 1984). Thus, the LADH/ADPR-LADH difference spectrum can not contain bands due to a protein conformational change. Since no band disappeared in the bound ADPR spectrum relative to the bound NADH spectrum (apart from bands which could be clearly identified as nicotinamide), none of the bands in the bound NADH spectrum can arise from the conformational change.

Using a similar analysis, presented below, we find that some of the bands in the LDH/NADH with LDH difference spectrum in figure 3.2.a contain features due to the protein conformational change which accompanies NADH binding to LDH. We labelled such peaks as Pr (for protein). As indicated above, it is also possible that the binding of NADH disrupts and/or forms strong interactions with protein moieties surrounding the bound NADH molecule, and some of the bands in figure 3.2.a may arise from motions located primarily on one or another of these protein moieties. However, we have not identified, conclusively, any bands which can be identified as such peaks, but a few peaks could not be assigned as either coenzyme peaks or bands arising from protein structural changes either.

From figures 3.2.a and 3.2.c, it is evident that the Raman spectrum of NADH bound to LDH differs markedly from the solution NADH spectrum. The binding of the nicotinamide moiety is clearly accompanied by the disappearance of the intense 1546 cm^{-1} band and an intensity decrease or disappearance in the 1458 cm^{-1} band found in the solution spectrum. The peak at 1084 cm^{-1} found in the solution spectrum consists of two bands, one arising from phosphate (ca. 30 % of the intensity) and one arising from the rocking motion of

the nicotinamide $-NH_2$ moiety (ca. 70 % of the intensity) (Yue et al., 1986). When the coenzyme binds to either LDH or LADH, there is a substantial loss in relative intensity at 1084 cm^{-1} and a concomitant increase in intensity at 1114 cm^{-1} which arises from the nicotinamide head group (see below). Thus, the rocking frequency of the nicotinamide $-NH_2$ moiety appears to move from 1084 cm^{-1} in solution to 1114 cm^{-1} when bound to the coenzyme binding pocket. Also the major nicotinamide band at 1688 cm^{-1} found in the solution spectrum is downshifted by 3 cm^{-1} to 1685 cm^{-1} when NADH binds to LDH. The binding of the adenine moiety is indicated by a number of very pronounced changes as well; these are more clearly seen in the spectrum of bound ADPR given below.

While there are pronounced changes in the Raman spectrum of nicotinamide when NADH binds to LDH, the observed nicotinamide bands are very much the same for NADH bound to either LDH or LADH as can be seen by comparing figures 3.2.a with 3.2.b. There are, however, some differences. The major nicotinamide band lies at 1688 cm^{-1} (figure 3.2.c) in the solution spectrum, at 1685 cm^{-1} for NADH (in LDH), and at 1681 cm^{-1} for NADH (in LADH). The exact assignment of this mode is unclear at the present time, but it very likely contains major contributions from C=O and C=C stretching motions (Bowman and Spiro, 1980; Rodgers and Peticolas, 1980; Chen et al., 1987; Bajdor et al., 1987). It is thus reasonable to suppose that differences in the position of this dominant mode can be correlated with the λ_{max} of the near UV $\pi\pi^*$ absorption band of NADH. In solution, this band is found at 340 nm, blue shifting to ~335 and 325 nm when NADH binds to LDH and LADH respectively (Fisher et al.,

1969). The intensity of the nicotinamide 1415 cm^{-1} band found in NADH (in LADH) (figure 3.2.b) appears to be reduced somewhat in NADH (in LDH) (figure 3.2.a), apparently concomitant with the formation of a shoulder at 1408 cm^{-1}. It is reasonable to suppose that the observed 1415 cm^{-1} band found in the NADH (in LADH) spectrum contains intensity from two degenerate normal modes; this degeneracy appears to be somewhat lifted when NADH binds to LDH. The 1600 cm^{-1} feature found in the NADH (in LADH) (figure 3.2.b) is not observed in the NADH (in LDH) spectrum (figure 3.2.a); likewise, there appears somewhat more intensity at 1577 cm^{-1} in the NADH (in LDH) spectrum as compared to the NADH (in LADH) spectrum due to nicotinamide.

Figure 3.3.a shows the difference spectrum of LDH/NAD^+ with LDH. The spectrum of NAD^+ in solution is shown in figure 3.3.b. The nicotinamide moiety of NAD^+ shows very few Raman active bands, as is clear from the solution data. The main nicotinamide peak at 1033 cm^{-1} is unaffected when NAD^+ binds to LDH.

Figure 3.4 shows the LDH/ADPR difference spectrum with LDH (figure 3.4.a) and, for comparison purposes, the analogous difference spectrum of ADPR bound to LADH (figure 3.4.b) and the Raman spectrum of ADPR in solution (figure 3.4.c). This bound ADPR spectrum is of interest for two reasons. First, it is very useful in assigning the bands to particular moieties since ADPR lacks the nicotinamide moiety of NADH but induces the same conformational change in LDH upon binding as does NADH (Grau et al., 1981). Secondly, the bands arising from adenine and other moieties are

more easily observed as the more intense nicotinamide bands are absent.

There are clearly a number of very pronounced changes in the spectrum of adenine when it binds to either LDH or LADH. The intense adenine solution band at 1338 cm^{-1} is absent in the bound data, and several new bands, the 1325 cm^{-1} band for example, appear in the bound spectra. In general, the spectra of bound ADPR in LDH and in LADH closely resemble each other with, however, important differences. For example, the band at 1245 cm^{-1} in ADPR (in LADH) (figure 3.4.b) appears to have moved to 1220 cm^{-1} in the ADPR (in LDH) spectrum (figure 3.4.a). Also new bands at 1290, 1606, and 1625 cm^{-1} appear in the ADPR (in LDH) spectrum compared to the ADPR (in LADH) spectrum. We have consistently observed a somewhat smaller intensity of the 1309 cm^{-1} peak relative to other nearby bands in the spectrum of ADPR bound to LDH compared to the apparently similar, but relatively more intense, band at 1303 cm^{-1} in the ADPR (in LADH) spectrum.

As discussed below, the adenine binding pocket in LDH and LADH is largely hydrophobic. In order to test whether or not the change from a hydrophilic to a hydrophobic environment is responsible for the rather dramatic changes in the Raman spectrum of the adenine moiety of the coenzymes upon binding to either LDH or LADH, we measured the Raman spectrum of 9-ethyladenine in various solvents including H_2O, propanol, chloroform, methyl cellosolve and para-dioxane. The Raman spectrum of 9-ethyladenine is quite close to adenosine and serves as a reasonable model compound for the adenosine moiety of NADH, NAD^+, etc (Yue et al.,

1986). The Raman spectra of 9-ethyladenine in all these solvents are very similar to each other. Relative to the H_2O spectrum, the spectrum of 9-ethyladenine in chloroform is found to be the most changed. In figure 3.5, we show the Raman spectra of 9-ethyladenine in water and in chloroform. As can be seen, there are very few differences between these two spectra. Hence, the change from a hydrophilic to a hydrophobic environment is quite unlikely to be responsible for the Raman spectral changes which accompany binding of the adenine moiety to either LDH or LADH.

Band Assignments: The assignment of a band to a particular moiety of NADH or NAD^+, a protein conformational change, or to a protein residue perturbed upon coenzyme binding is accomplished as follows. Nicotinamide bands are easily assigned by comparing the bound NADH, NAD^+, and ADPR spectra. X-ray crystallographic studies suggest that the protein structure is nearly the same for binary complexes of these three molecules with LDH (Chandrasekhar et al., 1973; Grau et al., 1981). The Raman spectra of oxidized and reduced nicotinamide differ markedly because of their very different electronic structure (Yue et al., 1986; see figures 3.2.c and 3.3.c), and ADPR lacks the nicotinamide head group. Thus, bands which vary amongst the three bound spectra are safely assigned to the nicotinamide moiety. We note one assignment in particular and that concerns the band at 1113 cm^{-1} in the NADH (in LDH) and the NADH (in LADH) spectra of figure 3.2.a and 3.2.b. The relative intensity of this band is clearly higher than found in the NADH solution spectrum (figure 3.2.c) or the bound and solution spectra of NAD^+ (figure 3.3). This can be seen by comparing the band intensities at 1084 cm^{-1}

and 1113 cm^{-1}. The 1084 cm^{-1} band arises from a phosphate mode, and the 1113 cm^{-1} band arises from a ribose-pyrophosphate mode. In addition, the rather broad peak at 1084 cm^{-1} in the NADH solution spectrum (figure 3.2.c) contains intensity arising from the nicotinamide $-NH_2$ rocking mode (Bowman and Spiro, 1980; Rodgers and Peticolas, 1980; Yue et al., 1986). The contribution of the $-NH_2$ rocking mode to signals at 1084 cm^{-1} disappears when NADH binds to LDH or LADH. The frequency of the $-NH_2$ rocking mode seems to have moved to 1113 cm^{-1} from 1084 cm^{-1} upon NADH binding. Corroborating this assignment is the observation that most of the intensity at 1113 cm^{-1} disappears in the NADH(in LDH) (data not shown) and in the NADH(in LADH) (Chen et al., 1987) spectra for samples suspended in D_2O, which deuteriates the $-NH_2$ hydrogens, as occurs at 1084 cm^{-1} for NADH in D_2O (Bowman and Spiro, 1980; Rodgers and Peticolas, 1980; Yue et al., 1986).

Having identified the nicotinamide bands, most of the remaining bands can be assigned by a close correspondence to a peak in the solution spectra of NADH, NAD^+, and/or ADPR or to a peak found in the spectrum of ADPR bound to LADH; the peaks in these spectra have been assigned previously (Yue et al., 1986: Chen et al., 1987). Thus in the bound ADPR data of figure 3.4.a, the 1309, 1324, 1340, 1375, 1421, 1481 1510, 1576 cm^{-1} are adenine related peaks, the the 1085 cm^{-1} peak is a phosphate mode, and the 1113 cm^{-1} peak is assigned to a ribose-pyrophosphate mode. The 1220 cm^{-1} peak in figure 3.4.a has the same relative intensity as the 1245 cm^{-1} peak found in the ADPR bound to LADH spectrum (figure 3.4.b) and the 1254 cm^{-1} band in the solution spectrum of ADPR (figure 3.4.c).

In the latter two cases, this band has been assigned to adenine, and we tentatively assign the 1220 cm^{-1} band in figure 3.4.a to adenine. We generally do not have sufficient data to label an adenine peak, for example, as having a small contribution from the bound ribose, a A/δR peak, in the bound spectra as we do in the case of solution spectra. Thus the adenine labelled peaks may or may not also contain a contribution from molecular motions of the bonded ribose. We have consistently observed a peak at 1670 cm^{-1} in the bound NAD^+ spectrum data of figure 3.3.a. We also appear to observe an intensity trough at 1650 cm^{-1}. For this reason and because NAD^+ has no bands in this frequency region while this is the Amide I region (see figure 3.1), we tentatively assign the 1670 cm^{-1} peak and the 1650 cm^{-1} trough to changes in the Amide I protein bands which accompany the binding of NAD^+. As mentioned above, the Amide I bands are sensitive to protein conformational changes. We have labelled these bands as (Pr) peaks for this reason. A similar pattern is observed in the NADH (in LDH) spectrum of figure 3.2.a. There are several peaks that we are currently unable to assign, and they have been labelled with a "?" mark.

3.3 Discussion

Adenine Binding. Our Raman results on the adenine moiety indicates that substantial molecular changes accompany its binding to LDH. The Raman spectrum of bound adenine differs markedly with that of adenine in solution. The strong 1338 cm^{-1} solution band disappears upon binding and is replaced by bands at 1325 and 1340 cm^{-1}. Also, the intensity of the 1308 and 1378 cm^{-1} solution bands seem to change upon binding, and the solution 1254 cm^{-1} band either disappears or, as we have tentatively suggested above, moves to 1220 cm^{-1} when the adenine moiety binds to LDH. There are also several bands in the spectrum of bound ADPR (figure 3.4.a), which we are unable to assign specifically to adenine and which may be protein bands (see above); but it is equally likely that one or more of these bands may be new adenine bands not found in the solution spectrum.

While the Raman spectrum of adenine bound to LDH differs considerably with its solution spectrum, its spectrum is quite similar to that of adenine bound to LADH. There are, however, differences; and these can be seen by comparing the ADPR data in figure 3.4.a and 3.4.b. For instance, the band at 1309 cm^{-1} in the LDH data (figure 3.4.a) probably has the same origins as the peak at 1303 cm^{-1} in the LADH data (figure 3.4.b). However, the 1303 cm^{-1} peak is not only slightly shifted but has somewhat higher relative intensity to that at 1309 cm^{-1}. The 1254 cm^{-1} peak found in the solution data (figure 3.4.c) appears to be found at 1245 cm^{-1} in LADH spectrum (figure 3.4.b) and at 1220 cm^{-1} in the LDH spectrum (see Results). The 1471 cm^{-1} peak, an adenine band, found in the

ADPR(in LADH) spectrum shifts to 1481 cm^{-1} in the ADPR (in LDH) spectrum. Also, one or more of the 1290, 1606, 1625, and 1668 cm^{-1} bands found in the spectrum of ADPR (in LDH) may be associated with adenine, and there is no corresponding band in the ADPR (in LADH) spectrum.

The environments of the adenine moiety of NADH and NAD^+ bound to LDH (Grau et al., 1981) and to LADH (Eklund et al., 1984) have been determined by X-ray diffraction to moderate resolution. The adenine binding pocket is very similar for both enzymes, the site being generally hydrophobic in both cases. However, a strongly conserved residue among dehydrogenases in the adenosine binding site is an aspartate, Asp-223 in LADH and Asp-53 in LDH. In the binary complex, tis Asp is buried in a hydrophobic environment and does mot form an ion pair with any enzyme residue. However, it does interact with the coenzyme. One of the side chain oxygens of the Asp forms a hydrogen bond with the 2'-oxygen atom of the NAD^+ or NADH adenosine ribose in the crystal structure of both LADH and LDH. The other Asp oxygen is close to adenine's N3, being 3.9 Å away in LADH and 3.3 Å away in LDH. In LADH, another polar group, Arg-271 (which forms an ion pair with Asp-273), is also near the adenine ring. The adenine binding site is close to the protein surface with adenine's $-NH_2$ moiety at the boundary. The adenine ring is somewhat more buried in LADH than LDH. For example, the calculated (Eklund & Brändèn, 1986) solvent accessibility of N6 (the $-NH_2$ moiety nitrogen) is 14 and 30 $Å^2$ in LADH and LDH respectively compared to its solution value of 55 $Å^2$ (Bajdor, et al.

1987). On the other hand, only N1, N6, N7, and C8 are accessible to solvent to any degree in both enzymes.

The changes in the Raman spectrum of adenine when NADH or NAD^+ binds to either LDH or LADH are difficult to explain based solely on a change from a hydrophilic to a hydrophobic environment. Experiments on 9-ethyladenine, which is a structural analog of adenosine and has a Raman spectrum very close to adenosine (Yue et al., 1986), shows an almost identical Raman spectrum in water and in chloroform (figure 3.5) and in a variety of other solvents (see Results). Moreover, It have been shown previously that there is no change in the Raman spectrum of ADPR under high salt conditions (4 M NaCl) or in 50% tert-butyl alcohol-water solutions (Chen et al., 1987). As the polar group of Arg-271 found in the LADH adenine binding site is not conserved in LDH, this arginine can not be an essential factor in the normal mode pattern of adenine bound to LADH since the spectrum of LADH-bound adenine is very close to that of LDH-bound adenine.

A plausible explanation of the pronounced changes in the adenine spectrum when it binds, in view of the above, is that the adenine ring protonates and forms an ion pair with the carboxylate of Asp-53 in LDH and Asp-223 in LADH. Protonation of the adenine was first proposed by Fisher (Fisher et al., 1967) to explain changes in adenine's 260-nm absorption band upon binding (Bajdor, et al. 1987), which are very similar, but not identical, to those found when adenine in solution is titrated to low pH. We have found that major changes in the Raman spectrum of adenine bands (in e.g. ADPR), particularly in the 1300-1400 cm^{-1} region, accompany protonation

of adenine in solution (Yue et al., 1986), and these changes show a major isotope effect when experiments are performed in D_2O. While the observed spectral changes upon protonation of adenine in solution are qualitively the same as those found when the adenine ring (in NADH, NAD^+, or ADPR) binds to either LDH or LADH, the specific patterns are distinctly different. Thus, the results indicate that the adenine tautomer found in the coenzyme cleft would not be the same as that for adenine in solution at low pH, under protonating conditions. It seems quite reasonable to suppose, because of the close distances involved, that the dehydrogenases' site conserved aspartate donates a proton to adenine's N3 and forms a stable salt bridge. There is just about the correct distance (see above) to place a H^+ ion between Asp (COO^-) and adenine N3 as determined from the X-ray crystallographic data. In solution, adenine's N1 nitrogen protonates with a $pK_a \approx 3.9$ (Moore & Underwood, 1969). Unfortunately, studies of bound NADH and ADPR in deuteriated samples are unable to confirm or exclude whether adenine is protonated when it binds. In both LADH (Chen et al., 1987) and in LDH (results unshown), the Raman spectra of deuteriated samples contain the strong 1338 cm^{-1} band found in adenine solution spectra. This represents a large isotopically induced spectral change upon deuteriation as would be expected. However, the data can be interpreted as resulting from a loosely bound, or solvent accessible unprotonated adenine ring in deuteriated samples compared to more tightly bound, solvent restricted bound ring in protonated samples (Chen et al., 1987).

Although unlikely in view of the pronounced changes that take place in adenine's vibrational spectrum when it binds to enzyme and the small changes that take place in different solvent types, it is also possible that the adenine group forms a very strong hydrogen bond in the binding site, sufficiently strong to cause the spectral changes. The pK_a's of the Asp groups mentioned above could shift substantially upward with the acid forming a strong hydrogen bond with N3 of the adenine ring. Alternatively, it is also possible that the solution structure of the protein relaxes sufficiently enough to accommodate a water molecule between adenine's N3 and the Asp, and this water molecule forms a strong hydrogen bond.

Nicotinamide Binding. The spectrum of NAD^+ contains few bands assigned to the nicotinamide moiety. The dominant 1033 cm^{-1} band is unchanged when NAD^+ binds to LDH (figure 3.3), and such a sharp band near 1000 cm^{-1} is characteristic of aromatic rings. For example, benzene's spectrum contains an intense band near 991 cm^{-1}, which has been assigned to a ring breathing mode. N-methylated pyridine, the simplest analog for oxidized nicotinamide, also has an intense band at 1029 cm^{-1} (Chen et al., 1987). Thus, the aromatic nature of the nicotinamide moiety of NAD^+ apparently is unchanged upon binding.

On the basis of X-ray structural determinations, strong hydrogen bonding between the apo-protein and the nicotinamide carboxamide moiety has been proposed for binary and ternary complexes of LDH and LADH. We are able now to observed these interactions directly. For instance, the weak broad peak at 1700 cm^{-1} found in the solution spectrum of NAD^+ is probably due to the

stretching motion of the amide C=O group of NAD^+ (Yue et al., 1986), and it is reasonable to suppose that the 1691 cm^{-1} band found in the bound spectrum is also the C=O stretching mode because of its high frequency (figure 3.3). The band is likely to sharpen when NAD^+ binds to the enzyme because of the more homogeneous bonding pattern found in the protein active site relative to that found in solution. An about 10 cm^{-1} shift in the frequency, between the bound and unbound amide C=O stretching motion resulting from different hydrogen bonding patterns is very reasonable. We will discuss this more detail in the next chapter, chapter 4. In addition, we have also shown in the Results section that the amide $-NH_2$ rocking mode, found at 1084 cm^{-1} in solution, shifts to 1114 cm^{-1} when NADH binds to LDH or LADH. This 30 cm^{-1} increase in frequency is in the correct direction for an increased hydrogen bonding interaction at the coenzyme binding pocket relative to solution interactions. An increased and/or more directional electrostatic interaction between the $-NH_2$ moiety and the apo-enzyme found at the coenzyme binding pocket compared to that found in solution would be expected to increase the frequency of the rocking motion. By study the steroreaction of LDH, LaReau (LaReau, 1990) point out that there is about 2.2 kcal/mol hydrogen bonding interaction between the protein and the $-NH_2$ group. We feel that the 30 cm^{-1} change in the rocking mode frequency just corresponds this interaction.

Upon binding to either LDH or LADH, the Raman spectrum of the reduced nicotinamide moiety of NADH shows some very interesting changes (figure 3.2). We have already discussed that the

shift in frequency of the NADH solution 1688 cm^{-1} band to 1685 cm^{-1} for NADH (in LDH) to 1681 cm^{-1} for NADH (in LADH) and correlated these changes to λ_{max} in Results. The largest change in the NADH spectrum is the disappearance of the solution spectrum's 1546 cm^{-1} band (figure 2.2.c) upon binding. This occurs in both the LDH spectrum and the LADH spectrum. It has been suggested (Bowman & Spiro, 1980) that the 1616 cm^{-1} and 1546 cm^{-1} bands are the in-phase and out-of-phase C=C stretches, respectively, of the reduced nicotinamide moiety by analogy with 1,4-cyclohexdiene bands at 1639 and 1680 cm^{-1} (Stidham, 1965; Bajdor et al., 1987). The lowered frequencies could be due to conjugation and coupling to the carboxamide C=O bond. The 1546 cm^{-1} band is upshifted somewhat upon deuteriation of the amide's protons (Yue et al., 1986).

It is difficult to rationalize how the 1546 cm^{-1} band could disappear upon NADH binding. Bowman & Spiro (Bowman & Spiro, 1980) speculate that the large relative intensity of this mode compared to the 1616 cm^{-1} band could result from the specific nature and direction of the transition dipole moment of NADH's 340 nm absorption band. This near UV $\pi\pi^*$ band likely extends from the reduced ring moiety to the carboxamide group. As we have seen above, the carboxamide moiety is strongly hydrogen bonded to the enzyme active site, and these interactions together with others 'fix' the orientation of the nicotinamide ring with respect to the carboxamide group. It is conceivable that a rotation about the ring-carboxamide bond could modulate the intensity of the out-of-phase 1546 cm^{-1} band by varying the relative direction of

the ring and carboxamide transition dipole moments which together sum coherently to form the total transition dipole moment. Thus, the particular orientation of this angle found at the active site could result in a marked decrease in the intensity of the 1546 cm^{-1} band. It is clear that studies of isotopically labelled nicotinamide compounds coupled with theoretical studies estimating the intensities of the observed coenzymes bands are needed so that accurate assignment of the modes and their strengths may be made.

Figure 3.1: Raman spectra of (a) LDH/NADH (LDH:NADH=1:2.5 mM) binary complex and (b) LDH, at 4 °C in 0.1 M phosphate buffer, pH 7.2.

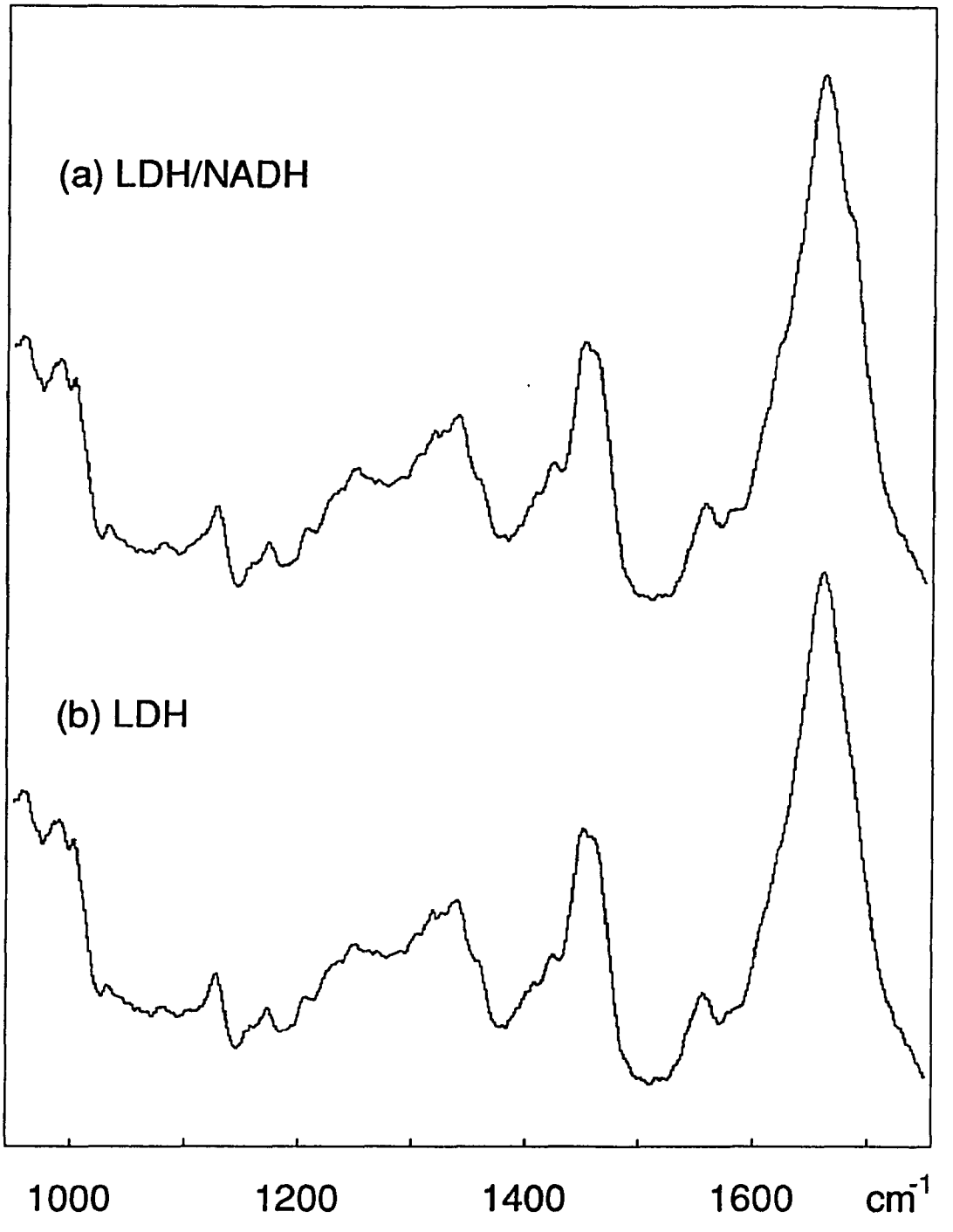

Figure 3.1

Figure 3.2: Raman spectra of (a) bound NADH in LDH (LDH:NADH=1:2.5 mM) at 4 °C in 0.1 M phosphate buffer, pH 7.2, (b) bound NADH in LADH (LADH:NADH=1:2 mM) at 4 °C in 0.1 M pyrophosphate buffer, pH 9.6, and (c) NADH in solution (70 mM) at 4 °C in 0.1 M phosphate buffer, pH 7.2. Assignments of the solution peaks in (c) are from Yue (Yue et al.,1986); assignments of the bound NADH peaks in LADH (b) are from (Chen et al., 1987); see text for the assignments of the bound NADH peaks in LDH (a): A=adenine; N=nicotinamide; P=phosphate; Pr=protein; PP=pyrophosphate; R(δR)=ribose; S=solvent; ?=unknown.

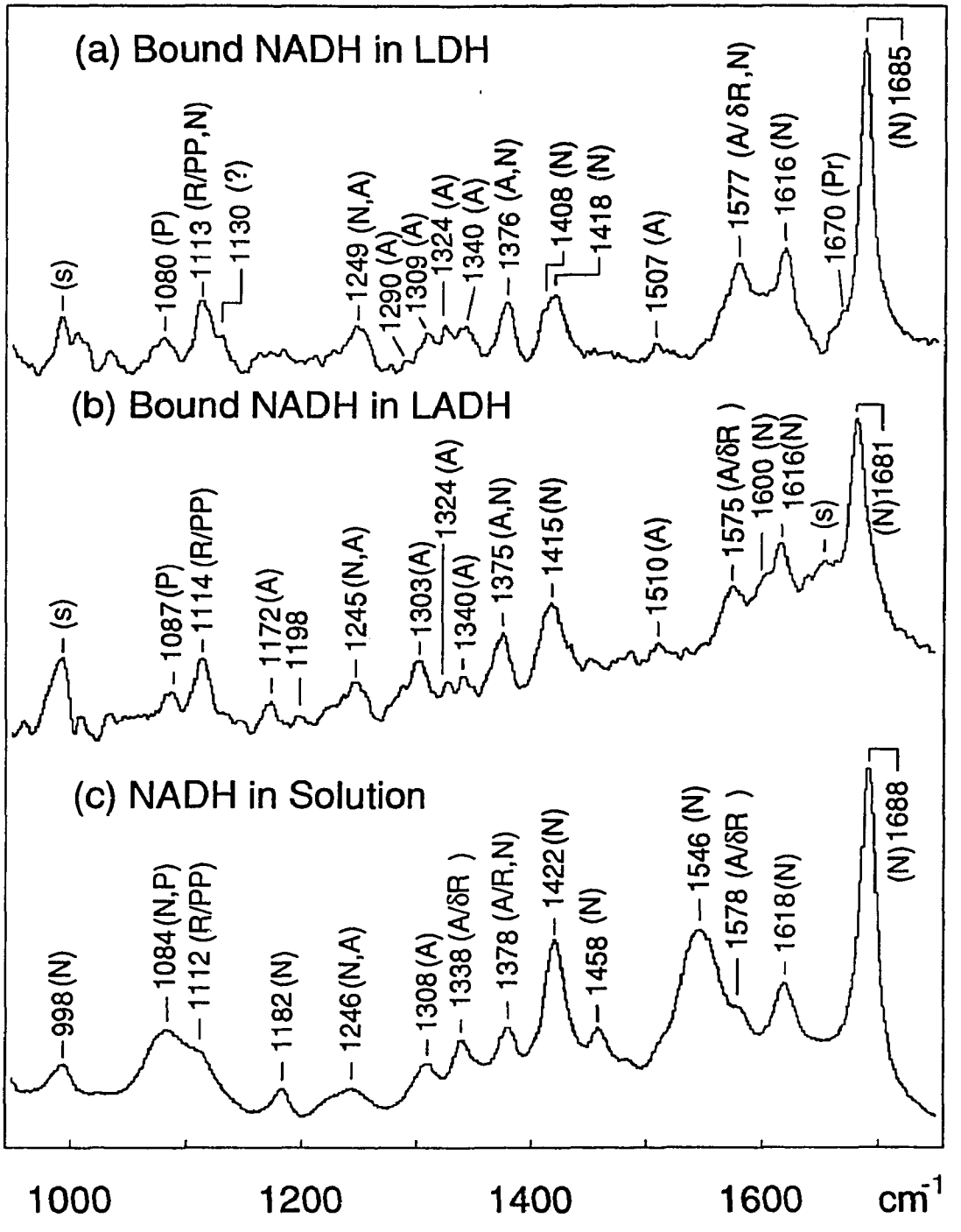
(a) Bound NADH in LDH
(s)
1080 (P)
1113 (R/PP,N)
1130 (?)
1249 (N,A)
1290 (A)
1309 (A)
1324 (A)
1340 (A)
1376 (A,N)
1408 (N)
1418 (N)
1507 (A)
1577 (A/δR,N)
1616 (N)
1670 (Pr)
(N) 1685
(b) Bound NADH in LADH
(s)
1087 (P)
1114 (R/PP)
1172 (A)
1198
1245 (N,A)
1303 (A)
1324 (A)
1340 (A)
1375 (A,N)
1415 (N)
1510 (A)
1575 (A/δR)
1600 (N)
1616 (N)
(s)
(N) 1681
(c) NADH in Solution
998 (N)
1084 (N,P)
1112 (R/PP)
1182 (N)
1246 (N,A)
1308 (A)
1338 (A/δR)
1378 (A/R,N)
1422 (N)
1458 (N)
1546 (N)
1578 (A/δR)
1618 (N)
(N) 1688
1000
1200
1400
1600
cm-1

Figure 3.2

Figure 3.3: Raman spectra of (a) bound NAD^+ in LDH (LDH:NAD^+ = 1.5: 5 mM) at 4 °C in 0.1 M phosphate buffer, pH 7.2, and (b) NAD^+ in solution (80 mM) at 4 °C in 0.1 M phosphate buffer, pH 7.2. See text and Figure 3.2 for the labelling scheme.

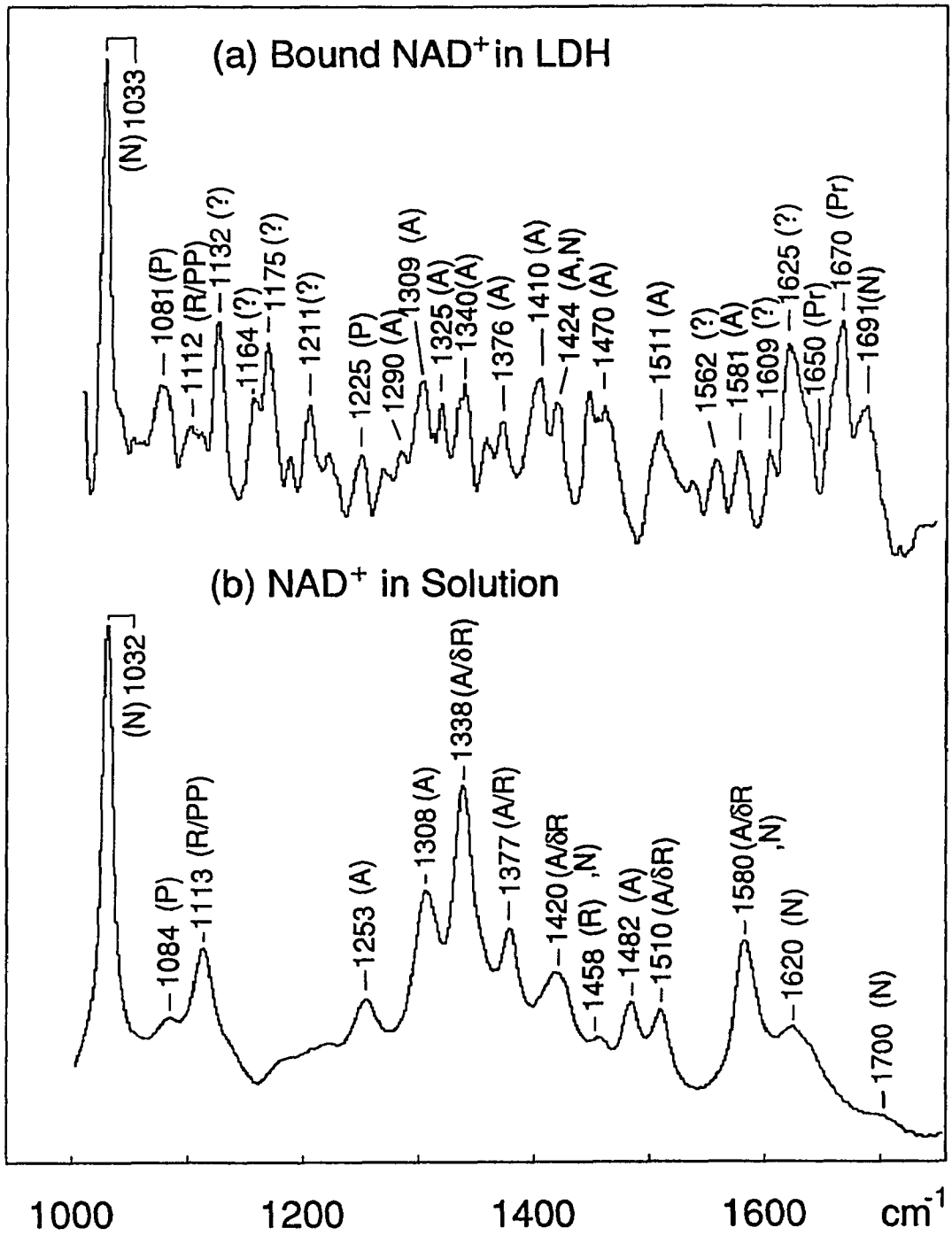
(a) Bound NAD+ in LDH
(N) 1033
1081 (P)
1112 (R/PP)
1132 (?)
1164 (?)
1175 (?)
1211(?)
1225 (P)
1290 (A)
1309 (A)
1325 (A)
1340(A)
1376 (A)
1410 (A)
1424 (A,N)
1470 (A)
1511 (A)
1562 (?)
1581 (A)
1609 (?)
1625 (?)
1650 (Pr)
1670 (Pr)
1691(N)
(b) NAD+ in Solution
(N) 1032
1084 (P)
1113 (R/PP)
1253 (A)
1308 (A)
1338 (A/δR)
1377 (A/R)
1420 (A/δR ,N)
1458 (R) ,N)
1482 (A)
1510 (A/δR)
1580 (A/δR ,N)
1620 (N)
1700 (N)
1000
1200
1400
1600
cm-1

Figure 3.3

Figure 3.4: Raman spectra of (a) bound ADPR in LDH (LDH:ADPR=1:2.5 mM) at 4 °C in 0.1 M phosphate buffer, pH 7.2, (b) bound ADPR in LADH (LADH:ADPR=1:1.8 mM) at 4 °C in 0.1 M pyrophosphate buffer, pH 9.6, and (c) ADPR in solution (80 mM) at 4 °C in 0.1 M pyrophosphate buffer, pH 9.6. See text and Figure 3.2 for the labelling scheme.

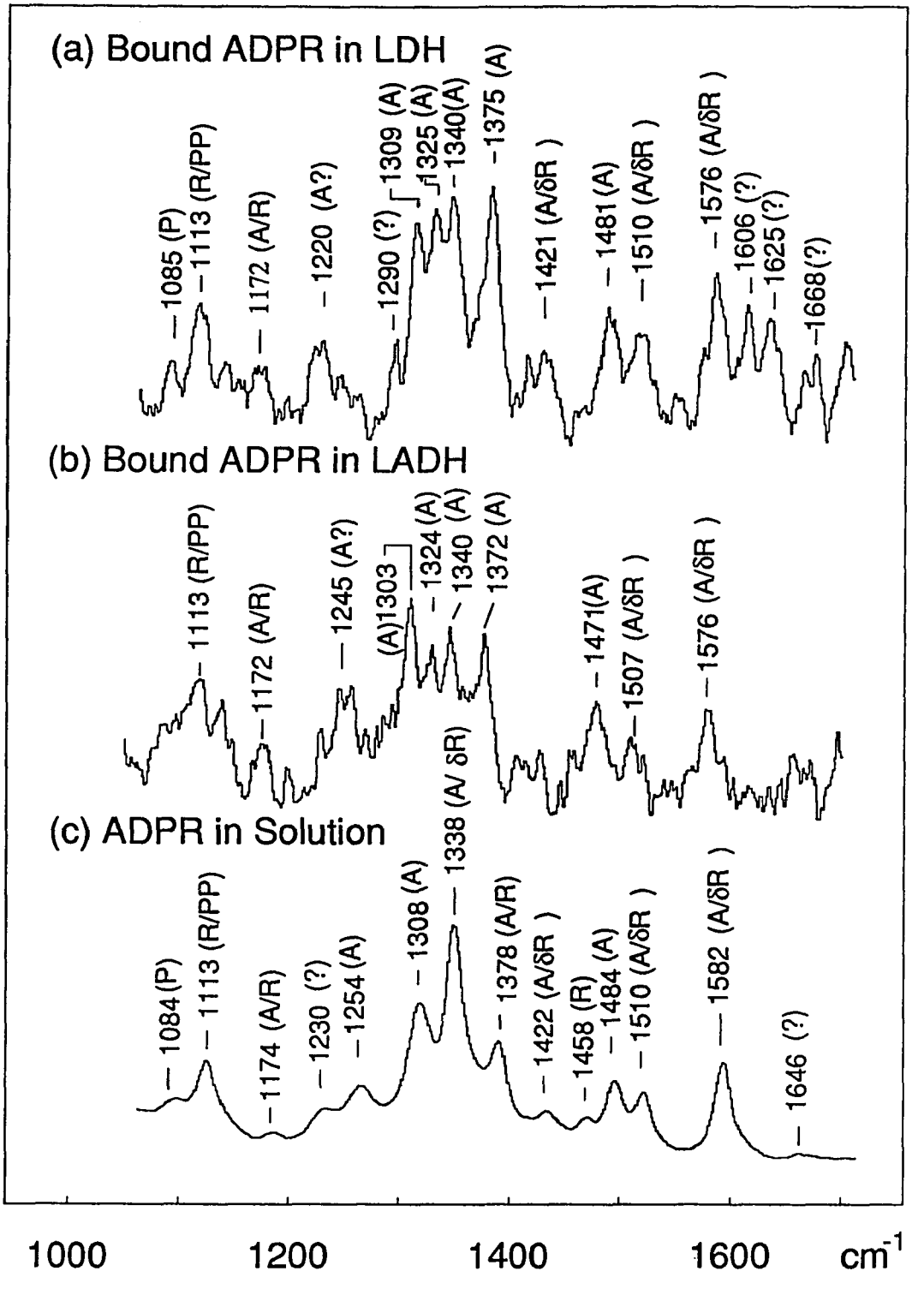
(a) Bound ADPR in LDH
1085 (P)
1113 (R/PP)
1172 (A/R)
1220 (A?)
1290 (?)
1309 (A)
1325 (A)
1340(A)
1375 (A)
1421 (A/δR)
1481 (A)
1510 (A/δR)
1576 (A/δR)
1606 (?)
1625 (?)
1668(?)
(b) Bound ADPR in LADH
1113 (R/PP)
1172 (A/R)
1245 (A?)
(A)1303
1324 (A)
1340 (A)
1372 (A)
1471(A)
1507 (A/δR)
1576 (A/δR)
(c) ADPR in Solution
1084(P)
1113 (R/PP)
1174 (A/R)
1230 (?)
1254 (A)
1308 (A)
1338 (A/ δR)
1378 (A/R)
1422 (A/δR)
1458 (R)
1484 (A)
1510 (A/δR)
1582 (A/δR)
1646 (?)
1000
1200
1400
1600
cm-1

Figure 3.4

Figure 3.5: Raman spectra of 9-ethyladenine (a) in chloroform and (b) in H_2O at 4 °C and 100 mM concentrations.

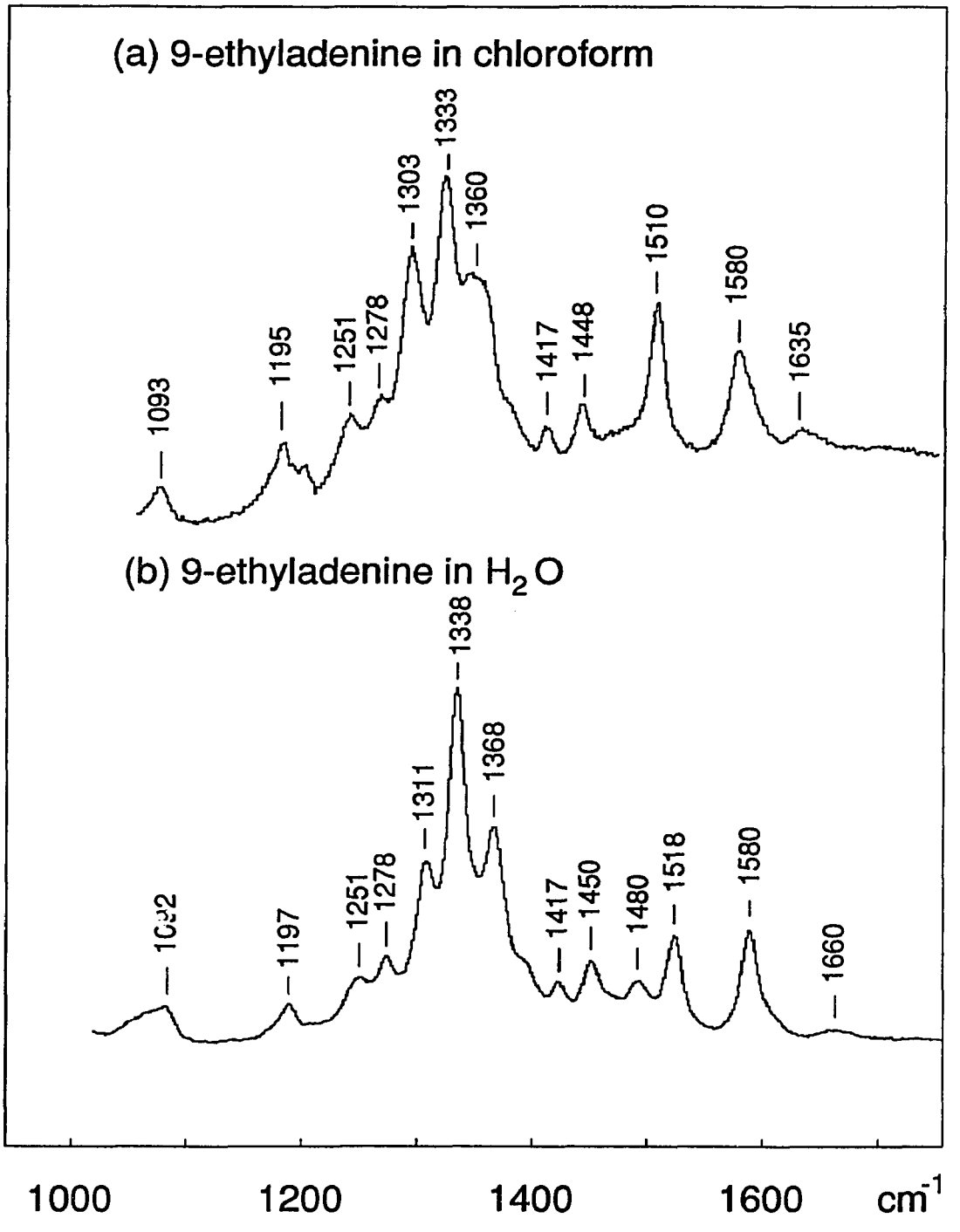
(a) 9-ethyladenine in chloroform
1093
1195
1251
1278
1303
1333
1360
1417
1448
1510
1580
1635
(b) 9-ethyladenine in H_2O
1092
1197
1251
1278
1311
1338
1368
1417
1450
1480
1518
1580
1660
1000
1200
1400
1600
cm^{-1}

Figure 3.5

Chapter 4
A STUDY TO UNDERSTAND THE MOLECULAR BASIS OF A-SIDE SELECTION IN LDH

4.1 Introduction

An important issue of enzymatic catalysis is that enzymes use noncovalent interactions to facilitate the making and breaking of covalent bonds and to perform stereospecific reactions (Fersht, 1985, and You, 1985). The energy and origin of these noncovalent interactions are generally difficult to assess experimentally. In this chapter, we investigate the origins of the bonds between enzyme and coenzyme that are at least partially responsible for the stereochemistry of the reaction catalyzed by lactate dehydrogenase and that are found generally in the pyridine dependent dehydrogenases, using classical Raman spectroscopy. Raman spectroscopy provides detailed information concerning these molecular properties and the interactions between molecules and molecular groups. In last two chapters, we showed that very good classical spectra of small molecules bound at the active site of proteins can be obtained using ultrasensitive difference techniques, which we have developed in our lab. In this approach, the classical Raman spectrum of the protein is subtracted from that of the enzyme-bound molecule complex.

In 1953, Westheimer, Vennlesland and coworkers discovered and reported the stereoscopically selectivity of alcohol dehydrogenase (Fisher et. al., 1953). In their work, they found that the enzyme could distinguish the two diastereotopically related faces

of the nicotinamide ring, and could also stereospecifically remove only one of the methylenic protons of ethanol. Later on, it had been found that among about 250 known pyridine-dependent dehydrogenases, there are two stereochemically distinct groups, some of them (A class enzymes) transfer only the pro-R proton of the the dihydronicotinamide ring and others (B class enzymes) transferred only the pro-S proton (see Scheme 5.1).

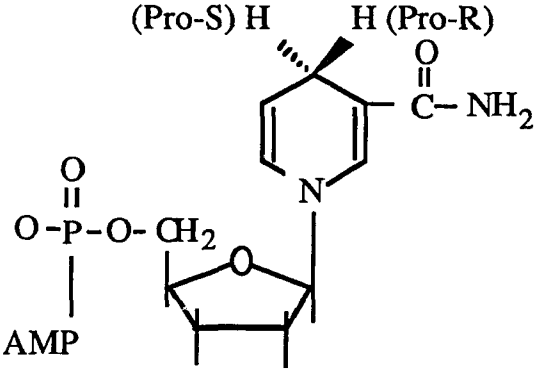

Scheme 5.1 Stereospecificity at cofactor in dehydrogenases.

The number of enzymes in the two groups are almost equal. The stereoselectivity of the enzymatic reaction is extremely high. For example, recent studies with lactate dehydrogenase, a A class enzyme, show that hydride transfer occurs with a high fidelity, only 10^{-8} of the total hydrogens are transfer to the "error place" (Anderson, et al. 1988). This is corresponds to about 11 kcal/mol difference in the relative energies of the two diastereotopic transition state. It is very interesting to compare this biological

reaction with the chemical one, in which there is almost no stereospecificity at all (You, 1985).

As we shall see before, the aromatic nature of the nicotinamide ring of NAD^+ is unaffected upon binding to LDH. Thus, the interactions between the carboxamide group and its protein environment are particularly interesting. We have already shown that the $-NH_2$ group of the carboxamide shows significant hydrogen bonding in the active sites of alcohol dehydrogenase (Chen et. al 1987), lactate dehydrogenase (see chapter 3) and DHFR (see chapter 5). Here our interest is focussed on the carboxamide carbonyl group. The stretching frequency of the C=O mode is expected to lie near 1710 cm^{-1}, but neither NADH nor NAD^+ contain a clearly identified carbonyl stretch (Rodgers, et al.,1980, and Yue, et al., 1986). With these molecules, the C=O stretch is likely coupled to other internal modes in both molecules, C=C stretches in NADH and with modes of the amide $-NH_2$ group in both NADH and NAD^+, and thus might be expected to be poorly defined. We have therefore studied the spectra of both free and bound acetylpyridine adenine dinucleotide, $APAD^+$, which also readily reacts catalytically with substrate (Colowick, et al., 1966). In $APAD^+$, an acetyl group replaces the carboxamide at the 3-position of the nicotinamide ring of NAD^+, and this replacement eliminates the resonance interaction between the amide and carbonyl groups, leaving a band in the observed Raman spectrum which can be clearly assigned to a C=O stretch. We observe the C=O stretch of $APAD^+$ when bound to LDH and find that it decreases 10 cm^{-1} upon binding. The particular hydrogen bonding pattern responsible for this shift is discussed and characterized.

4.2 Materials

$APAD^+$ was purchased from Boehringer Mannheim Co. (Indianapolis, IN), and it was used without further purification. Concentrations APAD was determined by UV-Vis absorption spectroscopy, ε_{259}=18000 $M^{-1}cm^{-1}$. Since LDH contains four independent active sites, binary complexes of LDH were prepared by mixing a 1:<4 molar ratio of LDH to $APAD^+$. Since the concentration of the enzyme is significantly larger than the dissociation constants (Stinson and Holbrook, 1973) for $APAD^+$, typically better than 90% is bound (see Results).

4.3 Results and Discussion

Spectra The Raman difference spectrum obtained by subtracting the spectrum of LDH from that of the LDH/APAD$^+$ binary complex is shown in figure 4.1.a. In these experiments and those described below, over 95% of the added APAD$^+$ is bound to LDH (based on a K_d of about 0.2 mM for the APAD$^+$ binary complex (Stinson, and Holbrook, 1973). The Raman spectrum of LDH has been reported in the chapter 3. In figure 4.1.b, we show the results from an identical experiment except that the LDH/APAD$^+$ and LDH samples are dissolved in $H_2{}^{18}O$. Since the carbonyl group of APAD$^+$ rapidly exchanges its ^{16}O oxygen for ^{18}O under these conditions, the changes in these spectra, which are discussed below, must result from changes in the molecular motions of the carbonyl. figure 4.1.c and 4.1.d show the solution spectra of APAD$^+$ in $H_2{}^{16}O$ and $H_2{}^{18}O$, respectively.

We found previously that the classical Raman bands of APAD$^+$ and the coenzymes NADH or NAD$^+$ arise from molecular motions generally located on smaller moieties of the larger molecule (see chapter 3). Peaks may be labelled as either adenine (A), nicotinamide (N), ribose (R), phosphate (P), or pyrophosphate (PP). We have so labelled all the peaks in the APAD$^+$ data of figure 4.1.c in this way. In some cases, a band is found to be largely located on a particular moiety but its position and/or strength is somewhat dependent on a connecting group. Some of the peaks of adenine are influenced by ribose binding to form adenosine, for example. The nomenclature A/δR identifies such peaks. Other peaks are strongly associated with two moieties, and these are identified as A/R. Finally, we have

assigned peaks in the protein difference spectra of figure 4.1.a to adenine, ribose and, phosphate groups based upon similar experiments on NADH and NAD^+ bound to alcohol and lactate dehydrogenases. We have discussed the binding properties of these coenzymes in chapter 3.

Two bands in the solution spectrum of $APAD^+$ are associated with the 3-acetylpyridinium moiety of $APAD^+$. The first of these is the dominant 1033 cm^{-1} band characteristic of aromatic rings. For example, benzene's spectrum contains an intense band near 991 cm^{-1}, which has been assigned to a ring breathing mode. A simple analog for oxidized nicotinamide, 1-methylpyridine, also has an intense band at 1029 cm^{-1}. This band is unaffected when $APAD^+$ binds to LDH as is shown in figure 4.1.a. The same result is found for the binding of NAD^+ to LDH and the binding of $NADP^+$ to DHFR. Thus, the aromatic nature of the nicotinamide moiety of $APAD^+$ (or NAD^+) apparently is unchanged upon binding. The other band associated with the 3-acetylpyridinium moiety is at 1710 cm^{-1} in the solution spectrum of figure 4.1.c, and this frequency is characteristic of carbonyl C=O stretches. This band shifts 28 cm^{-1} upon ^{18}O substitution of the acetyl oxygen as shown in figure 4.1.d. A simple reduced mass calculation yields a shift of 41 cm^{-1} for a 'pure' C=O diatomic molecule, which is within reasonable agreement to that observed. When $APAD^+$ is bound to LDH, this band shifts to 1700 cm^{-1} (figure 4.1.a), and, after labelling the carbonyl with ^{18}O, it shifts downward an additional 32 cm^{-1} (figure 4.1.b). Based on these shifts, we conclude that the carbonyl bond of the acetyl moiety has less double bond character when bound to the enzyme than in water.

Discussion The carboxamide moiety of both NAD^+ and NADH generally forms hydrogen bonds when bound to pyridine dependent dehydrogenases with either the protein backbone, the side chains, or tightly bound water molecules. The following discussion of the hydrogen bonding patterns involving the carboxamide of NAD and NADH is based on the refined structure of the dogfish LDH ternary complex, E/NADH/oxamate (K. Piontek and M. G. Rossmann, Purdue University, personal communication). In this structure, the amide is hydrogen bonded with the main chain carbonyl of residue 136 and the carbonyl oxygen interacts with a tightly bound water molecule with an O to O distance of 2.7 Å. In addition, His-193, which acts as a general acid/base during the normal catalytic process, is only about 3.3 Å from the carbonyl oxygen in the ternary complex. This is sufficiently close to interact electrostatically with the carbonyl. Based on these data and on the more limited structural data for LDH from pig heart (Chandrasekhar, et al., 1973, and Grau, et al. 1981) the enzyme used in this study, it is likely that a similar bonding patterns exists with this enzyme also.

Thus, it seems reasonable to ascribe the 10 cm^{-1} shift in the C=O frequency when $APAD^+$ binds to the protein to the formation to a hydrogen bond between the carbonyl group and the enzyme. We probed this assignment further by performing the same experiments with samples in D_2O. It is often possible to detect a shift in frequency of a bond being polarized by a hydrogen bond, if the polarizing electrophile is associated with a hydrogen which is exchanged for a deuterium. We found (data not shown) that the C=O mode of $APAD^+$ in solution shifted -2 cm^{-1} in D_2O relative to its value in H_2O and its

shift in the LDH/APAD$^+$ complex was -5 cm^{-1}. While small, the deuteriation effect was reproducible larger in the LDH/APAD$^+$ complex than for APAD$^+$ in solution.

It is intuitive that force constants, and hence vibrational frequencies, of localized modes will be affected by hydrogen bonding. Sometimes the relationship is very direct and simple. For example, Badger and Bauer suggested quite some time ago that the enthalpy of formation of a hydrogen bond, ΔH, is linearly related to the vibrational frequency shift, $\Delta\nu$, of the O-H stretch frequency of the hydroxylic accepter. A stronger hydrogen bond weakens the O-H bond and the stretch force constant; this gives rise to a significant decrease in the observed stretching frequency (for review, see Rao, 1975). A Badger-Bauer like rule has also been obtained for molecules containing the carbonyl, C=O, group (Thijs, 1984). The C=O stretch frequency, normally found near 1710 cm^{-1}, was found to decrease for the following molecules as a function of hydrogen bond strength:

Electron donor	
acetone	$-\Delta H$ (kcal/mol) = $(0.47)\Delta\nu$ - 0.11
acetophenone	$-\Delta H$ (kcal/mol) = $(0.31)\Delta\nu$ - 0.506
benzophenone	$-\Delta H$ (kcal/mol) = $(0.36)\Delta\nu$ - 1.05
methylacetate	$-\Delta H$ (kcal/mol) = $(0.40)\Delta\nu$ - 5.488

We note that the slope, and to an even greater extent, the intercept in these equations depends on the particular molecule. This relationship between carbonyl stretch and hydrogen bond energy has recently been investigated by *ab initio* calculations of $H_2C\,O$ interacting with various cations and water. It was found that the shift in C=O stretching frequency in H_2CO fits a linear correlation

with the computed interaction energy, ΔE, having a slope of 0.5 kcal/mol for every one cm^{-1} of frequency shift, agreeing remarkably well with experiment.

In our case, for calculating the the $\Delta\Delta H$ of C=O of $APAD^+$ in LDH, we use 0.47 kcal/mol/cm^{-1} that was found for acetone as a qualitative approximation. A 10 cm^{-1} shift would correspond to an increase of 4.7 kcal/mol electrostatic interaction energy for the C=O group of bound $APAD^+$ compared to its interactions with water. The data and this simple calculation suggest a substantial favorable interaction between the cofactor's carbonyl and the protein relative to its interaction with solvent (water).

The origin of the 99.999999% accuracy accomplished by LDH in the sterospecific transfer of a hydride ion between cofactor and substrate is unclear (Anderson, et al., 1984). This transfer between the C2 carbon of the substrate and the cofactor's C4 carbon depends on the correct positioning of the two molecules. We have showed that the substrate is strongly bonded to the enzyme by at least two interactions with specific residues. Hence, the bound substrate is unlikely to have significant rotational and translational freedom at the active site. Dehydrogenases bind the cofactor with the nicotinamide in either the *anti* or *syn* conformation relative to rotation around the gycosidic bond between the N-1 of the pyridinium ring and the C-1 of the ribose. Pro-R and pro-S dehydrogenases universally bind the coenzyme in the *anti* and *syn* conformation, respectively, and LDH belongs to the former group. Both our data and the X-ray structural results suggest that the enzyme presents a favorable hydrogen bond environment to the

carboxamide group of the cofactor when ring is in the *anti* conformation. From our data, we obtain 5 kcal/mol hydrogen bonding interaction between the C=O of carboxamide and protein, and about 2.2 kcal/mol hydrogen bonding interaction energy associated with the $-NH_2$ group (see chapter 3). In addition, model building studies based on the atomic coordinates for LDH show that carboxamide would be placed in a hydrophobic environment when the pyridinium ring is in the *syn* conformation. Since no other strong interactions between the cofactor's nicotinamide headgroup and the enzyme are apparent, the enzyme is apparently designed to accomplish reaction specificity by specific hydrogen bonding patterns with nicotinamide's carboxamide group. The facinating question from this is whether this bonding pattern is in place for important mechanistic reasons, as has been proposed (Benner, et al., 1986), or is merely an accident of the requirement that the cofactor must bind to the enzyme for catalysis and the protein is providing an accommodating environment for the polar nature of the carboximide group.

Conclusion: We have performed classical Raman difference spectroscopy on complexes of lactate dehydrogenase with and without $APAD^+$ and have obtained the spectrum of $APAD^+$ when bound to the active site of the enzyme. This result is compared to the solution spectrum of $APAD^+$. We have shown that the protein active site of LDH has been designed to interact through specific hydrogen bonding patterns with the carboxamide group, and apparently not with the ring moiety of $APAD^+$ (or NAD^+). The energy of the hydrogen bonding is favorable and probably substantial, in the order

of 10 kcal/mol. The hydrogen bonding between the coenzyme carboxamide moiety and enzyme and that with the ADPR group of the coenzymes may thus be significant factor in fixing the geometry of the ring of the coenzymes in a such a way that coenzyme-substrate hydride transfer occurs sterospecifically, as is found for this enzyme.

As we discused before (see Chapter 3), the bands in our difference spectra can also be raise from the following three sources. The first may come from the shot random noise. The second is due to an interaction between the bound ligand and surrounding protein moiety, this may affects a mode of the protein moiety. For example, due to the ligand binding, the pK_a of some protein residues in the active site can be dramatically changed. The third one may result from the changes in the secondary structure of the protein that occur when the coenzyme binds. For example Caughey and coworkers shown that the amide I of the spectra of proteins is relatively sensitive to the secondary structure of the proteins (Dong, et al., 1990). So, whether the Raman bands in our difference spectra come form the bound ligand or else where must always be considered carefully. In the chapter 3, by considering the relative Raman intensity and comparing the spectra of the bound coenzymes and their analogues, we assign the observed Raman band to particular molecular motions. Here, we show another way to handle this problem, using the isotope label. By this way, we can confirm where the Raman band come from.

Figure 4.1: Raman spectra of (a) bound $APAD^+$ in LDH (LDH:$APAD^+$=1:2.5 mM) at 4 °C in 0.1 M phosphate buffer, pH 7.2, obtained by calculating the difference spectrum between LDH/$APAD^+$ binary complex and LDH, (b) same as (a) except samples measured to calculate the difference were in $H_2{}^{18}O$, (c) $APAD^+$ in solution (70 mM) at 4 °C in 0.1 M phosphate buffer, pH 7.2, and (d) same as (c) except $APAD^+$ was in $H_2{}^{18}O$. See text and Figure 3.2 for the labelling scheme.

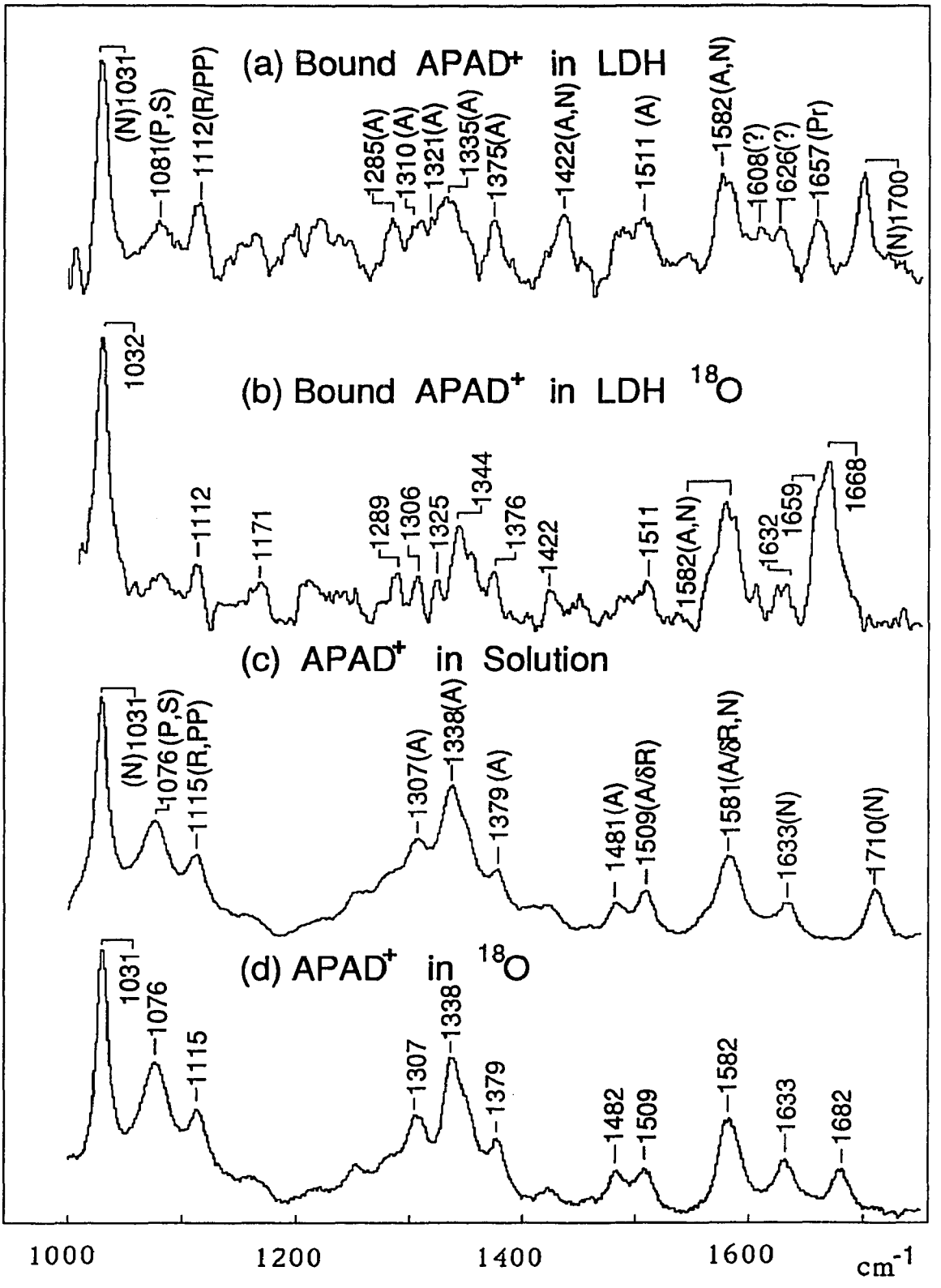
(a) Bound APAD+ in LDH
(N)1031
1081(P,S)
1112(R/PP)
1285(A)
1310(A)
1321(A)
1335(A)
1375(A)
1422(A,N)
1511 (A)
1582(A,N)
1608(?)
1626(?)
1657(Pr)
(N)1700
(b) Bound APAD+ in LDH 18O
1032
1112
1171
1289
1306
1325
1344
1376
1422
1511
1582(A,N)
1632
1659
1668
(c) APAD+ in Solution
(N)1031
1076(P,S)
1115(R,PP)
1307(A)
1338(A)
1379 (A)
1481(A)
1509(A/δR)
1581(A/δR,N)
1633(N)
1710(N)
(d) APAD+ in 18O
1031
1076
1115
1307
1338
1379
1482
1509
1582
1633
1682
1000
1200
1400
1600
cm-1

Figure 4.1

Chapter 5
THE BINDING PROPERTIES OF COENZYMES TO DIHYDROFOLATE REDUCTASE

5.1 Introduction

Dihydrofolate reductase (DHFR; tetrahydrofolate: $NADP^+$ oxidoreductase) is a widely occurring enzyme that catalyzes the NADP-dependent reduction of 7,8-dihydrofolate (FAH_2) to 5,6,7,8-tetrahydrofolate (FAH_4).

$$FAH_2 + NADPH + H^+ \rightleftharpoons FAH_4 + NADP^+$$

Like LDH, this enzyme performs pro-R (or A class) stereospecific hydride transfer from NADPH to substrate. The molecule of DHFR from *E. coli* is a monomer and consists of 159 amino acids having a molecular mass of 18000 daltons. DHFR is necessary for maintaining the intercellular pools of tetrahydrofolate and its derivatives, which are essential cofactors in many biosynthetic reaction. In eukaryotes, DHFR is also a target enzyme for a group of antifolate drugs that are widely used as antitumors and antibacterial agents, such as methotrexate (MTX, an anticancer agent) and trimethoprim (TMP, an antibacterial agent). Because of its biological and pharmacological importance, DHFR has been the subject of extensive structural and biochemical studies. DHFR also is the one of a few enzyme which can be easily purified by the application of affinity chromatography utilizing inhibitors (such as methotrexate) linked to a sepharose matrix. Thus, a wealth of information regarding this enzyme (Kraut and Matthews, 1987) is available. At present, refined high-resolution X-ray structures (to 1.7

Å) are available for some binary (enzyme + substrate or coenzyme) and ternary (enzyme + coenzyme + inhibitor) complexes (Filman et al., 1982, Bystroff et al., 1990).

DHFR is also a very good protein sample to enhance our difference Raman spectroscopy studies because of its small size, stability, and the detailed X-ray structure available. Comparing the spectra of the bound coenzymes to DHFR with that bound to LADH and LDH, should result in a better understanding our previous data and provide more generalized information.

5.2 Materials and Sample Preparation.

NADPH and $NADP^+$ were purchased from the Sigma Chemical Co. (grade III; St. Louis, MO) or from Boehringer Mannheim Co. (100%; Indianapolis, IN), and ATPR was purchased from Sigma and were used without further purification. DHFR from *E. Coli.* was kindly provided by Professor J. Kraut's group in University of California at San Diego, and store at 4°C in 10 mM Tris-HCl buffer, pH 8.0 with 0.5M KCl at 1 mg/ml. Before use, insoluble (probably denatured) protein was removed by centrifugation. The enzyme solution was concentrated to about 5 mM using a Centricon-10 centrifuge concentrator (Amicon, Lexington, MA). Concentration of the enzyme and coenzyme were determined by UV-Vis absorption spectroscopy, using ε_{280} = 31,000 $M^{-1}cm^{-1}$ for DHFR, ε_{340} = 6220 $M^{-1}cm^{-1}$ for NADPH, ε_{259} = 18,000 $M^{-1}cm^{-1}$ for $NADP^+$, and ε_{259} = 15,200 $M^{-1}cm^{-1}$ for ATPR. Unlike LDH, DHFR is monomer; each molecule of the enzyme contained only one active site. Thus, binary complexes of DHFR were prepared by mixing about 1:0.9 molar ratio of DHFR to NADPH, NADP+, and ATPR (typically 5 mM : 4.5 mM). Under these conditions, more than 99% of the coenzymes (or analogues) are bound.

5.3 Results

Spectra. Shown in figure 5.1 are the Raman spectra of apo-DHFR (a) and its binary complex with NADPH (b). Due to the protein's small molecular weight, we can really see differences between the two spectra that are clear even without applying the subtraction procedure (e.g. the strong NADPH peak at 1685 cm^{-1})

Using the same difference spectroscopic procedures discussed in chapter 3, we calculated the difference spectrum, shown in Figure 5.2.a, between the NADPH/DHFR binary complex and apo-DHFR. The band intensities of the Raman spectrum of the bound NADPH are 5-15% that of the DHFR. Compared with our previous LDH study, we obtain a better signal to noise ratio here. For comparison, the spectrum of NADPH in solution is shown in Figure 5.2.b. As was showing in last chapter, the Raman peaks may be assigned arise from the different moieties within the NADPH molecule i.e. adenine (A), nicotinamide (N), ribose (R), phosphate (P), pyrophosphate (PP). Additionally, we use (Pr) to indicate the contributions to the difference spectrum from protein changes.

From Figure 5.2, we can clearly see that the Raman spectrum of NADPH in DHFR differs remarkably from the spectrum of NADPH in solution. Most of these difference are very similar to the differences seen between NADH bound to LDH and NADH in solution. Like NADH bound in LDH, the binding of the nicotinamide moiety is clearly accompanied by the disappearance of the intense 1546 cm^{-1} band (which probably shifts to 1572 cm^{-1}) and an intensity decrease or disappearance in the 1458 cm^{-1} band found in the solution spectrum. When we compare the peaks due to the rocking motion of the

nicotinamide NH_2 moiety, we find the same features as in the spectra of NADH bound to LDH. The solution band at 1089 cm^{-1} shifts to 1119 cm^{-1} when NADPH binds. But the adenine moiety of bound NADPH in DHFR show a marked difference with that of the bound NADH in LDH and LADH.

Figure 5.3.a shows the difference spectrum of $NADP^+$/DHFR with DHFR and the figure 5.3b shows the spectrum of $NADP^+$ in solution. The nicotinamide moiety of $NADP^+$ shows very few Raman active bands, as is clear from the solution data. The main nicotinamide peak at 1032 cm^{-1} is unaffected when NAD^+ binds to LDH and $NADP^+$ binds to DHFR.

Figure 4.4 shows the ATPR/DHFR difference spectrum with DHFR (Figure 4.4.a), and the Raman spectrum of ATPR in solution (Figure 4.4b).

Band Assignments. Based on the analysis described in chapter 3, comparing the spectra of bound NADH in LDH and in LADH, we can assign the bands in the spectrum of the bound NADPH and $NADP^+$ to a particular moiety like nicotinamide (N), adenine (A), ribose (R) etc.

The difference between NADH (or NAD^+) and NADPH (or $NADP^+$) is the 2'-phosphate group. For the Raman spectra of NADPH (or $NADP^+$) in solution at pH 8.0, we can see that the peaks pattern almost exactly match that of NAD^+ and NADH, except for one additional peak at 980 cm^{-1} (which appears in $NADP^+$, NADPH, and ATPR spectra). This peak probably arises from the 2'-phosphate group attached to the adenosine ribose. Its position is just at the right frequency for the P=O symmetric stretching mode of the resonant $-PO_3^{-3}$ group. In the Raman spectra of DHFR-bound NADPH

and $NADP^+$ at pH 8.0, this peak is missing, and two new peaks appear at 876 cm^{-1} and 1072 cm^{-1}. It is reasonable to assign these peaks to the bound 2'-phosphate moiety. For free phosphate in solution at pH 4.5, which is in the HPO_2^{2-} structure (pK_a=7.21) the Raman spectrum is composed of two peaks, one around 876 cm^{-1}, rising from P-O stretching mode, and the other at 1072 cm^{-1}, from P=O symmetric stretching mode. In the spectrum of $NADP^+$ in solution at pH 4.0, in which the 2'-phosphate is in the monoionic state (pK_a=6.1), we do observe the two peaks around 876 cm^{-1} and 1072 cm^{-1}. So, although we need a isotope study to confirm these tentative assignments, we feel that is quite reasonable to assign those two peaks to 2'-phosphate. This means at least, when the coenzyme bind into DHFR, the three P=O resonance structure of the 2'-phosphate groups is broken to that of a two P=O double resonance and one P-O signal band structure.

5.4 Discussion

Nicotinamide Binding. For NADPH most features of the bound reduced nicotinamide moiety in DHFR spectra are very similar with those in LDH and LADH. One remarkable change for bound NADH in LADH and LDH is the amide NH_2 rocking mode. As discussed in chapter 3, this peak changes from 1084 cm^{-1} in solution to 1114 cm^{-1} upon binding to LDH and LADH. In the spectrum of bound NADPH in DHFR, we see this same change very clearly. Both the band shape and its 30 cm^{-1} upward shift upon binding are the same as NADH in LADH and LDH. We interpreted this shift to be due to the hydrogen-bonding interaction at the coenzyme binding pocket. From X-ray structure studies (Bystroff, et al., 1990; Filman, et al., 1982), it is evident that the carboxyamide side chain is bound to the backbone at Ala-7 with its O7 oxygen held *cis* to C4 of nicotinamide ring, while in solution, the lowest energy conformation for the carboxyamide has its oxygen *trans* to C4 of the pyridine ring (Kraut & Matthews, 1989). It is thus necessary that a hydrogen bond interaction keeps the conformation of carboxyamide at a relatedly higher energy. Following the same analysis of chapter 3, the observed shift is in the right direction and indicative of a strong hydrogen bond. It is interesting to see that the changes in the Raman band are just like those when NADH binds in LDH. The X-ray structure of NADH bound to LDH indicates that NADH's carboxyamide also rotates about 180° from the lowest energy conformation. Based on this, we may say that the hydrogen bond between the carboxyamide of the coenzyme and protein is strong enough to keep the group rotated from its most stable position. Kraut (Kraut & Matthews, 1989) has suggested that

this may can be interpreted as aiding transition-state binding of the nicotinamide. In LDH study, according to Anderson's studies, we estimate the energy of the hydrogen bond from that 30 cm^{-1} shift to be about 2.2 kcal/mol (see chapter 3). So, it is very reasonable to assume that in the DHFR case, the hydrogen bond is also around 2 kcal/mol.

In the spectrum of NADPH bound to DHFR, the 1546 cm^{-1} band disappears as found for LDH (see chapter 3) . In chapter 3, we tentatively assigned this band to the out of phase C=C stretch, and we suggest that this band's disappear is because of the orientation of the carboxamide is fixed at the active site. The DHFR studies here may give us a another evidence to support ours analysis in the chapter 3. We are looking forward the further isotopically labelled studies to assign this peak accurately.

Adenine Binding. In the spectrum of the NAD(P) and NAD(P)H the Raman bands due to to the adenine moiety are quite remarkable, especially around 1300-1350 cm^{-1}. In the chapter 3, we discussed the ionic state change of the adenine group when it binds to LDH. This was based on observation of the changes in the adenine Raman bands from free in solution to bound in the LDH or LADH. The peaks at 1308 cm^{-1} and 1338 cm^{-1} of adenine ring in solution were replaced by peaks at 1309 cm^{-1}, 1324 cm^{-1}, and 1340 cm^{-1} for adenine bound to LDH. Additionally, the intensities of other peaks changed. We proposed that these changes are due to an adenine ring ionization state change from unprotonated state in solution to a protonated state in protein (chapter 3). Alternative, by studying the Raman spectra of serial mononucleotides crystal sample, Tsuboi's

group in Japan (Nishimura et al., 1986) found that Raman's peaks from the guanine and cytosine in the 1200-1400 cm^{-1} range reflected the conformation of the guanosine or cytidine residues, namely their ribose-ring puckering state and the torsion angle around the glycosidic or cytidic bond. We note that these results are only obtained from crystal sample. If Tsuboi's analysis was also true for adenosine (a purine like guanosine), we would have to reconsider our model.

Combining the Raman results with X-ray crystallographic structural result, we are able to provide very good evidence to support the discussion we made in chapter 3. From the spectra of the bound adenine in the coenzymes data in Figure 5.2-5.4, we can see the three adenine "fingerprint" bands, at 1299, 1326, 1365 cm^{-1} are almost the same for adenine in solution or adenine bound to DHFR. Comparing with the adenine's peaks in solution, they all have a small red shift (about 5 to 10 wavenumbers). We have seen this general kind of the frequency shifts for adenine dissolved in a polar solvent (like water) to a hydrophobic one (like chloroform) (see Figure 3.5). Thus our data suggests that the environment of the adenine ring is a hydrophobic one when it binds to DHFR. It is very interesting to compare the difference the between the spectra of the bound adenine in DHFR and the bound adenine in LDH (chapter 3) or in LADH (Chen, et al. 1986). When adenine binds to DHFR, we do not see the the double bands of 1305 and 1341 cm^{-1} split into triple bands observed for LDH and LADH, but both shift down about 6 cm^{-1}. So by our hypothesis of chapter 3, there should be no change in the protonation state for adenine when it binds to DHFR. The X-ray

crystal structures on DHFR, LDH, and LADH structure confirm this. From the crystal structure of holo-enzyme ($NADP^+$/DHFR), the only direct contacts between the adenine ring and protein we can find are hydrophobic (Kraut & Matthews, 1989; Filman et al. 1982; Bystroff et al., 1990). Indeed, in the adenine binding site of DHFR, there is no such residue that like Asp-223 in LADH or Asp-53 in LDH to protonate the adenine ring and form an ion pair with it. But the backbone of residues 63 to 64 and backbone of 76 to 78 along with the side chain of Lys-62 form a strong hydrophobic adenine binding pocket.

The crystal structures of these holo-enzymes shows that the torsion angles for the glycosidic bond of the adenine mononucleotide moiety are clustered around -150° (Eklund & Branden, 1989). In LADH the torsion angles is -114°, while for DHFR it is -145° and for LDH it is -159°. For the ribose puckering state, adenosine bound to LDH is the same as DHFR, which is the 3'-endo pucker. In the ribose moiety of bound NADH to LADH, the ribose state is 2'-endo pucker. So, if the triple bands of bound adenine in LADH and LDH were due to conformational attributes of adenosine like Tsuboi's observed in crystal samples of guanosine and cytidine, our Raman data of bound coenzyme in DHFR should show a triplet. This is completely different from our Raman result and suggests that we can rule out of the possibility that the conformation of adenosine could effect the Raman data. So, taking all the data together on LDH, LADH, and DHFR and their X-ray structural results, we find that adenine's spectral changes upon binding to LDH and LADH is due to an ionization state change of adenine. Upon binding to DHFR, there are very strong hydrophobic

interactions between the enzyme and the adenine ring, but no ionization state change. As we saw above, we can find solid support for our analysis from the X-ray crystal structure data.

The 2'-phosphate binding. The difference between NADH and NADPH is the adenosine 2'-phosphate group. This "little" structural difference makes a big difference in DHFR's enzymatic specialities. The enzymatic activity using NADH as a cofactor is about 10% compared to that of NADPH. Also, NADH binds to DHFR 100 times weaker than NADPH dose (Feeney et al., 1975). The ^{31}P NMR studies on NADPH and $NADP^+$ bound to the *Lactobacillus casei* reductase have been interpreted to indicate that the 2'-phosphate is in the dianionic state in both enzyme-$NADP^+$ and enzyme-NADPH complexes at pH 5.0-8.0 and that the pK_a of the 2'-phosphate group shift down by at least three units from its value in free NADPH (Feeney et al., 1975). These authors have suggested that there is an electrostatic interaction between the phosphate group and protein cationic groups.

X-ray crystallographic studies of *E. coli* DHFR with bound $NADP^+$ have indicated that the $NADP^+$ 2'-phosphate makes hydrogen bond to the γ-hydroxyls of serines 63 and 64, Ser-64(N), Water-204, and the side chain of Agr-44. As we discussed in the band assignment section, the Raman spectra suggested that when the coenzymes binds to DHFR, the 2'-phosphate three P=O double bands resonance structure is broken into a two P=O double bond resonance structure and one P-O single bond. That indicates that a very strong hydrogen bond is needed, at least around the P-O single bond, to stabilize such a structure.

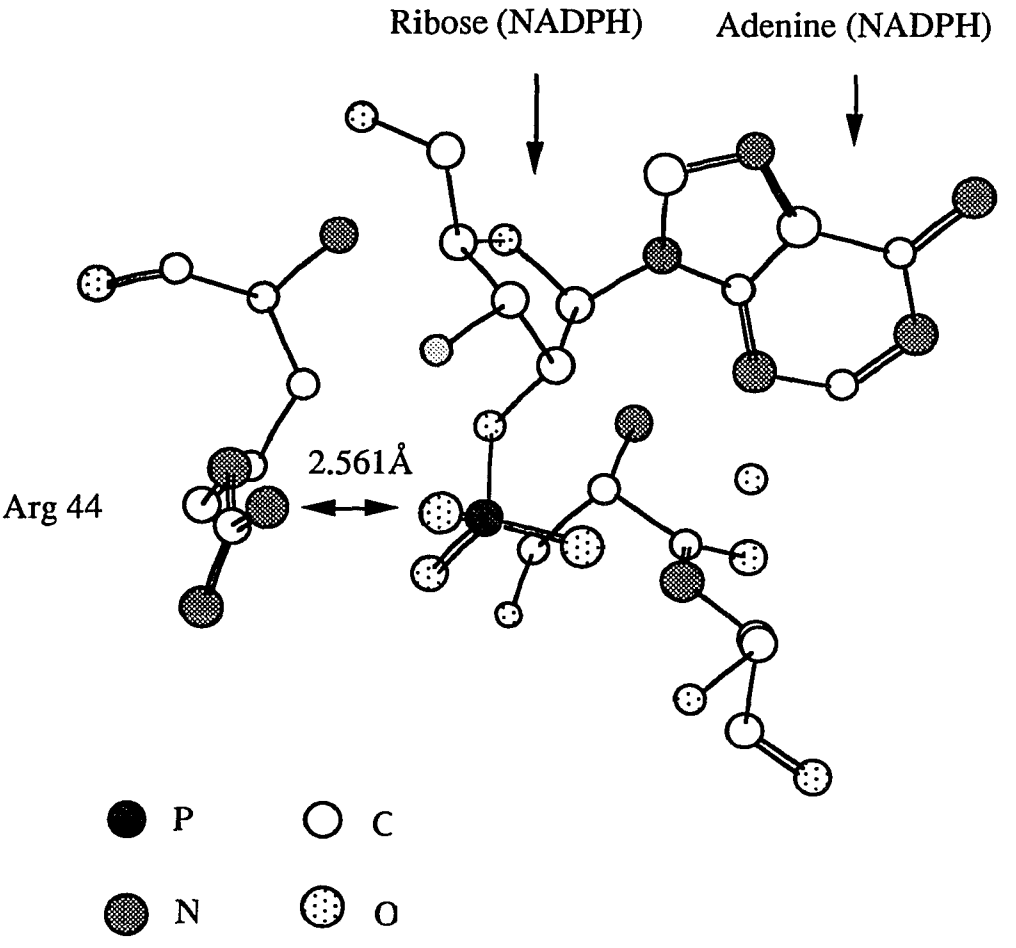

Scheme 5.1 The crystal structure of $NADP^+$ bound to DHFR.

On a closer look at crystal structure of the 2'-phosphate binding site, the nitrogen atom of $N^+=C$ of the side chain of arg 44 is very close to the one oxygen of the 2'-phosphate group, at about 2.5 Å (see scheme 5.1).This distance is such short that an ion pair could be formed between the two atoms. So, it is very possible that a very strong hydrogen bond interaction, $N^+...H...^-O$-P, is formed. These

strong hydrogen bond interaction may be the major effect to break down the resonance structure of the 2'-phosphate group apparently observed in the Raman data.

$NADP^+$ Binding. Like NAD^+, the Raman spectrum of $NADP^+$ contains a few bands assigned to the nicotinamide moiety. The strongest band at 1033 cm^{-1} due to the ring breathing mode of nicotinamide is still unchanged when $NADP^+$ binds to DHFR. Over all, from the our Raman results, we can see that the interaction between the oxidized nicotinamide moiety and the three enzyme, LADH, LDH, and DHFR are very similar.

Figure 5.1: Raman spectra of (a) DHFR/NADPH (DHFR:NADPH=5:4.5 mM) binary complex and (b) DHFR at 4 °C in 10 mM Tris-HCl buffer, pH 8.0 with 0.5 M NaCl in it.

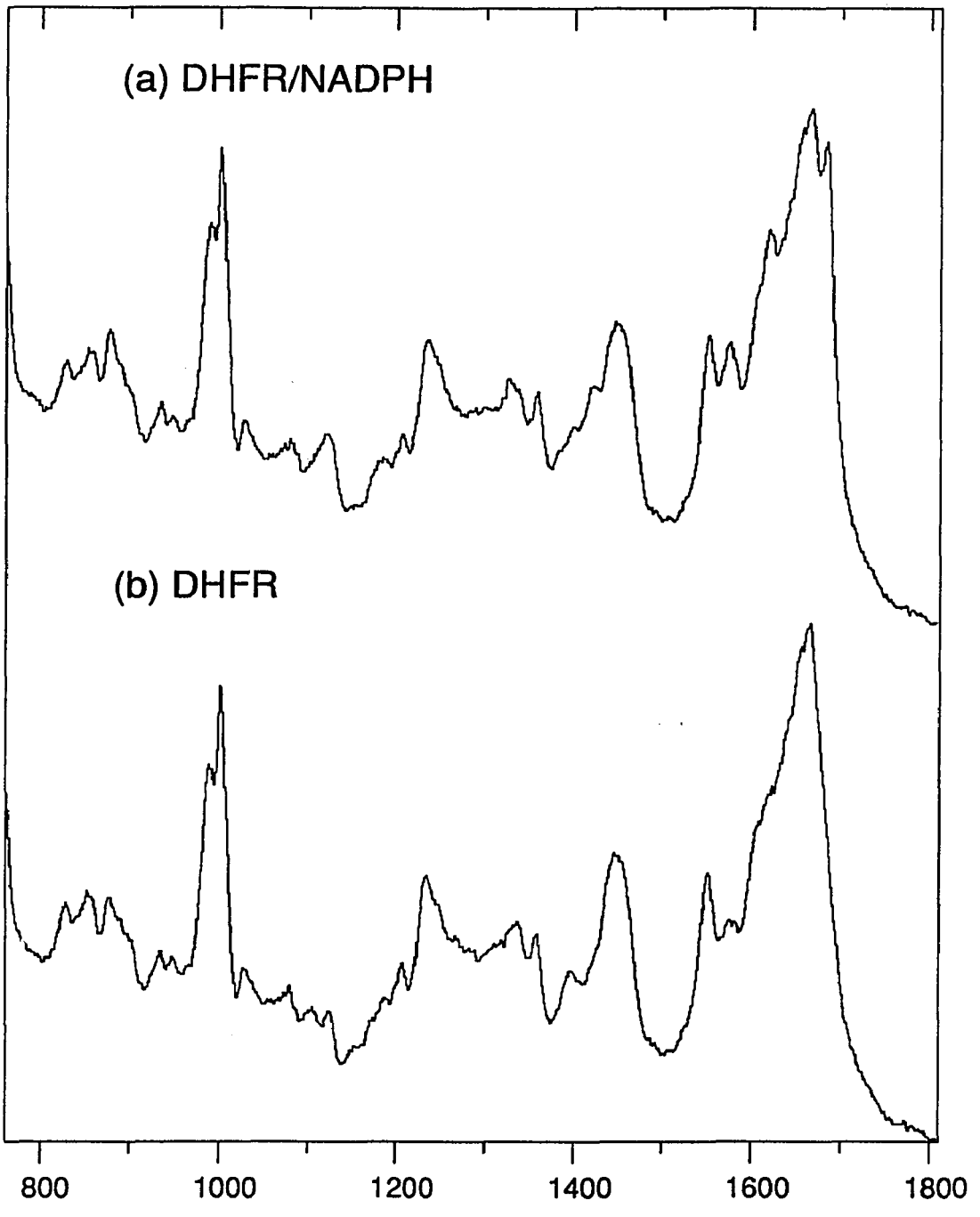

Figure 5.1

Figure 5.2: Raman spectra of (a) bound NADPH in DHFR (DHFR:NADPH=5:4.5 mM) at 4 °C in 10 mM Tris-HCl buffer, pH8.0, and (b) NADPH in solution (100 mM) at pH8.0. See text and Figure 3.2 for the labelling scheme.

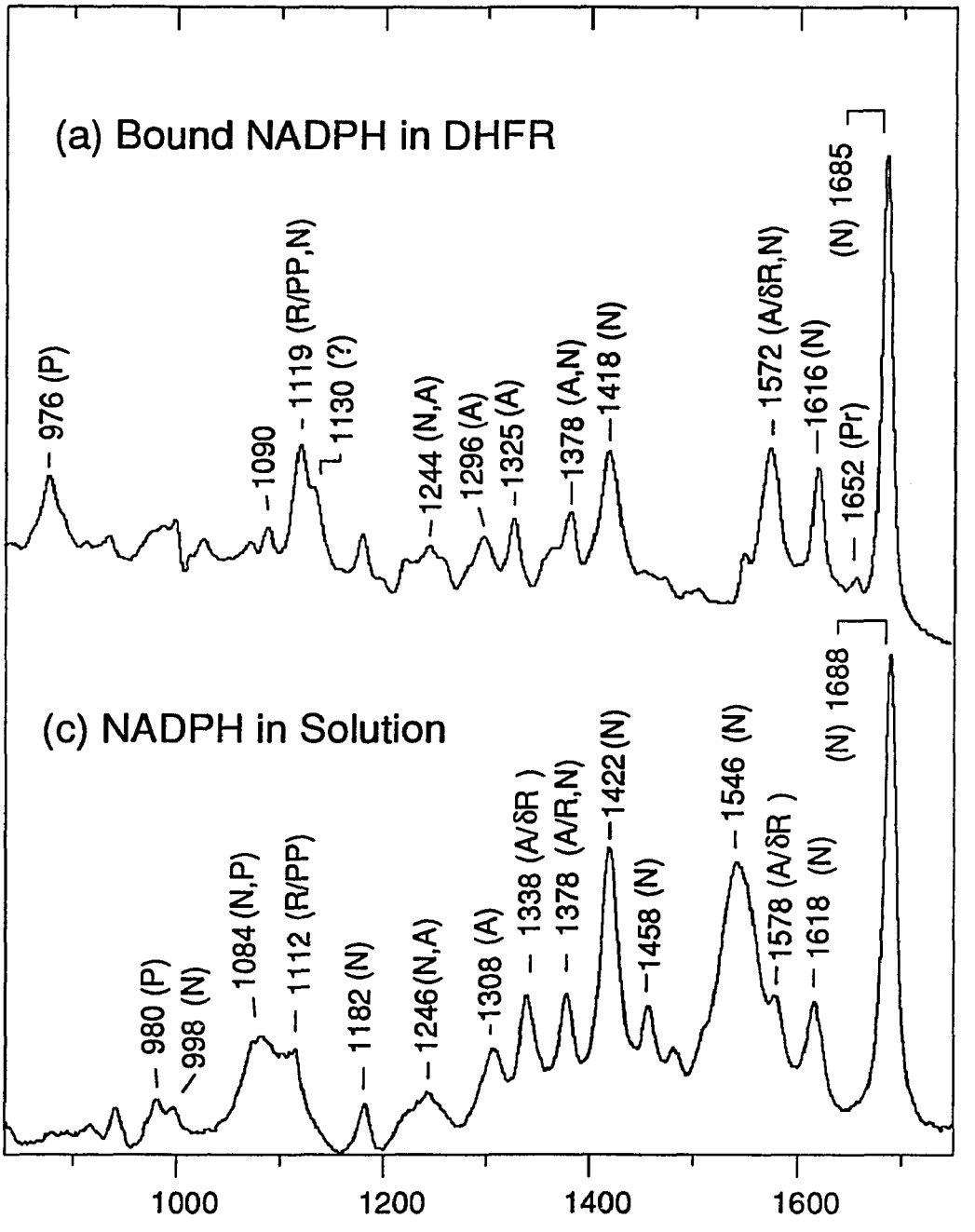
(a) Bound NADPH in DHFR
976 (P)
1090
1119 (R/PP,N)
1130 (?)
1244 (N,A)
1296 (A)
1325 (A)
1378 (A,N)
1418 (N)
1572 (A/δR,N)
1616 (N)
1652 (Pr)
(N) 1685
(c) NADPH in Solution
980 (P)
998 (N)
1084 (N,P)
1112 (R/PP)
1182 (N)
1246(N,A)
1308 (A)
1338 (A/δR)
1378 (A/R,N)
1422 (N)
1458 (N)
1546 (N)
1578 (A/δR)
1618 (N)
(N) 1688
1000
1200
1400
1600

Figure 5.2

Figure 5.3: Raman spectra of (a) bound NADP+ in DHFR (DHFR:$NADP^+$ = 5:4.5 mM) at 4 °C in 10 mM Tris-HCl buffer, pH8.0, and (b) $NADP^+$ in solution (100 mM) at 4 °C, ph 7.5. See text and Figure 3.2 for the labelling scheme.

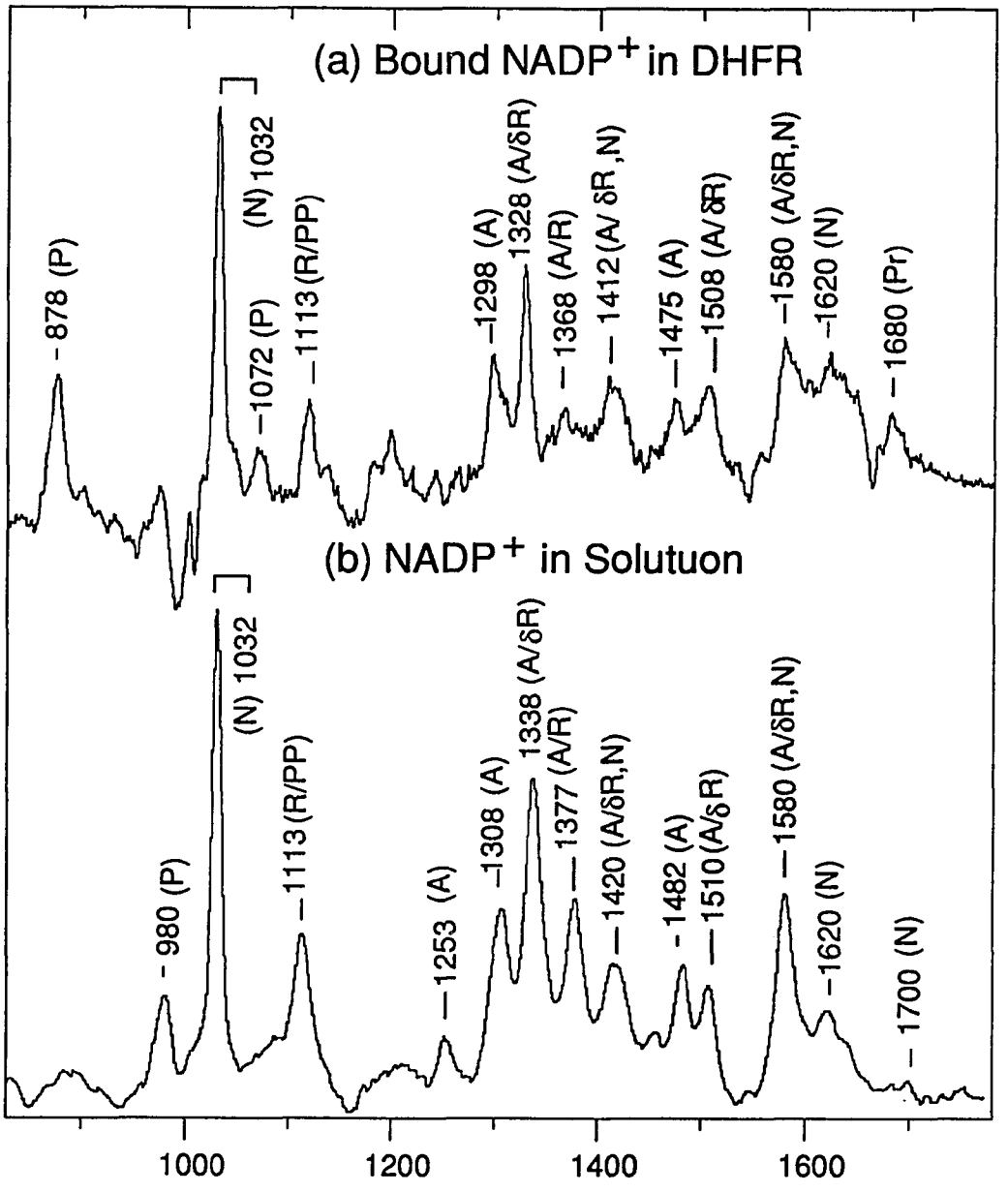
(a) Bound NADP+ in DHFR
878 (P)
1032 (N)
1072 (P)
1113 (R/PP)
1298 (A)
1328 (A/δR)
1368 (A/R)
1412 (A/ δR,N)
1475 (A)
1508 (A/δR)
1580 (A/δR,N)
1620 (N)
1680 (Pr)
(b) NADP+ in Solutuon
980 (P)
1032 (N)
1113 (R/PP)
1253 (A)
1308 (A)
1338 (A/δR)
1377 (A/R)
1420 (A/δR,N)
1482 (A)
1510 (A/δR)
1580 (A/δR,N)
1620 (N)
1700 (N)
1000
1200
1400
1600

Figure 5.3

Figure 5.4: Raman spectra of (a) bound ATPR in DHFR (DHFR: $NADP^+$= 5:4.5 mM) at 4 °C in 10 mM Tris-HCl buffer, pH8.0, and (b) ATPR in solution (100 mM) at 4 °C, pH 7.5. See text and Figure 3.2 for the labelling scheme.

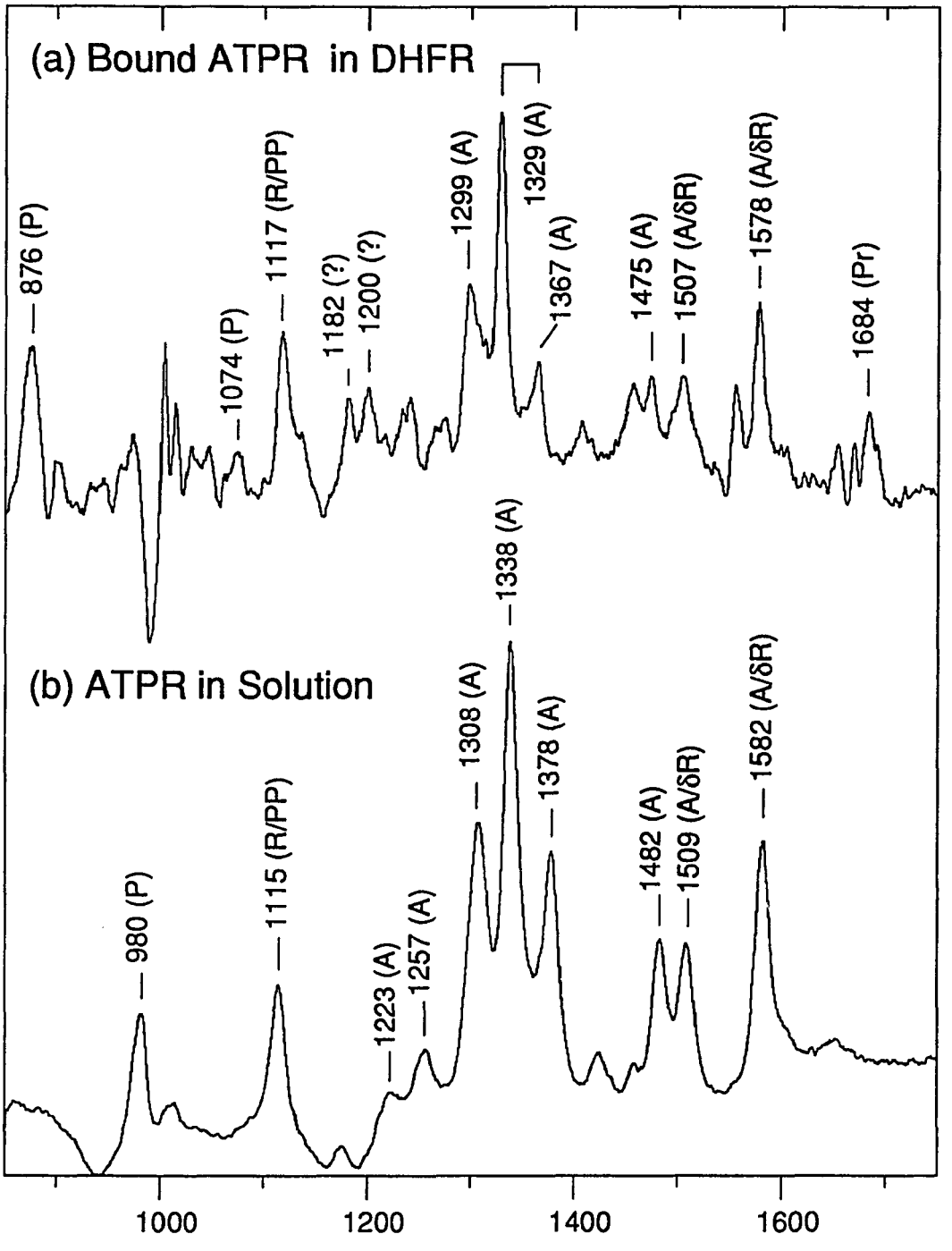
(a) Bound ATPR in DHFR
876 (P)
1074 (P)
1117 (R/PP)
1182 (?)
1200 (?)
1299 (A)
1329 (A)
1367 (A)
1475 (A)
1507 (A/δR)
1578 (A/δR)
1684 (Pr)
(b) ATPR in Solution
980 (P)
1115 (R/PP)
1223 (A)
1257 (A)
1308 (A)
1338 (A)
1378 (A)
1482 (A)
1509 (A/δR)
1582 (A/δR)
1000
1200
1400
1600

Figure 5.4

Chapter 6
STEREOSELECTIVITY IN DEHYDROGENASES AS PROBED BY THE C4-H STRETCH

6.1 Introduction

By examining a great number of the dehydrogenases near the end of the 60's, Colwick and Bentley introduced a set of empirical generalizations which characterizing the dehydrogenases. Often referred to as "Bentley's rules," these generalizations are (Colwick, et al, 1966, Bentley, 1971):

1. The stereospecificity of a particular enzyme does not depend on the source of the enzyme.

2. The stereospecificity of a particular reaction is the same in those cases where both NAD^+ and $NADP^+$ can be used as coenzymes.

3. If a single enzyme uses a range of substrates, the stereospecificity with respect to cofactor will be the same with all substrates.

These generalizations have only a few exceptions, but many remarkable confirmations. For example, all LDHs transfer the pro-R hydrogen, regardless of where they are isolated from. From mammals, birds, and fishes to plants, all the LDH which be isolated from are same, and they are A specific (Pro-R).

From a quick look, the stereoselectivity of enzymes seems quiet straightforward. Through specific binding geometries of the substrates and coenzymes at the active site, enzymes catalyze the reactions. So, because of the geography of the binding site, these conformations apparently present the ring to the substrate in such a

way that dictates the specific steric reaction. But as more experiments have been performed, it has been suggested that other factors may be involved.

About thirty years ago, Levy and coworkers (Levy et al., 1959) suggested a potential connection between the physical properties of the dihydronicotinamide ring and the stereochemical selectivity of the enzymatic reaction. They proposed that selectivity was based on the ability of a dehydrogenase to distort the dihydronicotinamide ring from planarity. By forcing one of the C4 protons axial, that proton would become activated and thus the one to be transfer. About twenty years later, by studying the ^{15}N isotope effect, Cook and coworkers (Cook et al, 1981) provided some evidence to support this. Unfortunately, due to the limit of the resolution of the current X-ray crystal structures, this conjecture can not be proven directly from the crystal structure.

However with the advent of X-ray crystal structure for over a half dozen different dehydrogenases, a more complete picture of the relative positioning of the substrate and coenzymes has emerged. Rossman (Rossman et. al., 1975), You (You et al., 1975) and their coworkers have suggested that the specificity of a dehydrogenase with respect to transfer of the C4 proton of the nicotinamide ring reflects the bound conformation of the nicotinamide-glycosyl bond. Their model is summarized schematically in the following figure, Scheme 6.1. Those enzymes that are pro-R specific bind the coenzyme with the nicotinamide ring *anti* whereas the pro-S specific enzymes bind the ring *syn*. It has to be noted that even among that half dozen dehydrogenases whose structure are known and their

binary and ternary complex, people have found some exceptions (Grau, et al., 1981).

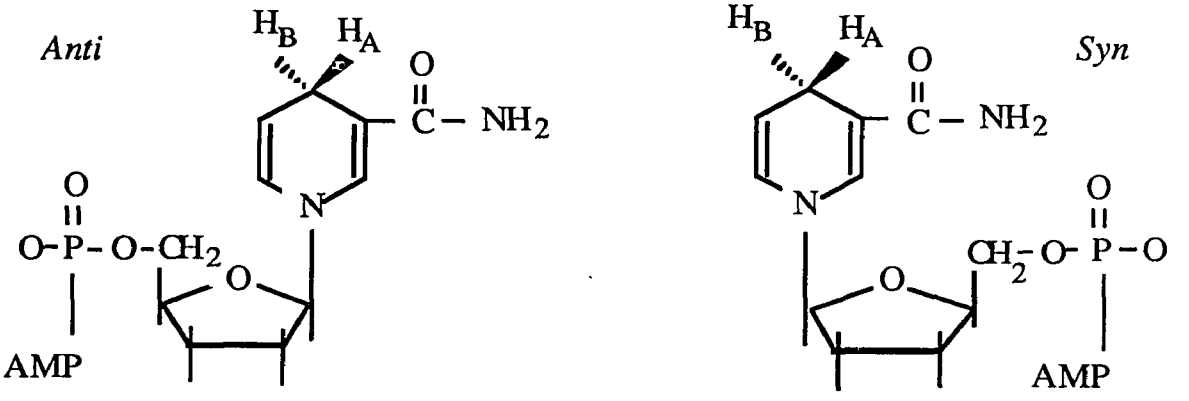

Scheme 6.1. The relation between the rotational isomers round the glycosyl bond and relative orientation of N4 methylene protons.

Thermodynamic studies on different dehydrogenases also seem to provide some common rules. It has been noted that aldehydes and α-ketoacids are reduced under the catalytic influence of enzymes that generally use the A-side of the dihydropyridine ring whereas the more stable ketones are reduced with enzymes that use B-side. Again, some exception have been found (You, 1985).

Based on the observation above and other considerations, Benner and coworkers (Benner et al., 1989) suggested four postulates to explain the stereoselectivity of enzymatic oxidation-reduction with respect to the A and B sides of NADH:

(1) the pro-R hydrogen atom is transferred when the nicotinamide cofactor is bound in an *anti* conformation, and the pro-S

hydrogen is transferred when the cofactor is bound in a *syn* conformation.

(2) *syn*-NADH is a stronger reducing agent than *anti*-NADH.

(3) "optimal" enzymes bind substrates so as to bring the ratio of free energies of the bound substrates closer to unity than they are in the unbound, or free condition, in accordance with the principle of matched internal states.

(4) evolutionary pressures push enzymes toward perfection, that is to the point where diffusion is rate limiting, or partially rate limiting, so that further changes in their chemistry can not improve their rate.

One way to directly see how the enzyme might distort the nicotinamide ring is to see how the enzyme affects the C4-H bond of the NAD(P)H upon binding to the enzyme. The C-H stretch mode of the bond could be used to indicate the "enzyme effect", when we see the frequency difference of that mode between that found for NAD(P)H in protein and in solution. It is known that there are significant differences between axial and equatorial C-H stretch frequencies (see below).

Measurements of C-H stretching mode are very difficult, since there are so many C-H bonds in the protein and cofactor. We solved this problem by deuteriating the cofactor's C4 hydrogen atom(s). This moves the stretching frequency down about 1000 cm^{-1} from 3100 cm^{-1} to near 2100 cm^{-1}. This is a spectrally silent region, apart from some very low intensity water combination bands.

6.2 Materials and Methods

Materials: Glucose dehydrogenase from *L. mesenteroides* was purchased from US Biochemical Corp. (Cleveland, OH), horse liver alcohol dehydrogenase and yeast aldehyde dehydrogenase were purchased from Sigma (St. Louis, MO), and L. *mesenteroides* alcohol dehydrogenase ($NADP^+$) was purchased from Research Plus Inc. (Bayonne, NJ). Glucose-1-D (98 atom% D) was purchased either from MSD Isotopes (St. Louis, MO) or Cambridge Isotope Laboratories (Woburn, MA). Ethanol-1,1-D2 (99 atom% D) was purchased from Cambridge Isotope Laboratories (Woburn, MA). Bio-Gel P-2, a polyacrylamide gel was purchased from Bio-Rad (Richmond, CA).

Stereospecifically deuterium labeled A and B side NAD(P)H and deuterium labeled C4-D-NAD^+ were prepared partly according to the procedure described by Cleland and coworkers (Viola, et al. 1979). The basic ideal is to use the dehydrogenases' stereospecificity and reduced NAD^+ by a stereospecific enzyme and deuterium labeled substrate.

Preparation of A-side NAD(P)D. For preparation of A side NADD, 60 mM ethanol-1,1-D2, 100 mM NAD^+, 100 units of horse liver alcohol dehydrogenase, and 200 units of yeast aldehyde dehydrogenase were mixed in 2 ml of 200 mM TAPS and 0.3 M KCl at pH 9.0 and 25 °C. The reaction was complete in 2 hours as determined by absorbance at 340 nm. Once the ratio of the absorbance at 260 to that at 340 nm reached 2.4, we stopped the reaction by separating the enzyme from the solution. Throughout the reaction, a small amount of 1 N NaOH solution was added to keep the mixture pH at 9.0. After reaction, the enzymes were removed by

filtration in centricon-10 (Amicon, Lexington, MA), and these proteins could be reused. For preparation of A-side NADPD, we used exactly same procedure, except that $NADP^+$ was used instead of NAD^+, and in place of horse liver alcohol dehydrogenase, we used *L. mesenteroides* alcohol dehydrogenase which is $NADP^+$ specific.

Preparation of B-side NAD(P)D. 110 mM of Glucose-1-D, 100 mM of $NAD(P)^+$, 1000 units of *L. mesenteroides* glucose dehydrogenase were mixed in 200 mM Tris-HCl buffer at pH 8.0. Again the reaction was complete in about 2 hours as determined by absorbance at 340 nm, and we stopped the reaction at the time the ratio 260 to 340 nm reached 2.4. Adding small amounts of 1N NaOH was needed to keep the pH at 8.0 throughout the reaction. Finally, the centricon-10 was used to separate the protein from the solution.

NAD(P)D Isolation. A Bio-gel P2 column was packed following the instruction provided by Bio-Rad in 4 °C. For purifying the NADD distilled water was used as eluent. Because the most stable pH range for NADPH is around pH 8.0, we used 10 mM Tris-HCl, pH 8.0 instead of distilled water. We pooled the fractions with $A_{260}/A_{340} < 2.3$. Finally, we lyophilized the samples to dryness, and then stored them below 0 °C.

6.3 Results

Spectra. Figure 6.1 shows the Raman spectrum of deuterated NADPH in solution. Panel (a) is the spectrum of the 200 mM $NADPD_A$ (i.e. A side deuterated) solution and (b) is the spectrum of the 200 mM solution of $NADPD_B$. Panel (c) is the the result of subtracting (b)-(a). The relative intensity scales between a, b, and c have been presented.

A very interesting question is whether, in solution, the dihydronicotinamide ring is in the planar form or puckered in a "boat" form. Similarly, what is the ring conformation when the coenzyme is bound to protein, and are there any difference between the coenzymes in solution and in protein? Using NMR studies, Oppenheimer and coworkers (Oppenheimer et al., 1978) pointed out that for NADH in solution the conformation of the ring pucker depend on whether the dihydropyridine and adenine rings are stacked together or not. It is now generally accepted a fraction of the molecular dihydropyridine and adenine rings are stacked together in solution and form a "folded" conformation. Oppenheimer and others have estimated that roughly 70% of NADH is in the "open" form with the rest of them in the "folded" form. Oppenheimer et al. proposed that the dihydronicotinamide ring was planar for those molecules in the "open" form, while in the "folded" form the ring take on a boat conformation. The evidence for this puckering was derived from the unusual vicinal coupling constant. The $^3J_{B\text{-}5}$ (3.9 Hz) is larger than the $^3J_{A\text{-}5}$ (3.1 Hz) in NADH. This kind of difference is not found in NMNH, in which both coupling constants have the same value of 3.5 Hz.

When the dihydronicotinamide ring puckers, one of the C4

hydrogens is in the equatorial position while the other is in the axial position. By calculation, Oppenheimer pointed out that the C-H bond of the equatorial displaced proton would approach an sp^2-1s hybrid orbital which has a bond energy of 109 kcal/mol, whereas that of the axially displaced hydrogen would approach a weaker 2p-1s hydride, whose energy would be approximately 80 kcal/mol. This kind of the bond energy difference should affect the C-H stretching mode, and so should be observed by vibrational spectroscopy. Studying the IR spectra of deuterated *exo*-Tricyclo[3.2.1.0]Octane, LaLonde and coworkers (LaLonde et al. 1971) did observe about 20 cm^{-1} difference in the C-D stretching mode between the deuterium atom on the equatorial position and axial position. The $C\text{-}D_{equatorial}$ stretching mode has a higher frequency than that of $C\text{-}D_{axial}$. We have studied the C-D stretch mode of the adduct of NAD-N4-D with sulfite and cyanide since the deuterium atom in these adducts are believed to be in the equatorial position (Oppenheimer, 1989). We have observed a C-D stretch mode in this case at 2180 cm^{-1}, about 65 wavenumbers upward from the C-D stretch mode of A side or B side NADD (see below). This also indicates that the equatorial C-D stretch mode has a higher frequency than axial C-D stretch mode.

The data in Figure. 6.1.c shows clearly a difference between A side (figure 6.1.a) and B side (figure 6.1.b) deuterated NADPD in solution. This difference spectrum can not be explained as due to a difference in frequency between the major peaks in (a) and (b) as based on the following analysis. In a study by Rousseau (Rousseau, 1981), when the separation of the two Raman peaks is about one tenth of the full width of the peak at half height (Γ), the separation of

the peak and the valley in the difference spectrum reaches a limit of 0.58Γ. In our case, the width of the peaks (Γ) is about 20 cm^{-1} and the separation of the peaks in figure (a) and (b) is less than 2 cm^{-1}. Thus the separation of the peak and the valley in the difference spectrum (c) should be around 0.58Γ which is about 12 cm^{-1}, but not 35 cm^{-1} as we observed in (c).

To explain the difference spectrum (c), it is reasonable to assume that spectra (a) and (b) contain a major peak and one or more small peaks as well. The major peak does not shift at all and the difference spectrum is due to the shift of the small peaks. The major peak can be assigned from the C-D stretch when the dihydronicotinamide ring in the planar conformation, which is the major population, and the small peaks come from the C-D stretch when the dihydronicotinamide ring puckers in the boat form. This idea is consistent with the previous NMR studies. For a further analysis, we need to estimate the width of the small peak, we take it to be the same as the major peak's width, about 20 cm^{-1}, and there is no reason to assume that the width is larger than 35 cm^{-1}. So, according to Rousseau's studies, if the band width (Γ) smaller than the separation of the the peak and the valley in the difference spectrum ($\Delta\nu_o$), then the two peaks separation ($\Delta\nu$) should be roughly equal to the separation of the peak and the valley in the difference spectrum ($\Delta\nu_o$). For two Lorentzian lines having a center intensity equal to I^o, the full width at half equal to Γ, a separation of the two peaks equal to $\Delta\nu$, and the intensity of the difference spectrum measured intensity difference at maximum and minimum in the difference spectrum equal to I^o_D, then Rousseau calculated a relation

as following: $\Delta\nu/\Gamma=0.38I^{o}_{D}/I^{o}$. Here, we take the $\Delta\nu=35$ cm^{-1}, $\Gamma\approx25$ cm^{-1}, $I^{o}_{D}\approx(0.3)I$, where, the I is the total center intensity of (a). Then, we get $I^{o}\approx(0.1)I$. We thus calculate that only about 10% of the total molecules in solution pucker to form the boat conformation and the rest of them are in the planar form. Also, from the (c) we can tell that when the dihydronicotinamide ring is in the boat form, the A side C-D stretch frequency is about 2105 cm^{-1}, and B side C-D stretch frequency is about 2140 cm^{-1}. This suggests that in the solution, when the dihydronicotinamide ring goes to boat pucker form, and the B side hydrogen (deuterium) atom is in the equatorial position and the A side one is in the axial position.

While deuteriating the C4 hydrogen(s) separates this C-H stretch frequency from other C-D modes, the C-H Raman cross section is very small. Also, for spectra of protein-bound coenzyme, the concentration of coenzyme is limited by the concentration limit of the protein solubility. Typically we can obtain the concentration of the bound coenzyme about 5 mM. It is thus not very easy to detected it *in situ.* Figure 6.2 shows the Raman spectrum of DHFR (b), its binary complex with A side NADPD from 2000 cm^{-1} to 2500 cm^{-1} (a), and the C-D stretch bands of A side NADPD bound in DHFR (c), obtained by the subtraction of (a) from (b). The main feature in the spectra of apo and holo enzyme, (b) and (a), is a very broad band. This is a band arising from the solvent (Carey, 1985). Comparing the two spectra carefully, we can see that the most of the small features are same, which are due to the fixed noise patten of the reticon detector as we discussed in the chapter 2. By subtraction, we can get rid of that and obtain a very clear C-D stretch spectrum (c).

In Figure 6.3, panel (a) is the C-D stretching mode of A side deuterated $NADD_A$ in solution after the water spectrum was subtracted. Panel (b) is the stretching mode when $NADD_A$ is bound to LDH. We can see that C-D stretch mode of bound A side $NADD_A$ in LDH remains almost unchanged compared with that in solution. Panel (c) is the spectrum of the bound A side NADPD in DHFR. Figure 6.4 shows that C-D stretch spectra of B-side NAD(P)D in solution (a), bound to LDH (b), and $NADPD_B$ bound to DHFR.

When NADD binds to LDH, we can see that C-D stretch modes for both A side and B side deuterated are extremely different. For A side C-D stretch (figure.6.3.b), the mode position is almost as same as that in solution (around 2112 cm^{-1}). But for the B side, the C-D stretch shifts to 2140 cm^{-1} (figure.6.3.a), about thirty wavenumbers higher than that of A side. As we mentioned before, C-H stretching modes for both equatorial and axial hydrogen are different, showing at higher frequency for the equatorial proton. Thus, our data suggest that the dihydronicotinamide ring is puckered into the boat form when NADH binds to LDH, with the A side hydrogen (or deuterium in our case) in the axial position and the B side hydrogen in the equatorial position. For A side bound $NADPD_A$ in DHFR (figure 6.3.c), the C-D stretch mode at 2120 cm^{-1} is very similar to C-D stretch mode of NADD in solution. For B side NADPD bound to DHFR, however, the C-D stretching mode shifts to 2160 cm^{-1}, suggesting, again, the dihydronicotinamide ring of NADPH is distorted to a boat form, with the A side hydrogen on the axial position and B side hydrogen on the equatorial position. It is interesting to note that both LDH and DHFR belong to the pro-R (or A side) class of dehydrogenases. It seems that

when NADH binds in A side host enzymes, the dihydronicotinamide ring puckers to the boat shape and A side hydrogen goes to the axial position. This may be a common rule for all the NAD-linked dehydrogenases. This needs farther study.

6.4 Discussion.

Distortion of the Dihydronicotinamide Ring in Solution. By NMR studies, Oppenheimer (Oppenheimer et al., 1978) pointed out that in solution when NADH is in the "folded" form and the dihydronicotinamide ring is puckered into boat form, the B side hydrogen faces to the adenine ring and in the equatorial position with the A side hydrogen in the axial position. As we saw in the result section, our Raman results can be rationalized within this analysis. In other words, we did see that some population of the dihydronicotinamide rings form a boat conformation, and the B side proton is in the equatorial position while the A side proton is in the axial position. However, the NMR studies suggested that about 30% of the NADH in solution is in the "folded" form. In our case, we used NADPH instead of NADH. Here the 2'-phosphate should help in stabilizing the "folded" form (Oppenheimer, 1978) and concentration of NADPH we used here (200 mM) is much higher than Oppenheimer used in his NMR studies. So we should expect no less than 30% of the molecular in "folded" form. But we only obtained about 10% of the molecules in the "folded" form. The reason for that is not clearly understood. One of the possibilities is that the structure of the "folded" form of NADPH in solution is not very stable during our Raman measurement. It is possible that inside the fairly strong laser beam most of the "folded" form is disrupted and so we see only about 10% of molecules in the the "folded" form.

Distortion of Dihydronicotinamide Ring when Cofactors Bind to Enzyme. By studying ^{15}N secondary isotope effect, Cook and coworkers (Cook et al. 1981) suggested that when NAD and NADH

bind to liver alcohol dehydrogenase, the protein distorts the coenzyme's nicotinamide/dihydronicotinamide rings. They proposed that for the bound NAD or NADH molecule, the N-1 to C-1 bond of the ribose is no longer co-planar with the nicotinamide ring but is bent far enough out of plane to destroy any resonance between a lone pair on N-1 and the remaining double bonds in the ring. The ring does not remain planar but forms a boat conformation in respose to the deformation brought to bear by the enzyme. For bound NAD(P)H in LDH and DHFR, our Raman data agree very well with this idea. We do clearly see that kind of dihydronicotinamide ring conformation change when the coenzyme binds to those proteins. And the coenzymes in the both enzyme, LDH and DHFR, pucker in the same way, the A side proton goes to the axial position and B side one goes to the equatorial position.

We believe that the ring pucker form of bound NAD(P)H in proteins is partly due to the host enzyme, or in the other words, is due to the interaction between the enzyme and NAD(P)H. For example, from the X-ray crystal structure, Kraut and his coworkers (Bystroff et al. 1990, Filman et al. 1982) have found that there is an oxygen atom of the protein backbone, carbonyl oxygen O:97, that is very close to the C4 carbon of the nicotinamide ring. The distance between the oxygen and the carbon is 3.3 Å which is too close to be considered as normal van der Waals interaction (about 3.6 Å from carbon to oxygen). Therefore, they have suggested that there must be a some kind of hydrogen bond formed between the C-H and the oxygen atoms.

As discused before, the $C\text{-}D_{equatorial}$ bond has a higher bond

energy than that C-D_{axial}. By calculation, Oppenheimer suggested this kind of the energy can be as different by as much as 30 kcal per mole. That much bond energy difference is large enough to prohibit B side proton transfer relative to A side transfer. Also, more than thirty years ago, Levy and Vennesland pointed out that the axial hydrogen was likely to be oxidized in the reaction because it was this hydrogen that caused the smallest shift of atoms from the positions they occupied in the oxidized, planar form of the coenzyme.

Figure 6.1: Raman spectra of (a) A side NADPD (200 mM), B side NADPD (200 mM) at 4 °C in 200 mM Tris-HCl buffer, pH 8.0, and (c) difference spectrum of (b) and (a). This latter spectrum Y axis was amplified by a factor 2.5 for clarity. The laser line to probe the sample was 647.1 nM with 600 mW incident power.

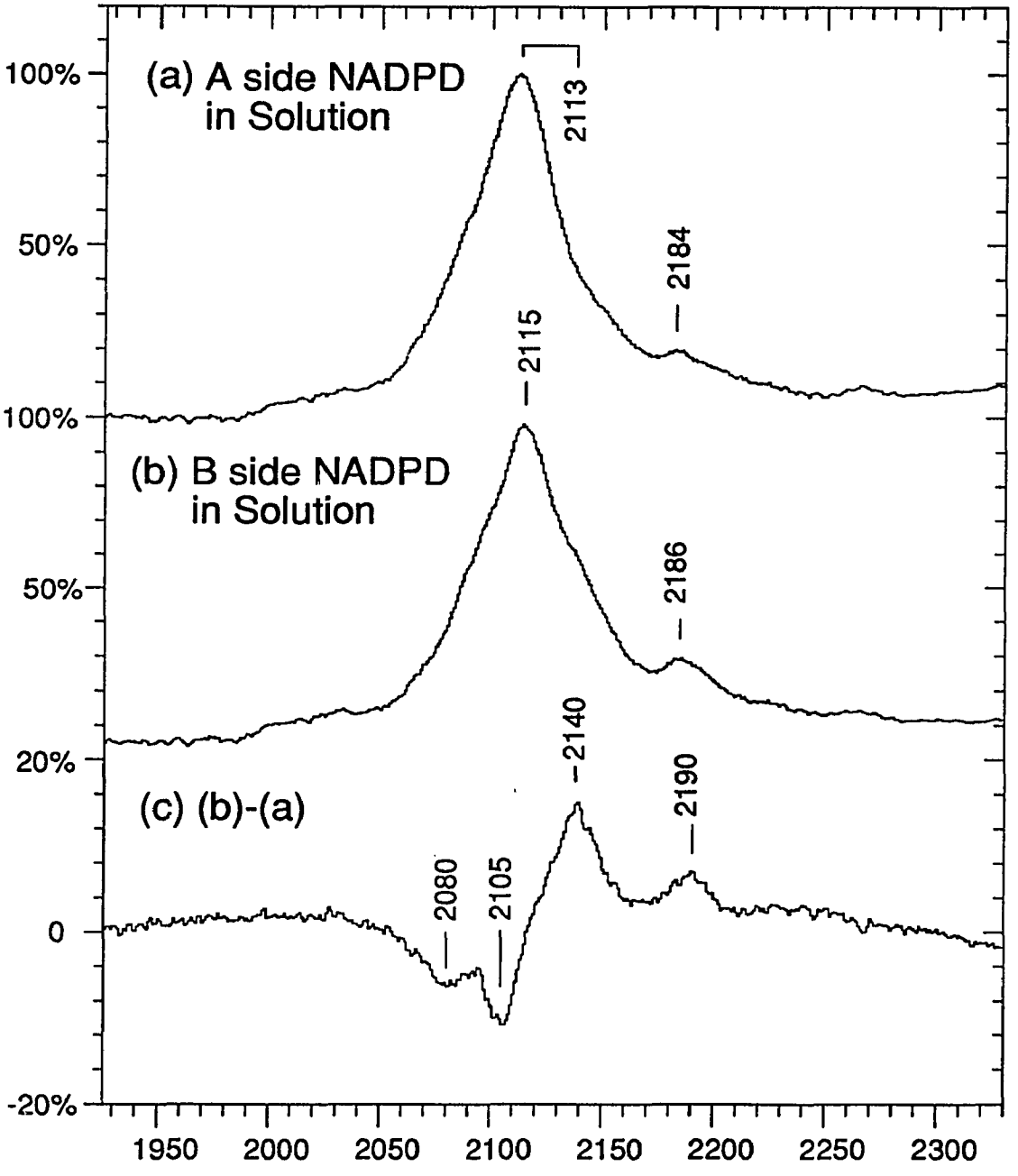
100%
50%
100%
50%
20%
0
-20%
(a) A side NADPD
in Solution
2113
2184
2115
(b) B side NADPD
in Solution
2186
2140
2190
(c) (b)-(a)
2080
2105
1950
2000
2050
2100
2150
2200
2250
2300

Figure 6.1

Figure 6.2: Raman spectra of (a) binary complex of DHFR and A side deuterium labelled NADPH (LDH:NADPD=5:4.5 mM); (b) apo-DHFR at 4 °C in 10 mM Tris-HCl pH 8.0; and (c) bound A side NADPD in DHFR, obtained by calculating the difference spectrum between binary complex and apo enzyme. The 514.5 nM laser line from an argon laser were used to probe the samples, and the laser power on the sample was 200 mW.

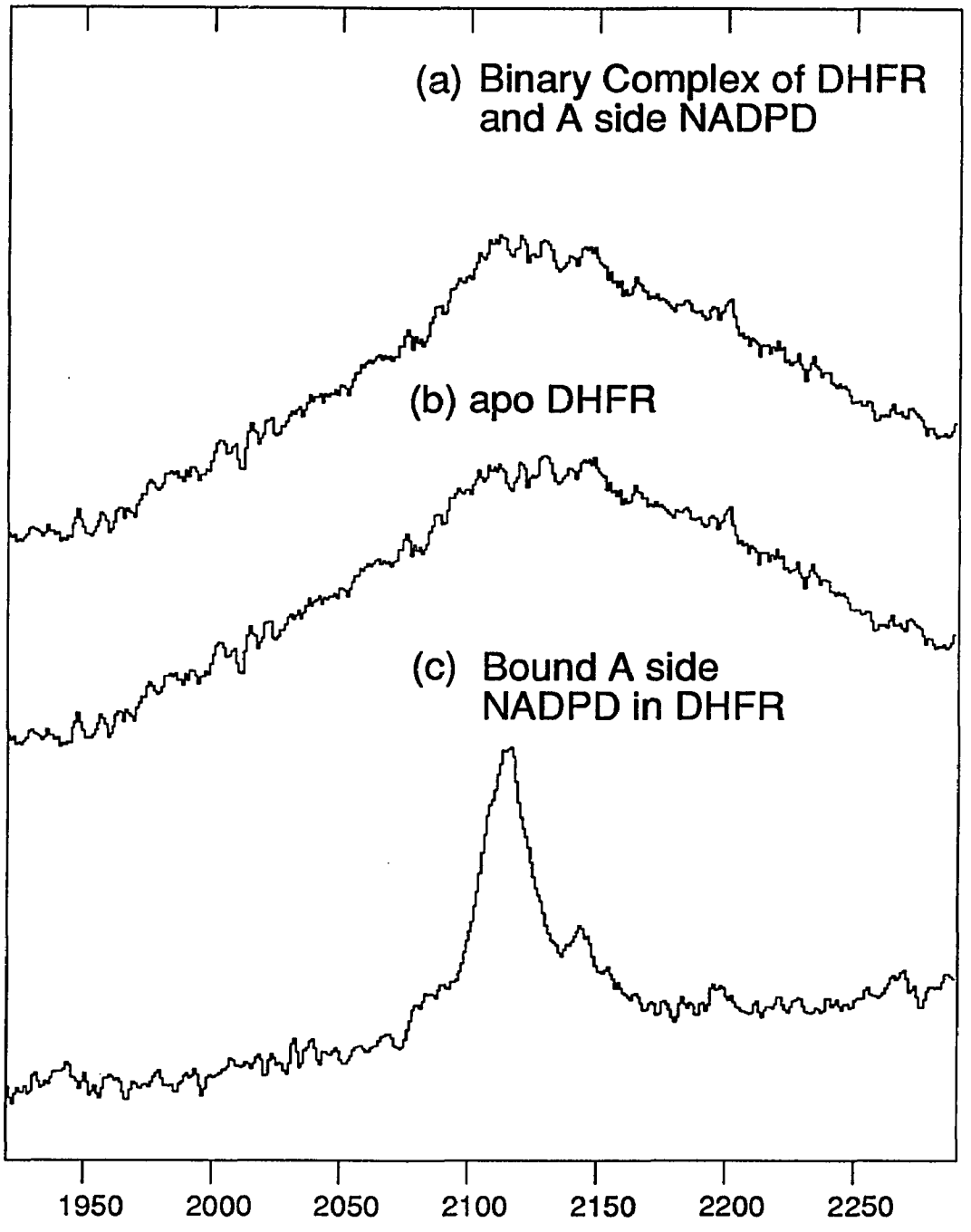
(a) Binary Complex of DHFR and A side NADPD
(b) apo DHFR
(c) Bound A side NADPD in DHFR
1950
2000
2050
2100
2150
2200
2250

Figure 6.2

Figure 6.3: Raman spectra of (a) A side NADPD in solution (same as in Figure 6.1.b); (b) bound A side NADD in LDH (LDH:NADD=1:3 mM) at 4 °C in 10 mM Tris-HCl pH 7.4; and (c) bound A side NADPD in DHFR (DHFR:NADPD=1:0.9 mM) at 4 °C in 10 mM Tris-HCl pH 8.0. For the protein studies, the 514.5 nM laser line from an argon laser were used to probe the samples, and the laser power on the sample was 200 mW.

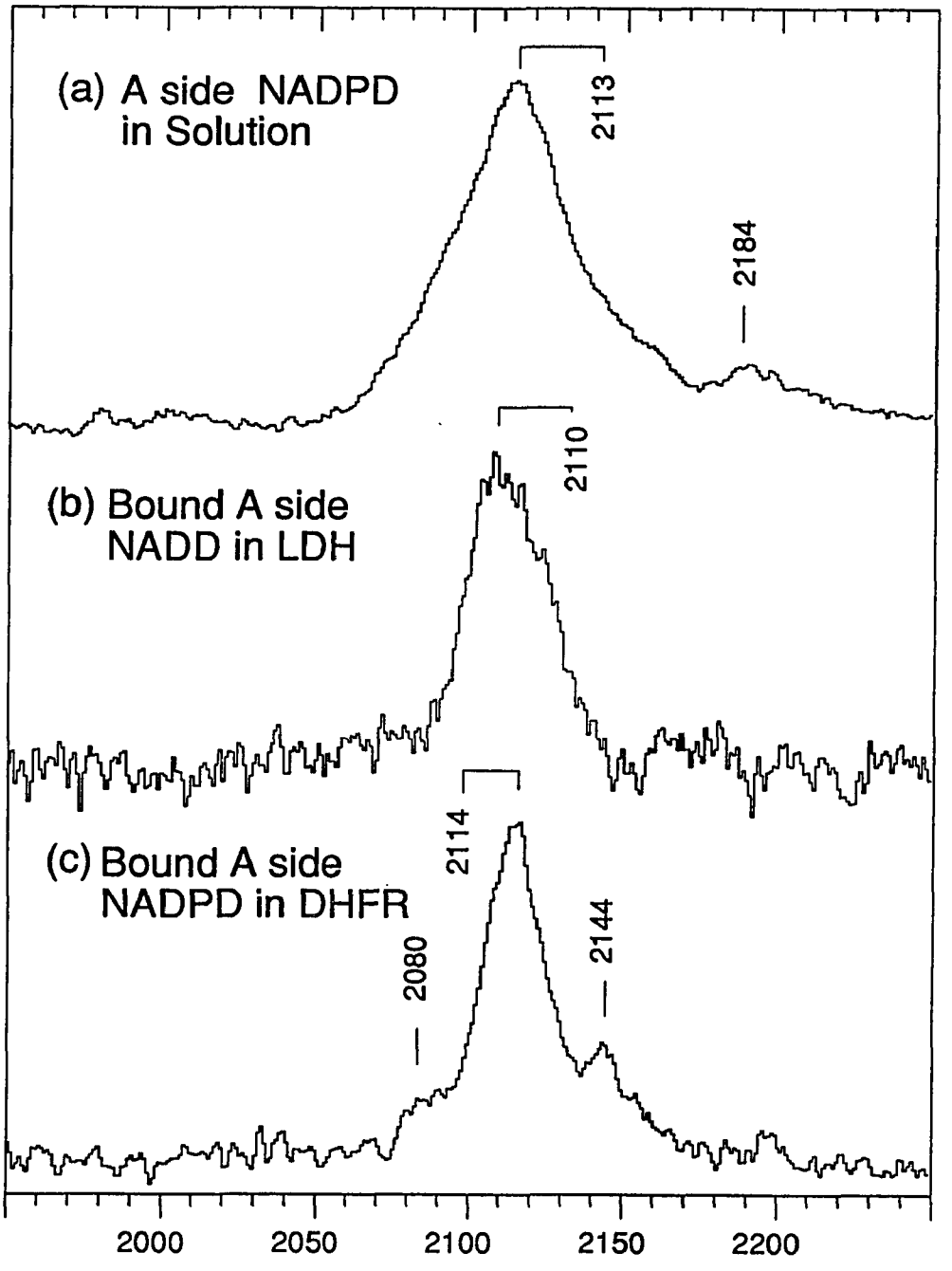
(a) A side NADPD
in Solution
2113
2184
(b) Bound A side
NADD in LDH
2110
(c) Bound A side
NADPD in DHFR
2114
2080
2144
2000
2050
2100
2150
2200

Figure 6.3

Figure 6.4: Raman spectra of (a) B side NADPD in solution (same as in Figure 6.1.b); (b) bound B side NADD in LDH (LDH:NADD=1:3 mM) at 4 °C in 10 mM Tris-HCl pH 7.4; and (c) bound B side NADPD in DHFR (DHFR:NADPD=1:0.9 mM) at 4 °C in 10 mM Tris-HCl pH 8.0. For the protein studies, the 514.5 nM laser line from an argon laser were used to probe the samples, and the laser power on the sample was 200 mW.

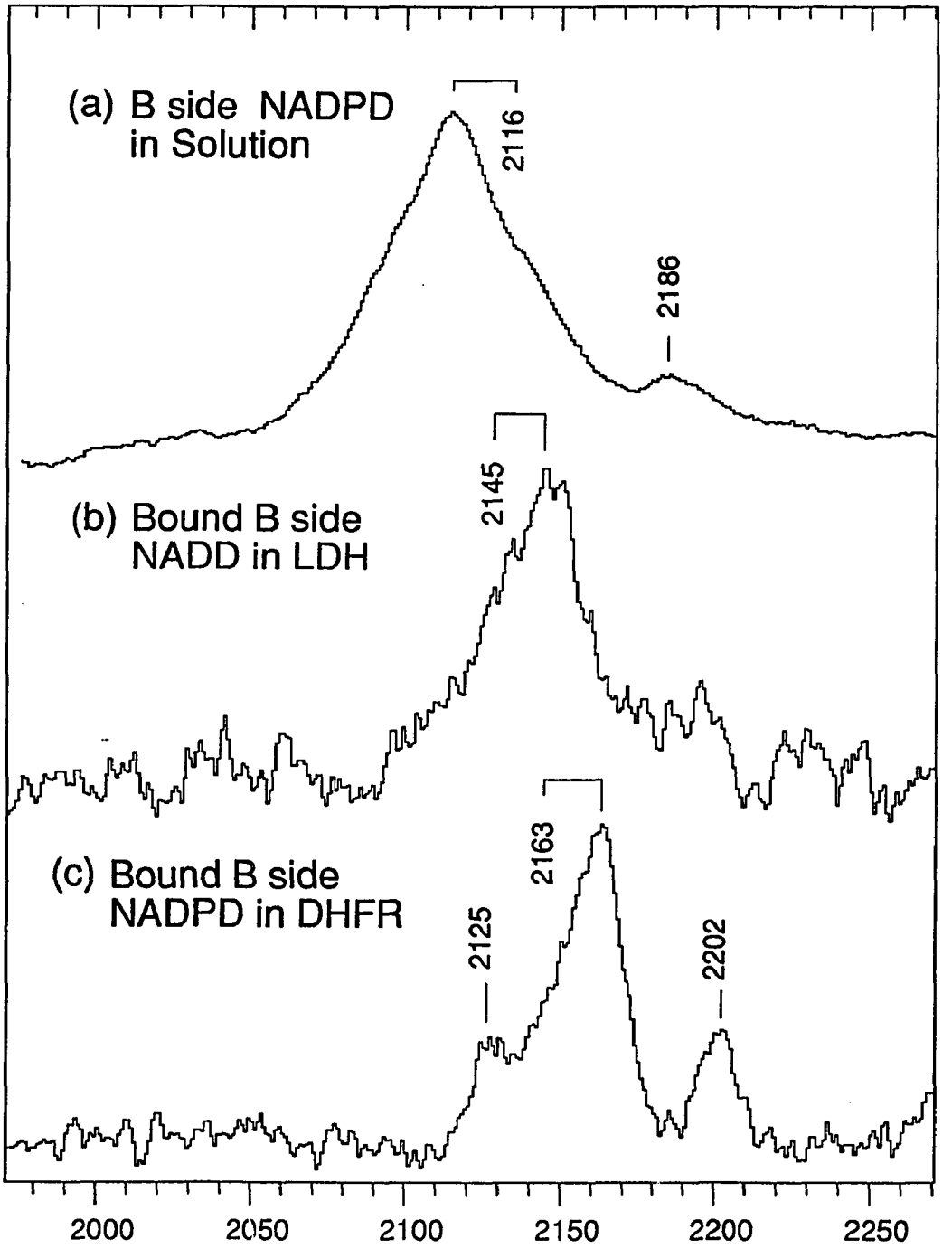
(a) B side NADPD
in Solution
2116
2186
(b) Bound B side
NADD in LDH
2145
(c) Bound B side
NADPD in DHFR
2125
2163
2202
2000
2050
2100
2150
2200
2250

Figure 6.4

Appendix

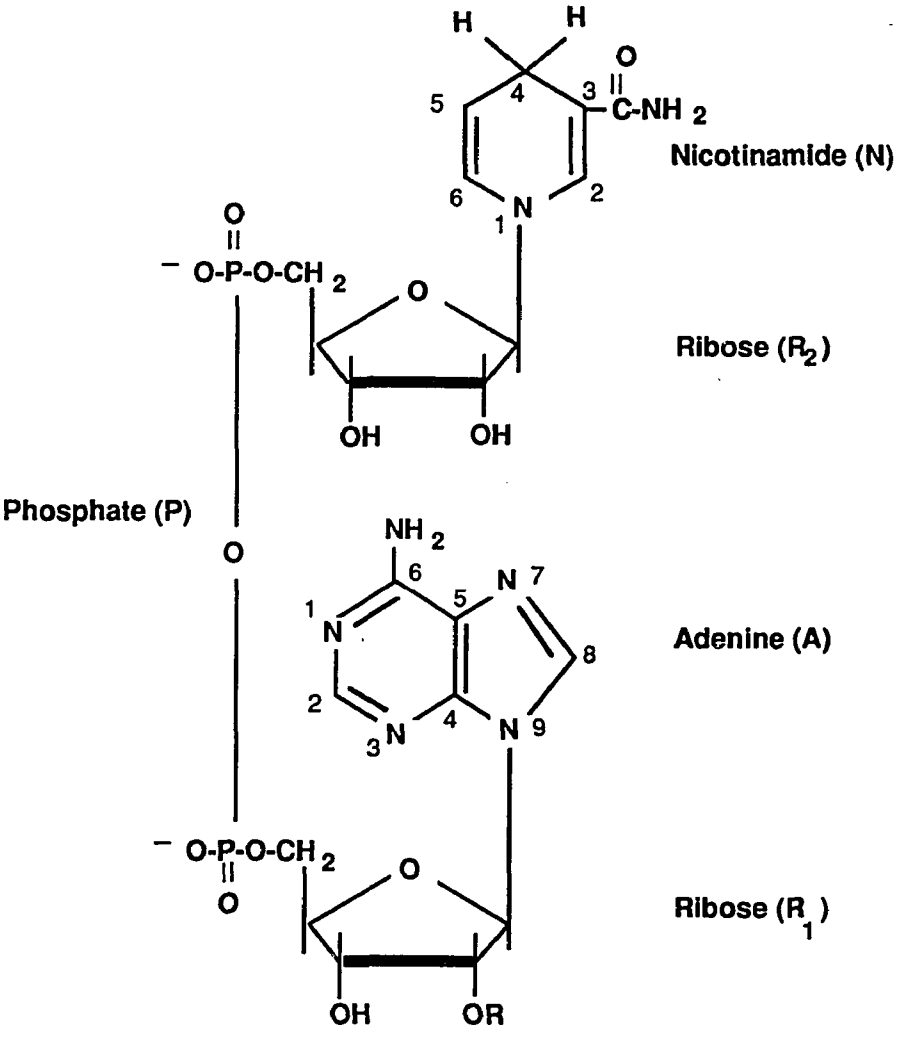

R = H : NADH

R = PO_3^{2-} : NADPH

Scheme of NAD(P)H

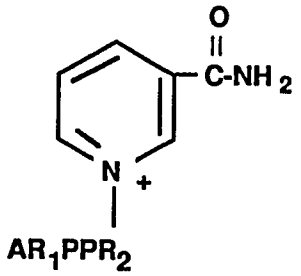

NAD+

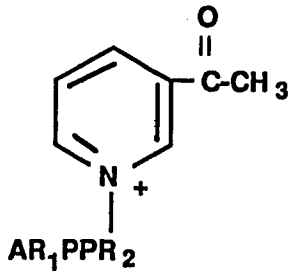

APAD+

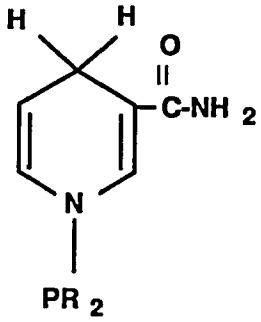

NMNH

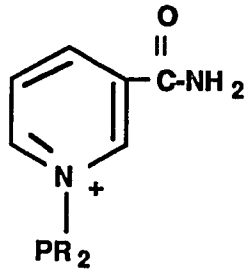

NMN +

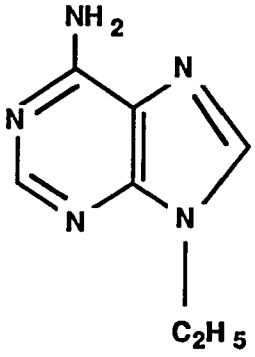

9-EtAd

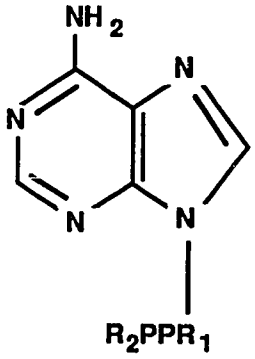

ADPR

Scheme of NAD-Coenzymes

REFERENCES

Albrecht, A. C. *J. Chem. Phys.* **1961**, *34*, 1476.

Anderson, V. E.; LaReau, R. D. *J. Am. Chem. Soc.* **1988**, *110*, 3695.

Bajdor, K.; Nishimura, Y.; Peticolas, W. L. *J. Am. Chem. Soc.* **1987**, *109*, 3514-3520.

Benner, S. A. *Experientia* **1982**, *38*, 633-637.

Benner, S. A.; Nambiar, K. P. in *Functional Explanations for Stereoselectivity in Dehydrogenases*; Frey, P. A.; Elsevier Science Publishing Co., New York, 1986; pp 28-43.

Bentley, R. *Molecular Asymmetry in Biology 2*; Academic: New York, 1970; .

Bowman, W. D.; Spiro, T. G. *J. Raman Spectrosc.* **1980**, *9*, 369-371.

Burgner II, J. W.; Ray, W. J. *Biochem.* **1984**, *23*, 3636-3648.

Burgner II, J. W.; Ray, W. J. *Biochem.* **1984**, *23*, 3626-3635.

Burgner II, J. W.; Ray, W. J. *Biochem.* **1984**, *23*, 3620-3626.

Burgner II, J. W.; Oppenheimer, N. J.; Ray, W. J. *Biochem.* **1987**, *26*, 91-96.

Bystroff, C.; Oatley, S. J.; Kraut, J. *Biochem.* **1990**, *29*, 3263-3277.

Callender, R.; Deng, H.; Sloan, D.; Burgner, J.; Yue, T. K. *Proccedings of International Society for Optical Engineering*, **1989**, 154-160.

Carey, P. R. *Biochemical Applications of Raman and Resonance Raman Spectroscopy.*; Academic Press: New York, 1982; pp 1-262

Chandrasekhar, K.; McPherson, A.; Adams, M. J.; Rossmann, M. G. *J. Mol. Biol.* **1973**, *146*, 561-587.

Chen, D.; Yue, K. T.; Martin, C.; Rhee, K. W.; Sloan, D.; Callender, R. *Biochem.* **1987**, *26*, 4776-4784.

Clarke, A. R.; Wigley, D. B.; Chia, W. N.; Holbrook, J. J. *Nature* **1986**, *324*, 699-702.

Colowick, S. P.; van Eys, J. ;. P., J. H. in *Comprehensive Biochemistry*; Statz, F. &.; Elsevier, 1966;

Cook, P. F.; Oppenheimer, N. J.; Cleland, W. W. *Biochem.* **1981**, *20*, 1817-1825.

Deng, H.; Zheng, J.; Burgner, J.; Sloan, D.; Callender, R. *Biochem.* **1989**, *28*, 1525-1533.

Deng, H.; Zheng, J.; Burgner, J.; Callender, R. *J. Phys. Chem.* **1989**, *93*, 4710-4713.

Eklund, H.; Samama, J.-P.; Wallen, L.; Branden, C.-I.; Akeson, A.; Jones, T. A. *J. Mol. Biol.* **1981**, *146*, 561-587.

Eklund, H.; Samama, J.-P.; Jones, T. A. *Biochem.* **1984**, *23*, 5982-5996.

Eklund, H.; Branden, C.-I. *Pyridine Nucleotides*; Wiley: New York, **1988**; pp 250-260.

Euler, v. H.; Alber, H.; Schlenk, F. *HoppeSeyler's Z. Physiol. Chem.* **1936**, *240*, 113-122.

Feeney, L.; Birdsall, B.; Roberts, G. C. K.; Burgen, A. S. V. *Nauture* **1975**, *257*, 564-566.

Fersht, A. *Enzyme Structure and Mechanism*; Freeman and Co.: New York, 1985; pp 1-475 .

Filman, D. J.; Bolin, J. T.; Matthews, D. A.; Kraut, J. *J. Biol. Chem.* **1982**, *257*, 13663-13672.

Fisher, H. F.; Adija, D. L.; Cross, D. G. *Biochem.* **1969**; pp 4424-4430.

Grau, U. M.; Trommer, W. E.; Rossmann, M. G. *J. Mol. Biol.* **1981**, *151*, 289-307.

Hanson, K. R.; Rose, I. A. *Acc. Chem. Res.* **1975**, pp 1-14.

Holbrook, J. J.; Liljas, A.; Steindel, S. J.; Rossmann, M. G. in *Lactate Dehydrogenase*; Academic Press, New York, 1975; pp 191-293.

Johnson, B. B.; Peticolas, W. L. *Ann. Rev. Phys. Chem.* **1976**, *27*, 465.

Kraut, J.; Matthews, D. A. in *Dihydrofolate Reductase*; Jurnak, F. A. McPherson, A.; John Wiley, New York, 1987; pp 1-72.

LaLonde, R. T.; Ding, J.-y.; Tobias, M. *J. Am. Chem. Soc.* **1967**, *89*, 6651-6657.

LaReau, R. D.; Wan, W.; Anderson, V. E. *Biochem.* **1989**, *28*, 3619-3624.

LaReau, R. D. **1990**. *Thesis*, Brown University.

Michaelis, L.; Menten, M. L. *Biochem. Z.* **1913**, 49, 333

Nambiar, K. P.; Stauffer, D. M.; Kolodziej, P., A.; Benner, S. A. *J. Am. Chem. Soc.* **1983**, *105*, 5886-5890.

Nishimura, Y.; Tsuboi, M. *J. Molec. Str.* **1986**, *146*, 123-153.

Oppenheimer, N. J.; Arnold, J., Lyle J.; Kaplan, N. O. *Biochem* **1978**, *17*, 2613-2619.

Oppenheimer, N. J.; Marschner, T. M.; Malver, O.; Kam, B. L. in *Stereochemical Aspects of Coenzyme-Dehydrogenase Interactions*; Frey, P. A.; Elsevier Science Publishing Co., New York, 1986.

Parker, D. M.; Holbrook, J. J. Sund, H.; de Gruyter, Berlin, 1977; pp 485-502.

Piontek, K.; Chakrabarti, P.; Schar, H.-P.; Rossmann, M. G.; Zuber, H. *Proteins* **1990**, *7*, 74-92.

Rafilipomanana, C.; Cavagnat, D.; Lassegues, J. C. *J. Mol. Strut.* **1985**, *129*, 215-227.

Rao, C. N. R.; Dwivedi, P. C.; Ratajczak, H.; Orville-Thomas, W. J. *J. Chem. Soc. Faraday Trans.* **1975**, *71*, 955-966.

Rodgers, E. G.; Peticolas, W. L. *J. Raman Spectrosc.* **1980**, *9*, 372-375.

Rousseau, D. L. *J. Raman Spec.* **1981**, *10*, 94-99.

Stidham, H. D. *Spectrochim. Acta.* **1973**, *21*, 23-32.

Stinson, R. A.; Holbrook, J. H. *Biochem. J.* **1973**, *287*, 291-296.

Stryer, L. *Biochemistry*; W.H. Freeman and Company: **1988**; pp 201-232 .

Tang, J.; Albrecht, A. C. *J. Chem. Phys.* **1968**, *49*, 1144.

Tang, J.; Albrecht, A. C. *Raman Spectrosc.* **1970**, *2*, 33.

Thijs, R.; Zeegers-Huyskens, T. *Spectrochemica Acta.* **1984**, *40A*, 307-313.

Thompson, C. P.; Grady, J. K.; Chasteen, N. D. *J. Biol. Chem.* **1986**, *261*, 13128-13134.

Tsuboi, M.; Nishimura, Y.; Hirakawa, A. Y.; Peticolas, W. L. in *Resonance Raman Spectroscopy and Normal Modes of the Nucleic Acid Bases*; Spiro, T. G.; John Wiley & Sons, 1987;

Viola, R. E.; Cook, P. F.; Cleland, W. W. *Anal. Biochem.* **1979**, *96*, 334-340.

Waldman, A. D. B.; W., H. K.; Clarke, A. R.; Wigley, D. B.; Barstow, D. A.; Atkinson, T.; Chia, W. N.; Holbrook, J. J. *Biochem. Biophys. Res. Comm.* **1988**, *150*, 752-759.

Warburg, O.; Christian, W. *Biochem, Z.* **1936**, *287*, 291-296.

Westheimer, F. H. in *Mechanism of Action of the Pyridine Nucleotides*; Dolphin, D.; Poulson, R. Avramovic, O.; John Wiley & Sons, New York, 1987; pp 253-322.

White, J. L.; Hackert, M. L.; Buehner, M.; Adams, M. J.; Ford, G. C.; Lentz, P. J.; Smiley, I. E.; Steindel, S. J.; Rossmann, M. G. *J. Mol. Biol.* **1976**, *102*, 759-779.

You, K. *CRC Crit. Rev. Biochemistry* **1982**, *17*, 313.

Yue, K. T.; Yang, J. P.; Martin, C. L.; Lee, S. K.; Sloan, D.; Callender, R. *Biochem. Biophys. Res. Comm.* **1984**, *122*, 225-229.

Yue, K. T.; Yang, J. P.; Charlotte, M.; Lee, S. K.; Sloan, D.; Callender, R. *Biochem.* **1984**, *23*, 6480-6483.

Yue, K. T.; Martin, C. L.; Chen, D.; Nelson, P.; Sloan, D. L.; Callender, R. *Biochem.* **1986**, *25*, 4941-4947.

Yue, K. T.; Deng, H.; Callender, R. *J. Raman Spec.* **1989**, *20*, 541-546.